Thermal chamber for adhesives creep testing machine

Manuel Brito Janeira

Master Dissertation

Supervisor: Prof. António Mendes Lopes

Co-supervisor: Inv. Carlos Moreira da Silva

Co-supervisor: Prof. Lucas F. M. da Silva

Integrated Master in Mechanical Engineering

January 2020

“Every chess master was once a beginner”

Irving Chernev

Resumo

Os adesivos são cada vez mais utilizados num vasto leque de indústrias de ponta, devido às suas excelentes propriedades, quando comparadas com métodos de ligação convencionais. Assim, fabricantes e académicos estão empenhados em estudar estes materiais e as suas caraterísticas.

O objetivo principal do Grupo de Adesivos (AJPU) da FEUP é estudar e avaliar diferentes tipos de adesivos sujeitos a várias condições de trabalho. Um dos equipamentos disponíveis no AJPU é uma máquina de ensaios à fluência com três postos de trabalho, desenvolvida em Dissertações de Mestrado de Engenharia Mecânica realizadas em anos anteriores. Os ensaios à fluência devem realizar-se a uma temperatura controlada, sendo assim necessária a implementação de uma câmara térmica.

Com esta dissertação pretende desenvolver-se uma câmara térmica para a máquina de ensaios à fluência já existente. A câmara tem de ser capaz de operar entre -100 e 200 ℃ e apresentar baixo gradiente de temperaturas.

O primeiro passo foi conceber um isolador térmico para cada veio superior da máquina, de modo a reduzir a temperatura nas células de carga para valores de serviço. O desenvolvimento e validação do design do isolador térmico foi realizado recorrendo a simulações numéricas no SolidWorks.

Posteriormente, o conceito da câmara foi desenvolvido, explorando diferentes soluções. Quando conveniente, diferentes opções com influência na eficácia térmica da câmara foram suportadas por explicações matemáticas. Ao mesmo tempo, os projetos de controlo e automação necessários para o funcionamento da câmara foram desenvolvidos. Durante o processo de desenvolvimento, os materiais e os componentes foram selecionados com base nas suas propriedades, disponibilidade e preço.

Por fim, foram realizados os desenhos técnicos, definindo os materiais e as dimensões dos componentes desenvolvidos.

Abstract

Adhesives have been increasingly used in a wide range of industries, due to their good proprieties when compared with traditional joining methods. Therefore, manufacturers and researchers have been making an effort to study these materials and their characteristics.

The main goal of the Adhesives Group (AJPU) of FEUP is to study and evaluate different types of adhesives under different conditions. One equipment available at the AJPU is a creep testing machine with three independent working stations, developed in the context of previous Mechanical Engineering Master Dissertations. As the creep tests must be performed under controlled temperature, the implementation of a thermal chamber was required.

The main goal of this masters' dissertation is to design a thermal chamber for the existing creep testing machine. The chamber needs to be capable of operating between -100 and 200 ℃ and have a low temperature gradient.

The first step was to design a heat insulator for each upper rod of the creep testing machine, in order to limit the temperature at the load cells to service values. The development and validation of the design were made using thermal simulations on SolidWorks.

Subsequently, the concept of the chamber was developed, exploring different possible designs. When convenient, the solutions with influence on the thermal efficiency of the chamber were supported analytically. The development of the chamber was made side by side with the required control and automation project of the chamber. During this process, the materials and the components were selected based on their proprieties, availability and market price.

Finally, the technical drawings were defined and the materials were selected.

Acknowledgments

Firstly, I would like to thank my supervisors Prof. António Mendes Lopes, Inv. Carlos Moreira da Silva and Prof. Lucas da Silva for all the support and knowledge they gave me during the dissertation.

To Prof. Paulo Coelho and Mr. Joaquim Silva, for the availability and patience that was fundamental to conclude all the work.

To my family, friends and especially to my girlfriend who during all my academic life encouraged me to move forward and fight for my goals.

Finally, to all members of the AJPU for their help in every issue along this dissertation.

Contents

List of Figures

List of Tables

Acronyms

AJPU – Advance Joining Processes Unit

AC – Alternating Current

CFM – Cubic Feet per Minute

DC – Direct Current

FEUP – Faculdade de Engenharia da Universidade do Porto

LED – Light Emitting Diode

RCBO – Residual Current circuit Breaker with Overcurrent protection

rpm – Rotations per Minute

RT – Room Temperature

SSR – Solid State Relay

UTM – Universal Test Machine

1 Introduction

1.1 Background and motivations

Adhesives have increasing importance in today's industry, with a strong presence in the aerospace, automotive, railway and marine industries, as well as in civil construction, electrical equipment and even in medicine and dentistry areas.

The use of natural adhesive is very ancient, but just in recent years, the humankind started to use adhesives based on synthetic polymers. The advantages of adhesive joints compared to traditional mechanical joints led to an increase in the studies in this field [1].

At Faculdade de Engenharia da Universidade do Porto (FEUP), a research group (Advance Joining Processes Unit - AJPU) was created to study the proprieties and behavior of adhesives and adhesive joints, contributing with their research for the advance of the state-for-the-art in the field. The AJPU is involved in different projects; therefore, the use of a large variety of equipment is unceasing. An important equipment is the multi-station creep testing machine. Being creep a typical characteristic of a material, adhesives included, its study and understanding are fundamental. Due to the correlation between creep and temperature, studying creep under different values of temperature is of paramount importance.

Freire [2], Pina [3] and Silva [4] developed the AJPU multi-station creep testing machine. In their projects, the construction of a thermal chamber was mentioned, but it was never developed.

1.2 Objectives

The main goal of this dissertation is to develop a thermal chamber that can operate between -100 ℃ and 200 ℃. The chamber has to be integrated with the existing multi-station creep testing machine developed by Freire [2], Pina [3] and Silva [4].

Besides operating in a specified range of temperatures, the thermal chamber has to ensure a low temperature gradient over its inner volume and to respect the dimensions imposed

by the creep testing machine. It must also guarantee human safe values of on the exterior casing and safe temperature values for all the components that constitute the equipment.

The chamber also needs to work autonomously, meaning that the temperature control has to perform automatically over long periods of time, and the interface for setting up the thermal tests should be user-friendly.

1.3 Methodology

Initially, a literature review on creep testing machines was done. For that propose, the previous master dissertations of Freire [2], Pina [3] and Silva [4] were analyzed, books and papers on the subject were read, and the state-of-the-art on such machines was revised.

After understanding the previous work and the solutions available on the market, another literature review was done, now focused on thermal chambers. The principles of the constructive solutions were understood, namely on how the insulation is made, how the heating and cooling systems operate and what solutions for integrating thermal chambers in creep testing machines exist in the market.

Then, the thermal and dimensional restrictions for the thermal chamber were established and a heat insulator was designed. After performing thermal and static force simulations, the solution was validated. Then, the design of the chamber was developed, having in mind the thermal needs of the equipment.

Finally, the automation project was executed. All the required electric components were selected, and the command and control circuits were established.

1.4 Dissertation outline

This dissertation is organized in six chapters, each one covering a subject of relevance for the understanding of the content developed.

The first chapter gives a brief introduction to the dissertation, the background, the motivation for the project and its main objectives.

In the second chapter, a small introduction to adhesives is made, followed by a literature review on creep testing machines and thermal chambers.

In the third chapter, the development and the design of the thermal chamber, and the conceived heat insulator are described. Afterwards, the steps for the material selection, the mechanical connections between components, and all the features for the good functioning of the chamber are contemplated. The thermal simulations necessary to validate the design of the heat insulator are also presented in this chapter.

The fourth chapter addresses the automation of the chamber. The development of the command and control circuits are described and all electrical components are presented.

The fifth and last chapter compiles the most relevant conclusions of the dissertation. A critical analysis is made, regarding the obtained results, and suggestions for further improvements are presented.

2 Literature review

This chapter presents a brief literature review on adhesives, creep testing machines and thermal chambers.

2.1 Introduction to adhesives

An adhesive may be defined as a material that, when applied on the surfaces of two substrates join them together and the formed joint can resist against separation loads [5]. For thousands of years adhesives have been used by men. Originally, they were made of natural products such as skin, bone, milk, fish, beeswax and tree sap. At the beginning of the twentieth century, adhesives based on synthetic polymers started to be used, and their application on the industry grew exponentially. Nowadays, it is possible to find adhesives in everyday products and across different industries [1].

Adhesives can be classified in a variety of ways according to their form, type, chemistry or their load-carrying capability. Regarding the latter, those materials can be defined as structural and non-structural [6]. It is imperative that structural adhesives are capable of transmitting structural stress without loss of structural integrity. Their major function is to join parts together, in a way that the stress transmitted between the parts is distributed much more evenly than when conventional mechanical fasteners are used. Consequently, adhesives often permit the fabrication of structures that are mechanically equivalent to, or even stronger than, conventional assemblies, at lower weight and cost [7].

Despite, being a very interesting material, with many useful proprieties, adhesives still have some downsides when compared with other joining technologies. Careful preparation of the surfaces that are to be bonded is required. The bonding is usually not instantaneous, which requires the use of tools to maintain the parts in place, and their resistance to extreme conditions of temperature and humidity is limited [1].

2.2 Creep testing machine

A creep testing machine is an apparatus that measures the creep of a specimen of a given material at constant stress and temperature. Creep is a deformation that accumulates with time. According to the scale and the duration of the stress applied to a specimen, the deformation may become so large that rupture occurs [8].

At certain temperatures, large creep strains may occur in adhesives, in which a leathery or rubbery state is achieved. Thus, it is of extreme importance knowing the behavior of such materials at different temperatures and loads.

There are different methods for creep testing, but the most common consists of applying a constant force, either in compression or in tension, over the main axis of the specimen that is being tested. The data obtained in creep tests are normally presented as a plot of strain versus time, as shown in Figure 1. It is possible to identify three phases in the plot. Phase I corresponds to the primary or transient creep, where the creep rate decreases continuously. At the end of phase I, instantaneous elastic strain and delay elastic strain are complete. Then, phase II corresponds to the secondary or steady-state creep. At the end of phase II, Phase III initiates, where creep increases in an unsteady manner, accelerating towards the rupture of the specimen. This part is denominated by tertiary creep [8] [9].

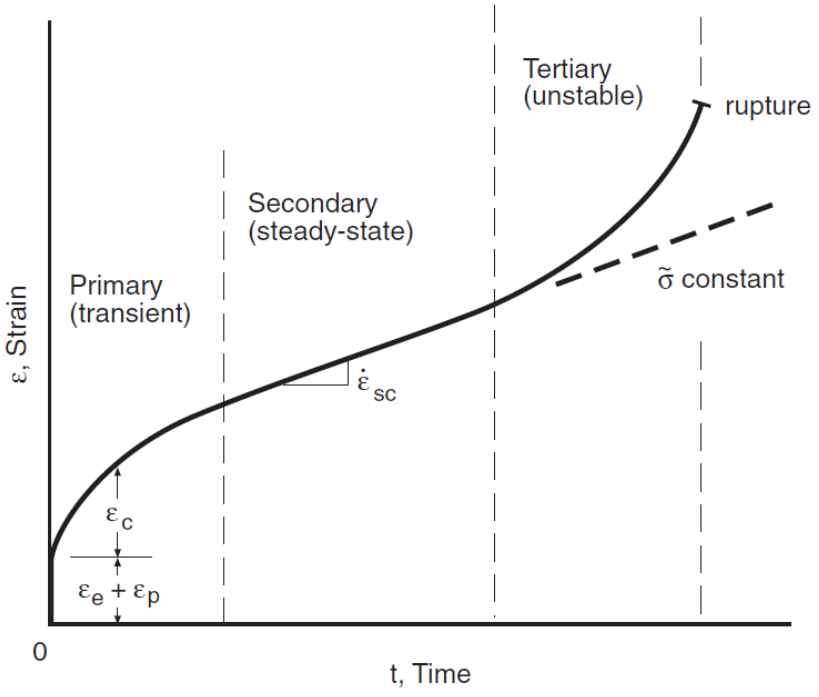

Figure 1 – Strain versus time behavior during creep [8].

2.2.1 The AJPU creep testing machine

The AJPU group has a dual column tabletop testing machine, model 3367 from INSTRON – Figure 2. The machine is equipped with an environmental chamber, model 3119 from the same manufacturer – Figure 3. Although this equipment is capable of performing creep tests, the group uses it on a daily basis, so the long duration of creep tests makes the use of the INSTRON machine impracticable.

Figure 2 – INSTRON model 3367 testing machine.

Figure 3 – INSTRON model 3119 environmental chamber.

The creep testing machine developed by Freire [2], Pina [3] and Silva [4] – Figure 4 – tries to respond to the AJPU needs. It is fully functional for tests at room temperature (RT), but since it does not include a thermal chamber, its usability is limited. The AJPU resorted temporarily to simple creep tests, using calibrated weights hanging on the specimen, as shown in Figure 5. This set (calibrated weights plus specimen) is then put in a thermal chamber and the displacement is measured at defined time intervals.

Figure 4 – AJPU creep testing machine.

Figure 5 – Creep test using hanging weights.

2.2.2 Creep testing machines in the market

Different manufacturers, such as INSTRON, ZWICK, and SHIMADZU offer solutions capable of performing creep tests. They have a variety of Universal Test Machines (UTM's) that are able to execute creep tests, and also have the option for including thermal chambers. However, the vast majority of the models available are single-station. When looking for multi-station solutions, the options drop exponentially and the prices rise. Moreover, a multi-station machine with a climate chamber incorporated is scarce.

ZWICK offers an electromechanical creep testing machine – Figure 6 – with five or six individually controlled test axis, each one with a maximum load capacity of 10 kN. This equipment was designed to perform tests for long periods of time, up to 10,000 h. It is also possible to have incorporated an irremovable climate chamber that can operate between -70 and 250 °C [10].

Figure 6 – ZWICK's multi-station creep testing machine [10].

INSTRON has a multi-station solution – Figure 7 – with five test axes, that can perform simultaneous and independent tests using a single load frame. The single load frame can have a total load capacity of 30 kN, being able to have other capacities upon request. The load capacity per station is the total load capacity divided by the number of load stations that are being used. Only the central station can work at the full capacity of the load frame. The other stations can work at a maximum of 10 kN. There are four models available. Just two of them offer the possibility of incorporating a five port environmental chamber with a roller mount that works from -40 to 200 °C [11].

Figure 7 – INSTRON's multi-station creep testing machine [11].

2.3 Thermal chambers

Generically, a thermal chamber is an equipment that allows temperature control in a confined volume. Depending on the application, thermal chambers can work above, below or both above and below RT. They can have humidity control and allow the introduction of different gases in the inner volume to create a specific atmosphere. These equipments are commonly used in many applications, namely in the food industry, medicine, pharmacology, and chemistry [12] [13] [14] [15].

No matter the size nor the application, a thermal chamber needs to have its walls insulated, in order to prevent heat losses and assure the safety of people that may be in contact with the external walls of the chamber. Different layers of insulation are set, forming a sandwich structure, as shown in Figure 8. Depending on the application, the wall can have more or fewer layers, made of various types of material [14] [15] [16].

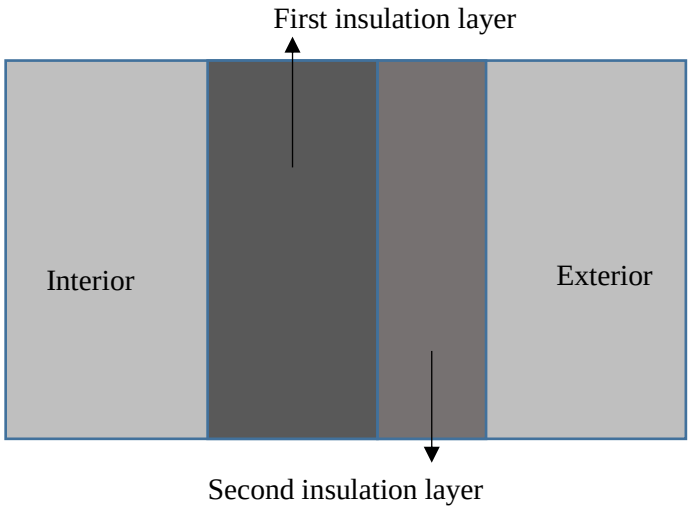

Figure 8 – Scheme of the sandwich structure of a chamber.

2.3.1 Heating system

The heating process in thermal chambers for creep testing machines is usually done by forced convection. A fan either blows or vacuums air through or from the heating element, increasing the air's temperature, which spreads over the volume of the chamber. With this method, the temperature inside the chamber reaches its set point quicker and with smaller temperature gradients, when compared with the heating process by natural convection, in which the heating element is set at the bottom part of the chamber, creating upwards convection currents [13] [16].

According to Joule's first law, when an electrical current flows through a conductive material it generates a heat power that is directly proportional to the product of the material's resistance per the square of the current [17]. This is the principle of functioning of a heating element, where a piece of conductive material with a certain resistance carries an electrical current, generating heat.

There are several types of heating elements composed of different alloys and shapes that fulfill the needs of each application [18]. By reading the product data sheets of two major heating element manufacturers – KANTHAL and WATTACO – it becomes evident that the combinations of alloys that exist in the market are vast, so naming all of them would be too extensive for the purpose of this dissertation. Three examples of heating elements are depicted in Figure 9.

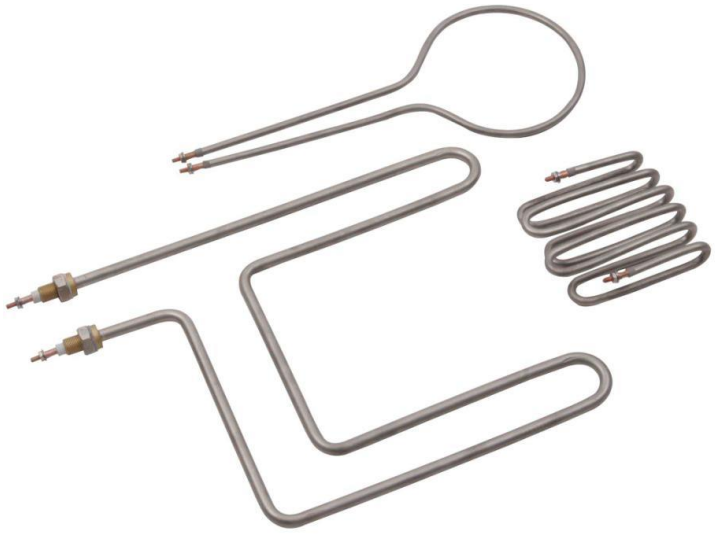

Figure 9 – Examples of heating elements [18].

According to the KANTHAL Appliance alloys handbook, this manufacturer has heating elements of:

- NiFe;
- Austenitic alloys – NiCr, NiCrFe;
- Ferritic alloys – FeCrAl;
- Copper-nickel alloys [19].

WATTCO does not give much information about their heating elements, only indicating that the main alloy for all tubular heating elements is NiCr and providing the sleeve material and the type of application they are designed for. These characteristics are shown in Table 1 [20].

Table 1 – Application and sheath material of heating elements [20].

Application	Sleeve material
Water Water solutions non-corrosive to copper	Copper
Oil Grease Alkaline cleaning solutions Tars Asphalt	Steel
Corrosive liquids Food processing equipment	Stainless steel
Air heating Radiant heating Cleaning and degreasing solutions Plating and picking solutions Corrosive liquids	Incoloy® Inconel®
Acid Corrosive liquids	Titanium

2.3.2 Colling system

There are different processes for cooling a material or a workspace. Generally speaking, it is possible to divide them into two categories:

- Mechanical cooling;
- Cryogenic cooling;

A mechanically cooled system is a closed system that recovers and reuses the coolant fluid. In order to operate, these systems need at least a metering valve, a throttling device, a condenser, an evaporator, one compressor, two heat exchangers coils, a fan and its motor, electronic relays, a thermostat, and innumerous process controls, making it complicated and expensive. However, the equipment responsible for the cooling and recompression of the coolant fluid is usually integrated with the thermal chamber, turning it in a convenient self-contained system. Nevertheless, these systems are limited by the capacity of the compressor, which in turn is restricted by space, power availability and heat and noise tolerances.

In terms of refrigerating capacity, mechanical cooling systems can reach temperatures of -65 ℃, taking more or less time to reach a certain temperature value depending on the power of the compressor. However, these times are significantly higher, when compared with the cryogenic cooling systems, as is illustrated in the graph of Figure 10 [21].

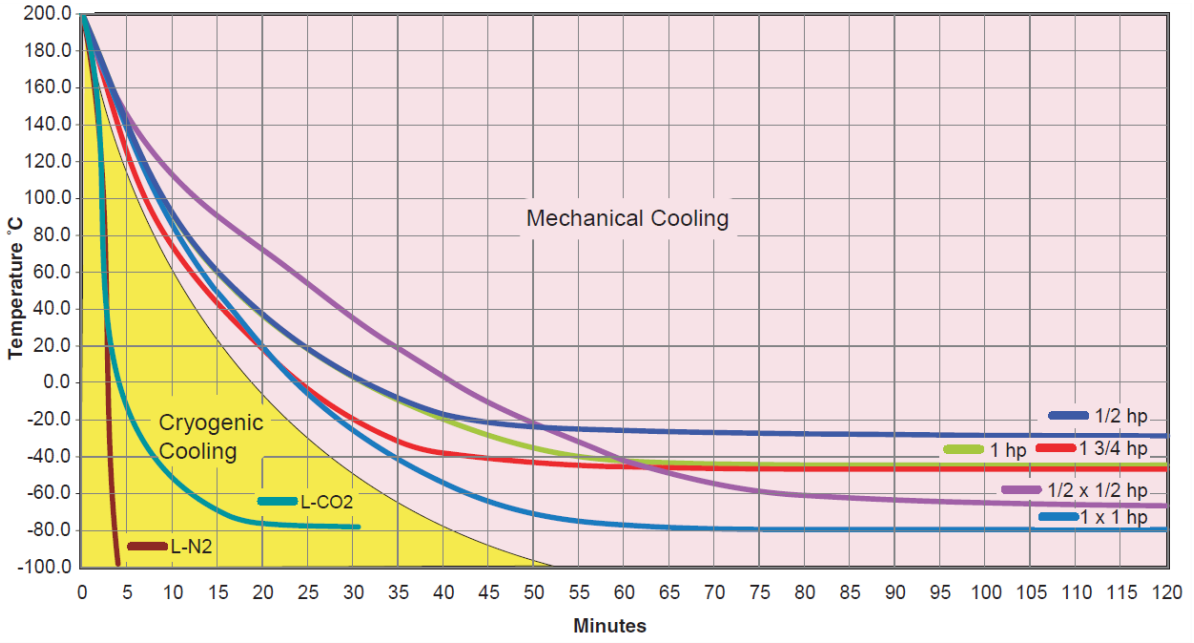

Figure 10 – Temperature versus time for different methods of cooling [21].

Contrary to the previous systems, the cryogenic solution is, in general, open. A cryogenic coolant is injected in the chamber, cooling it down and is then expelled to the atmosphere. The most common coolants are CO_2 and N_2. Being part of the Earth's atmosphere, they do not represent any harm to the environment. Although, if the workspace where the cryogenic coolant fluids are being exhausted is not big enough and/or well ventilated, the concentration of oxygen in the room can drop to levels that could be harmful to humans.

The main components of a cryogenic cooling system are a supply vessel with the cryogenic coolant, pressure reducer, a hose, a filter, a safety valve, a metering valve, and a throttling device. This is a shorter and less complex list than the one mentioned for mechanical cooling systems. The hardest part of cryogenic cooling is to compress and liquefy the coolant. That responsibility is removed from the user of the system, since the vessel containing the cryogenic coolant can be bought to a supplier that does all of the work. This way of cooling is easy and cheap to implement and achieves great results in terms of temperature and time. However, the cost of the coolant is much higher than the cost of electricity required for the mechanical cooling system.

A cryogenic cooling system that uses L-CO_2 (liquid CO_2) can reach a temperature of -80 ℃ in much less time than a mechanical system – Figure 10. If L-N_2 (liquid N_2) is used instead, the temperature can drop to -175 ℃ or even more [21] [22].

2.3.3 Market solutions for thermal chambers

As said in section 2.2, the availability of multi-station creep testing machines is very reduced due to the lack of market demand. Therefore, the information regarding thermal chambers for these machines is also scarce. To bypass this absence of information, it is

necessary to resort to the data of thermal chambers designed for single-station creep testing machines and then interpret and adapt the information to bigger volumes chambers.

ZWICK has a large option of thermal chambers for their different types of machines. For the models that belong to the AllroundLine, it has five thermal chamber options, being one of them depicted in Figure 11. All chambers can operate between 10 and 250 ℃ and have the option of installing a cryogenic cooling system able to reach -80 ℃ that runs on L-N_2. The consumptions of the coolant required to reach the lowest temperature vary from 6 to 19 l. In terms of ramps of heating and cooling, 14 to 23 minutes are required to reach the maximum temperature, when departing from RT. In order to reach the minimum temperature from RT, the equipment needs between 12 and 17 minutes. Every chamber model has temporal instability and a local inhomogeneity of ± 1 ℃. The power supply required is 400 V and the power consumption varies from 3.3 to 5.2 kVA. The wide range of values presented is due to the different internal volumes that every thermal chamber has, and can be visualized in Table 2.

Figure 11 – Example of creep testing machine with a thermal chamber by ZWICK [23].

The details provided by the manufacturer lead to the conclusion that the chamber is mounted in guide rails and slides back and forth to be put in place. ZWICK also offers the possibility of having an additional door opening, to minimize the temperature variations during change or removal of the specimen. A safety door function and Light Emitting Diode (LED) light module are also included.

Table 2 – Characteristics of ZWICK's thermal chambers [23].

		Values				
Model No.		**1022207**	**1022208**	**1022209**	**1022210**	**1022211**
Temperature range		[-80; 250] ℃				
Typical L-N_2 consumption in liter from RT to -80 ℃		6	9	13	14	19
Hating time, in minutes from RT to 250 ℃		15	17	23	14	19
Cooling time, in minutes from RT to -80 ℃		12	14	16	19	17
Temporal instability		±1 ℃				
Local inhomogeneity						
Power supply [V]		400				
Power supply frequency [Hz]		50/60				
Power supply consumption [kVA]		3.3			5.2	
Internal dimensions [mm]	**Height**	500	700	900	700	900
	Width	260	260	260	460	460
	Depth	445	445	445	655	655
External dimensions [mm]	**Height**	640	840	1040	840	1040
	Width	400	400	400	600	600
	Depth	1,015	1,015	1,015	1,225	1,225

Another main manufacturer of creep testing machines is INSTRON. They also have a large number of thermal chamber models for single-station test machines. For their 3119-600 Series – Figure 12 – six different options are available for the floor models and other four for tables models, being also possible to choose the coolant to be used. Most of the chambers can achieve 350 ℃ and one of them can reach 600 ℃. The chambers that work with CO_2 coolant can reach -70 ℃, the ones operating with N_2 reach -80 ℃ or -150 ℃. In order to achieve these temperatures, these equipments require more time, compared with the chambers from ZWICK, since they are powered with 200-240 V instead of 400 V. The maximum temperature is reached in less than 50 minutes in some chambers. Some models need less than 120 minutes. On the other hand, to reach the minimum temperature it takes between 20 and 120 minutes. The overall accuracy of the temperature inside the chambers ranges from ±3.5 to ±5.5℃. Appendix A contains a table giving an overview of the main characteristics of the INSTRON models for the 3119-600 Series [16].

Figure 12 – Example of two creep testing machines with thermal chambers from INSTRON [16].

The chambers use forced convection to spread the heated air or the coolant, accelerating the heat transfer and ensuring a more homogenous temperature inside the chamber. Air at RT flows through a case that is between the insulation and the outer panels, allowing more efficient insulation, as it is depicted in Figure 13. These equipments have other features, such removable wedge ports ensuring a quick and easy setup of the chambers without interfering with the pull rods and roller mounting can be installed to remove the chamber from the test space.

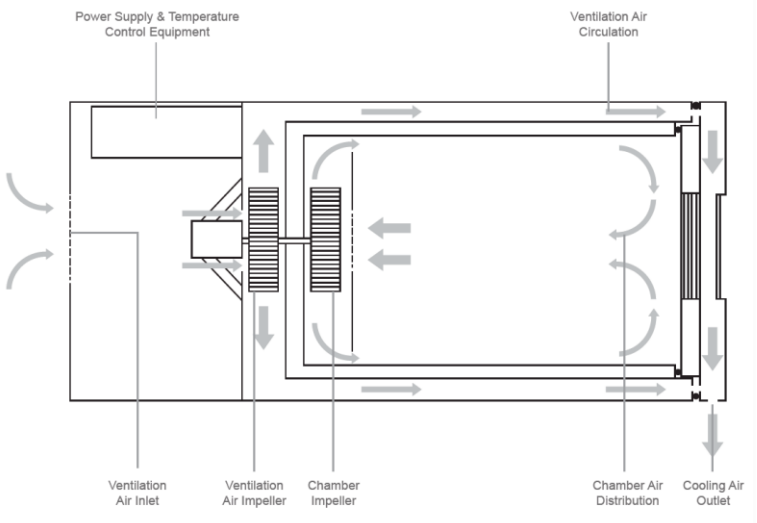

Figure 13 – Scheme of the airflow through the chamber [16].

2.4 Discussion

The implementation of a thermal chamber in the already existing creep testing machine will add significant value to the AJPU group, allowing them to have a fully equipped creep testing machine

The main idea of how a thermal chamber should behave, and how the heating and the cooling systems work was described in this chapter. Cryogenic cooling was also shown to be a good option. Moreover, the need for an extra layer of insulation, where air flows through it, ensuring better insulation and limiting the exterior case temperature to levels not harmful to humans, was perceived.

3 Thermal chamber design

This chapter describes the design and validation of the thermal chamber and the heat insulator that prevents the overheating of the load cells implemented in the top of the creep testing machine.

3.1 Heat transfer concepts and principles

Heat transfer consists of the change of energy in the form of heat, which occurs every time a difference of temperature difference exists in a medium, or between different media. In Figure 14 the three modes of heat transfer are shown: conduction, convection, and radiation.

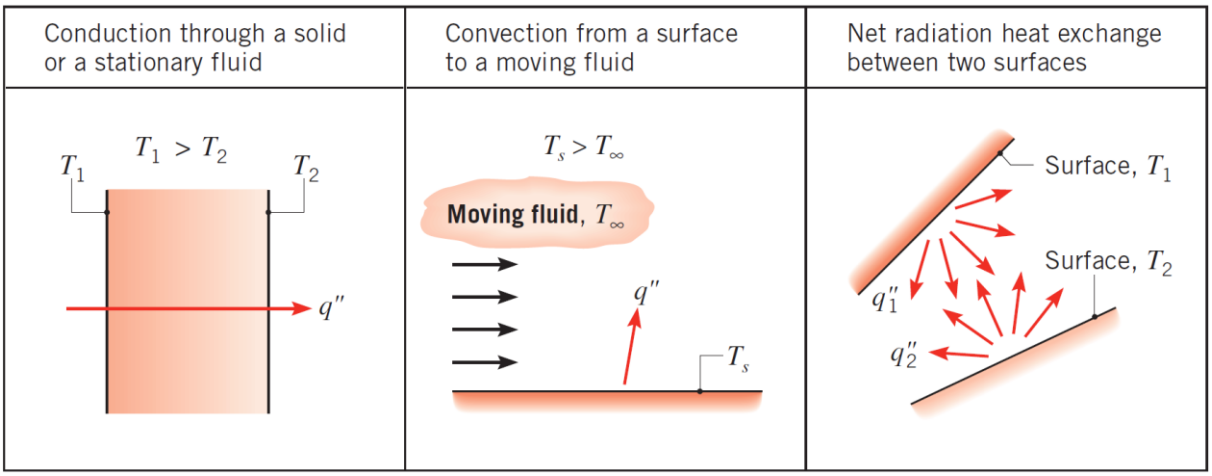

Figure 14 – Scheme of the three modes of heat transfer [24].

The transfer of energy from a more energetic to a less energetic particle is a way to interpret conduction. The particles that constitute a substance interact with each other transferring energy, from the more (associated with a higher temperature) to the less energetic. Thus, a temperature gradient leads to heat transfer by conduction towards the lower temperature.

The Fourier' law is used to quantify the heat flux that flows through a material. This law translates into the following equation, under the steady-state conditions shown in Figure 15,

$$q''_x = k\frac{\Delta T}{L} \tag{3.1}$$

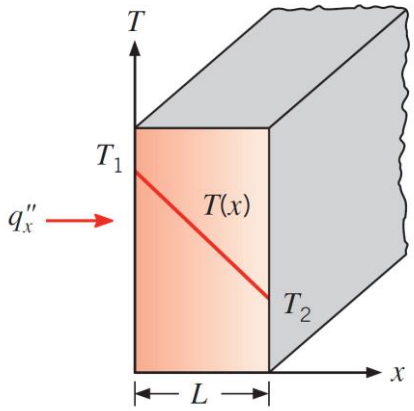

Figure 15 – One-dimensional heat transfer by conduction [24].

where q''_x is the conduction heat flux, expressed in W/m^2 and k is the thermal conductivity, a propriety that varies with the material and is expressed in W/m·K. The length of the material, where the heat flows is represented by L and is expressed in meters and the difference of temperature between T_1 and T_2 is represented by ΔT.

The heat transfer by convection is divided into two mechanisms: diffusion – heat transfer by random molecular motion – and the energy transferred by macroscopic motion of the fluid. It can be classified in forced or free (or natural) convection, according to the nature of the flow. In forced convection, an external source forces the movement of the fluid that transfers heat with a surface – Figure 16. In natural convection the flow is induced by a buoyancy force, which occurs due to the variation of temperature in the fluid, generating density differences.

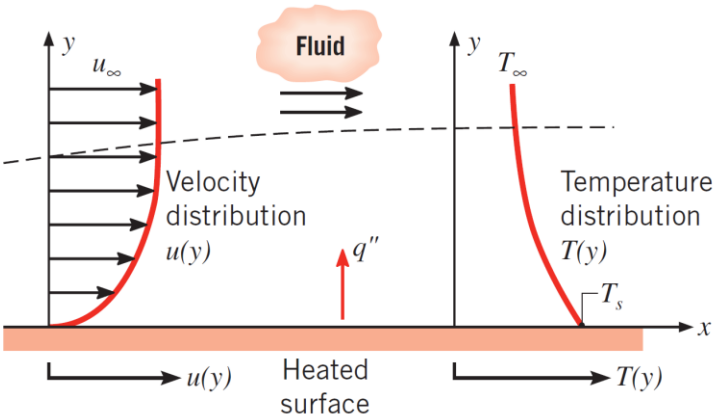

Figure 16 – Scheme of heat transfer by convection [24].

Regardless of the convection being forced or natural, the equation that quantifies the amount of heat flux is the same and called Newton's law of cooling

$$q'' = h(T_\infty - T_s) \tag{3.2}$$

where q'' represents the convection heat flux, expressed in W/m^2 and h is the convection coefficient, expressed in W/m^2·K. This coefficient is determined by the fluid motion and thermodynamic proprieties, boundary layer, and surface geometry. The heat flux is proportional to the difference of temperatures, being T_∞ the temperature of the fluid and T_s the temperature of the surface.

The Nusselt number is a dimensionless parameter, which correlates the convection coefficient, the thermal conductivity of the fluid and a spatial coordinate. It can be defined as the ratio of convection to pure conduction heat transfer and is expressed by the equation

$$Nu = \frac{hL}{k_f} \tag{3.3}$$

The Nusselt number can also be calculated based on empirically and assumes drastically different values according to the geometry of the surface and the nature (internal or external) of the flow. Combining the equation above and one of the equations obtained by empirical experience, it is possible to reach a value of the convection coefficient.

Thermal radiation is the energy emitted by any substance at a temperature greater than absolute zero (0 K). This energy is transported by electromagnetic waves, not requiring the presence of a material medium for heat transfer to take place. The Stefan-Boltzmann law quantifies the energy that is emitted from a surface per unit area by radiation and is represented in the following equation

$$E = \varepsilon \sigma T_s^4 \tag{3.4}$$

where E represents the heat flux by radiation and is denominated surface emissive power, expressed in W/m^2. The parameter ε is called emissivity and measures how efficiently a body emits energy when compared to a blackbody. Its values are in the interval $0 \leq \varepsilon \leq 1$. The Stefan-Boltzmann constant is represented by σ, with a value of 5.67×10^{-8} W/m^2·K^4. Finally, the temperature of the body is defined by T_s [24].

3.2 Thermal and dimensional restrictions for the chamber

The thermal chamber will be incorporated in the creep testing machine developed by Freire [2], Pina [3] and Silva [4]. In order to fit between the existing two support columns, the chamber cannot exceed 625 mm in width. Evidently, this value should be a little bit lower to

ensure that the equipment does not hit the columns when installing it. In terms of height, the chamber has to accommodate the entire stroke by the grips of the rods of the machine. Regarding the chamber's depth, it should comply with the size of the rods and fit the workspace.

The chamber has to operate in a range of temperatures between -100 ℃ and 200 ℃. The homogeneity of the temperature has to be as high as possible, avoiding thermal gradients that can lead to dubious test results. On the top of each rod of the creep machine a load cell is installed – Figure 17. This device has an admissible range of temperature to operate, as presented in Table 3, which must be respected.

Figure 17 – Load cells from AEP transducers [25].

According to Table 3, there are two ranges of values to take into consideration. From the available information, there is no apparent difference between "temperature nominal range" and "service temperature". After asking the manufacturer, it was concluded that the load cell can work within the range of "service temperature". The values of the "temperature nominal range" are the ones that the manufacturer uses to perform thermal compensation during production.

Table 3 – Temperature values for the load cell [25].

Characteristic	**Temperatures [℃]**
Reference temperature	+23
Temperature nominal range	-10/+40
Service temperature	-20/+70
Storage temperature	-20/+80

When Pina developed the creep test machine, he also considered the hypothesis that a thermal chamber could be designed in the future. Therefore, he made an approximate calculation of the temperature that would reach the load cells, when the chamber operated at its extreme values, concluding that the temperature where beyond the appropriate range [3].

3.3 Heat insulator

As said in section 3.2, the value of temperature that reaches the load cells is not low enough to ensure the proper functioning of these transducers. Therefore, it is necessary to create a device for protecting these equipments. A heat sink was the first idea considered, because it would allow the dissipation of heat that flows through the upper rod of the creep testing machine, reducing the temperature that reaches the load cells. In addition, Pina suggested the same approach during the development of the creep testing machine [3].

The main goal of a heat sink is to dissipate heat, so it is necessary to increase the heat flux going out of the upper rod. According to what has been presented in section 3.1, the best way to increase the heat flux is to expand the surface area. So, a heat sink constituted by a stainless steel slotted tube with aluminum fins attached was designed. A representation of the heat sink is depicted in Figure 18 and the most relevant characteristics of the materials are summarized in Table 4. The choice of material is due to the fact that aluminum has a much higher thermal conductivity than stainless steel. Therefore, in order to prevent the increase of heat flux by conduction, which results in a higher temperature near the load cell, the tube around the upper rod needs to have a low thermal conductivity coefficient.

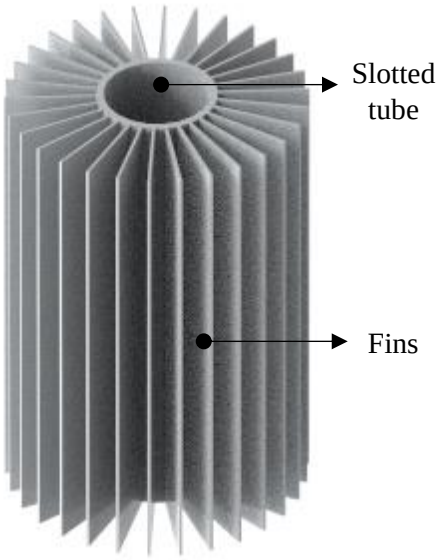

Figure 18 – Example of a heat sink [3].

The heat transfer that occurs in the heat sink is due to conduction, natural convection, and radiation. Those phenomena occur simultaneously and in three spatial dimensions, making them very hard to study without resort to simulation software. In order to obtain fast results that allow implementing eventual changes to the heat sink, heat transfer by radiation was temporally suppressed from the thermal analysis.

Table 4 – Characteristics values of stainless steel AISI 304 and aluminum 1060 alloy.

	Values	
Characteristic	**Stainless steel AISI 304**	**Aluminum 1060 alloy**
Mass density [kg/m^3]	8000	2,700
Thermal expansion coefficient [K^{-1}]	1.8×10^{-5}	2.4×10^{-5}
Thermal conductivity [J/m·K]	16	200
Specific heat [J/kg·K]	500	900

The software utilized for the simulations was SolidWorks, since it was the one used to design the components of the heat sink. To set up the thermal simulation it is required to create a mesh, input the thermal loads and specify the materials and their proprieties. The mesh divides the components under study in small geometric elements and analyzes each of them. It is possible to refine the mesh adjusting the number of small geometric elements and making them smaller. In the thermal load section, it is possible to set the values of temperature, convection, heat flux, heat power and radiation for the desired surfaces. To choose the materials, the software has a very complete database from which it is possible to select different materials or even create new ones.

With all restrictions defined, the simulation parameters have to be specified. At this point, the heating elements and the type of cooling system were still not determined. Therefore, a temperature was defined in one section of the rod where the heat sink was supposed to be connected. This temperature corresponds to the extreme values that the thermal chamber can operate at, that is -100 ℃ and 200 ℃. Evaluating the convection coefficient is not an easy task. The literature on the subject is vast and there are innumerous equations that try to establish the best approximation to the reality. The Nusselt equation for a cylinder can be used for a vertical plane [24]. So, utilizing an online tool from QuickField that calculates the natural convection coefficient [26] – Figure 19 – those values were obtained for the range of temperatures needed, obtaining a graph of the evolution of the coefficient for different temperatures, as shown in Figure 20. Now it is possible to define all the thermal loads required to run the thermal simulation.

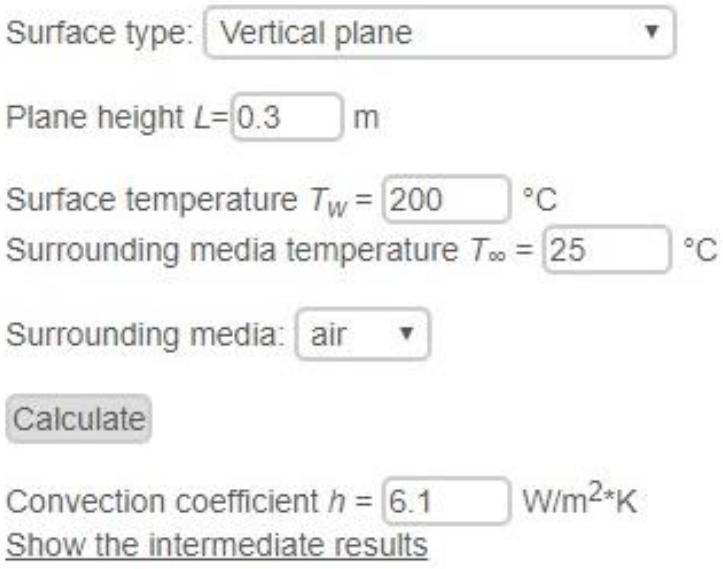

Figure 19 – Print screen from the QuickField tool [26].

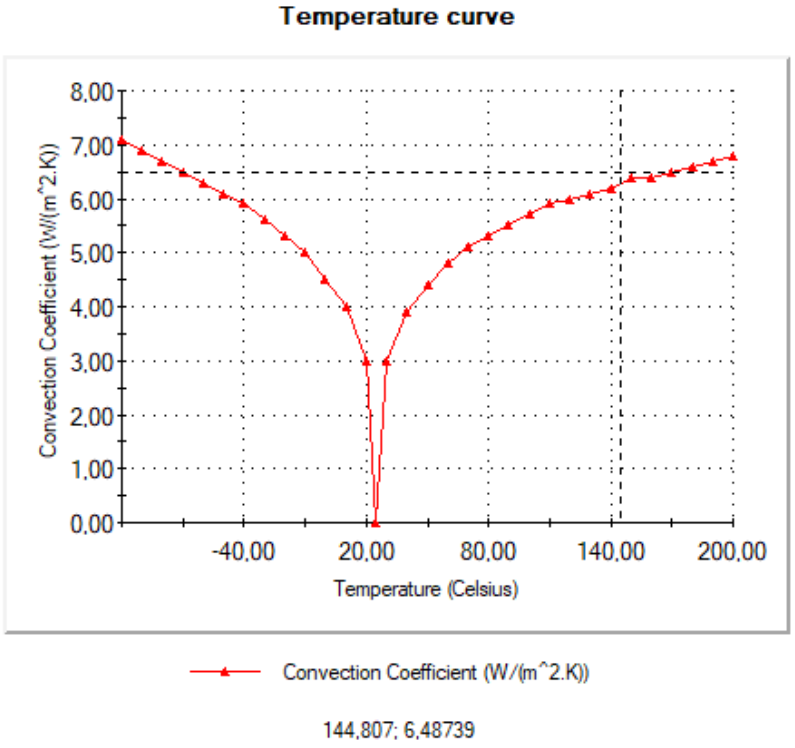

Figure 20 – Graphic of convection coefficient versus temperature.

The heat sink – Figure 21 – was initially defined with a height of 151 mm, using as much space as possible, in order to increase the area of the fins. The 20 fins have a thickness of 2 mm and a width of 25 mm. With this configuration, the simulation was performed, setting a temperature value of 200 ℃ in the section below the heat sink. As Figure 22 shows, the reduction of temperature is not low enough for the load cell to operate properly.

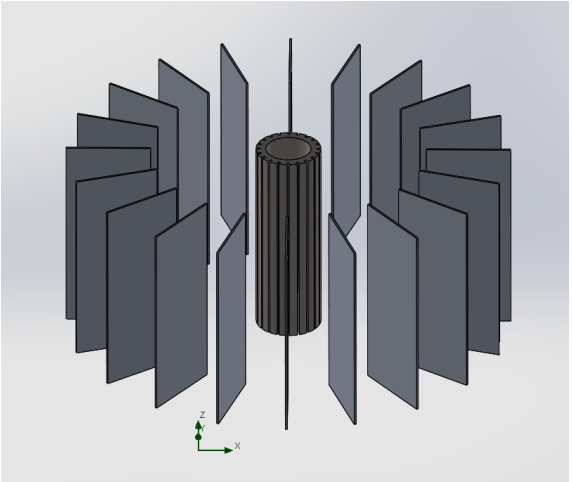

Figure 21 – Heat sink.

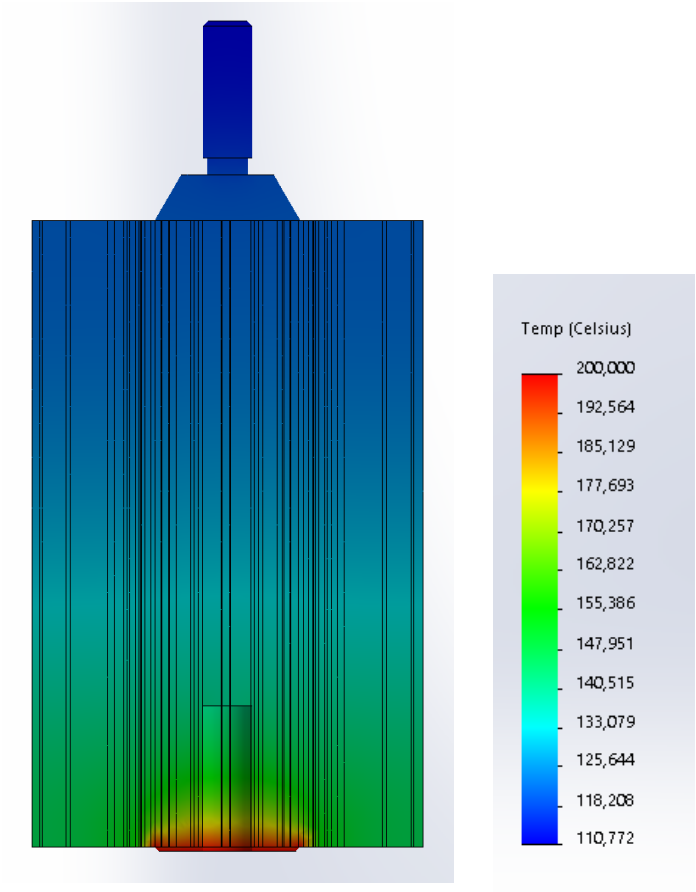

Figure 22 – Results of the thermal simulation with 20 fins, each one with 25 mm of width and 2 mm of thickness.

To improve the heat transfer, the number of fins and its width were increased and the thickness of every fin was reduced. Each iteration in the geometry of the heat sink led to a slightly better result than the previous one, but never achieving the required temperature values. The results of the various simulations are shown in the follow-up. The best result was the one with 40 fins, having each one 50 mm of width and 1.5 mm of thickness.

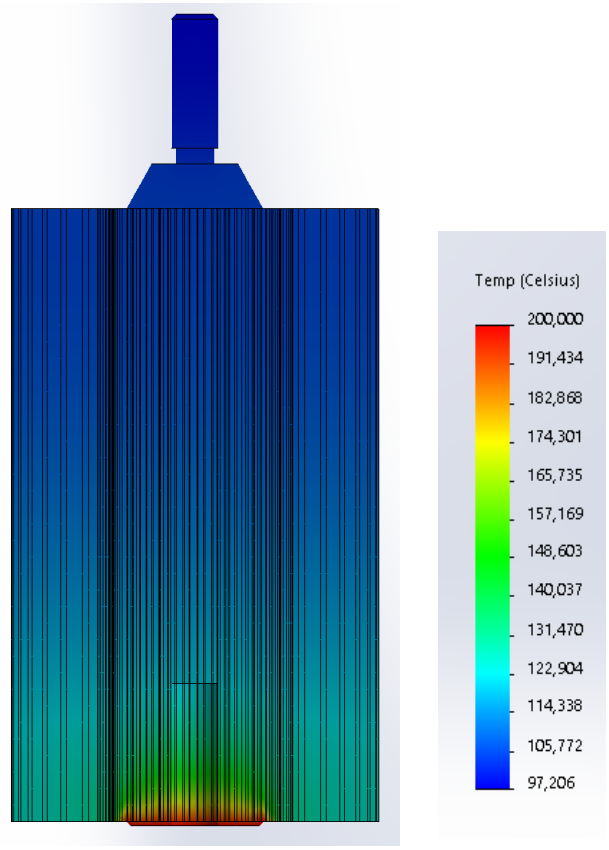

Figure 23 – Results of the thermal simulation with 40 fins, each one with 25 mm of width and 2 mm of thickness.

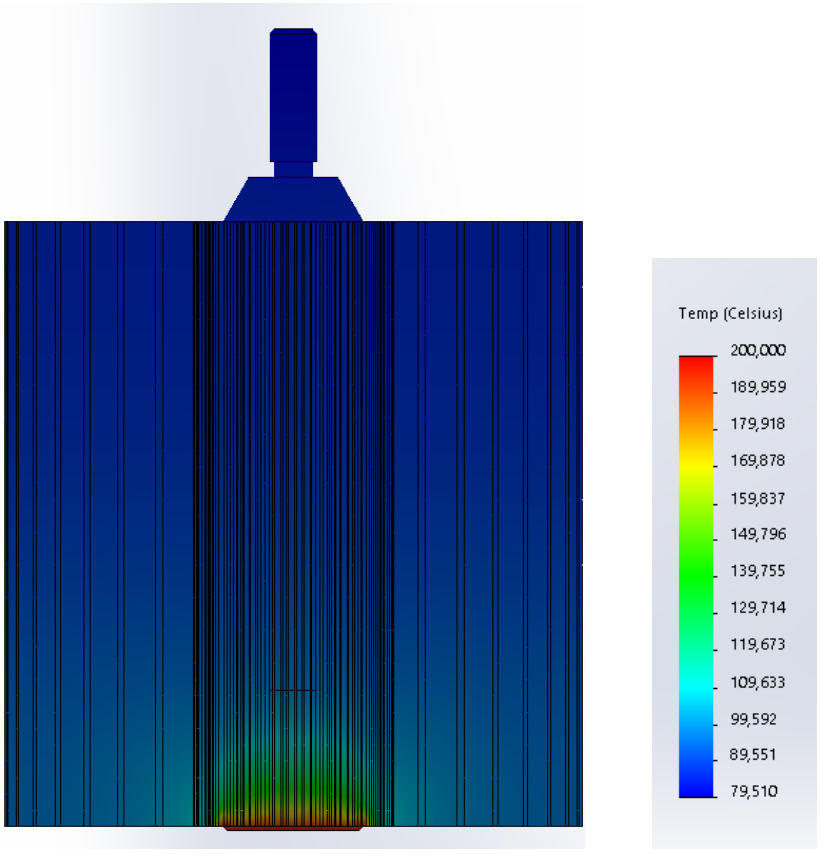

Figure 24 – Results of the thermal simulation with 40 fins, each one with 50 mm of width and 2 mm of thickness.

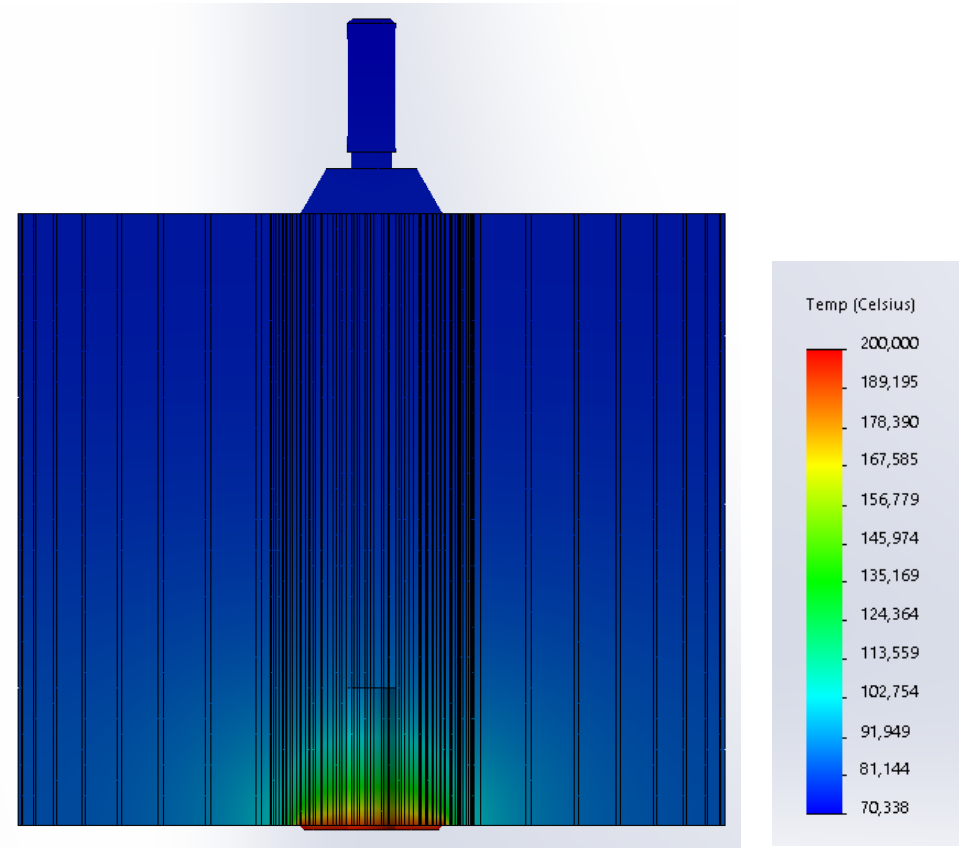

Figure 25 – Results of the thermal simulation with 40 fins, each one with 60 mm of width and 1.5 mm of thickness.

In order to improve the heat sink, more iterations could have been made. Starting with the material, a different aluminum alloy could have been used, namely one with lower thermal conductivity, to decrease the conduction of the heat through the height of the fins. Also, changing the chamber's height could eventually have allowed to increase the surface of the fins or reduce their thickness.

A different design using a heat insulator was also tried. The purpose of this insulator is to avoid heat dissipation caused by the heat sink, thus helping to achieve the thermal chamber's main purpose of avoiding heat losses across its components and reduce the temperature that reaches the load cells.

The concept of the heat insulator is demonstrated in Figure 26. The upper rod extension of the creep test machine needs to be altered for this new design, but the total length should be preserved, avoiding changing the total length of the upper part of the machine.

The heat insulator is constituted by a three-piece stainless steel cylindrical casing, in which the bottom and top lids screw. Inside the casing, the bottom part of the modified upper rod extension is attached to a cylindrical base plate by two nuts. Between the base plate and the bottom lid of the casing, a ceramic insulator is lodged. On the top lid, the other half of the modified upper rod extension is attached (not in the figure). The empty space inside the casing is covered by rock wool to avoid heat transfer by radiation and increase the insulation.

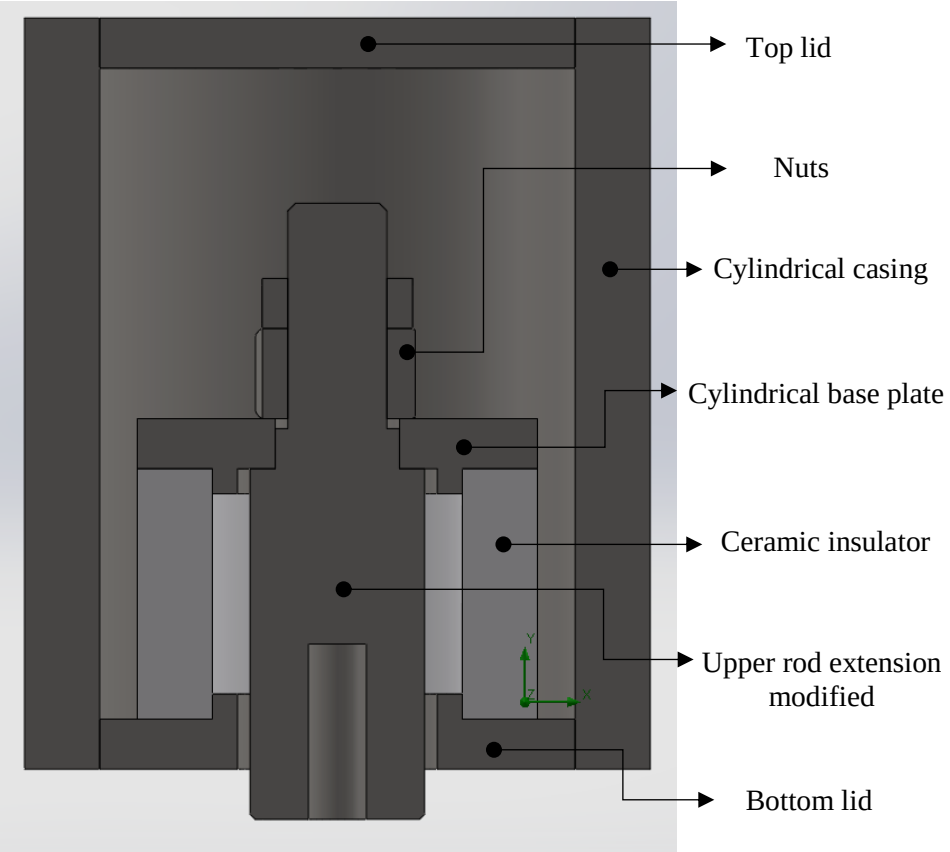

Figure 26 – First concept of the heat insulator.

This configuration allows the required force transmission for the creep test. A traction force is exerted on the upper rod, compresses the ceramic insulator and finally is transmitted to the bottom of the casing.

The ceramic insulator has to have a very low conduction coefficient, to minimize the heat flow that reaches the top of the casing and to have a compression stress that holds the forces of the creep testing machine. After investigating the best ceramic that fulfils the requirements, the company MJAmaral advised using cordierite, which characteristics are described in Table 5.

Table 5 – Cordierite proprieties.

Characteristic	**Value**
Density	1,600 [kg/m^3]
Elastic modulus	120 [GPa]
Compressive strength	600 [MPa]
Thermal conductivity	1.3 [J/m·K]
Specific heat	800 [J/kg·K]
Maximum service temperature	1,300[°C]

The rock wool used in the heat insulator suppresses the heat transfer by radiation between the internal components and the external casing. It also offers good thermic insulation, because it has a very low thermal conductivity, as shown in Table 6.

Table 6 – Rock wool proprieties.

Characteristic	Value
Density	25 [kg/m^3]
Thermal conductivity	0.04 [J/m·K]

To avoid losing more time developing the design of the heat insulator and without guarantees that it would be a viable solution, a quick thermal simulation was executed. The definition of thermal loads followed a similar principle of the ones performed before. Convection was defined based on the values shown in Figure 20. A temperature value of 200 °C for the bottom part of the upper rod extension was also defined. The heat transfer by radiation that occurs between the exterior case and the atmosphere was characterized by an emissivity of 0.4 and a view factor of 1, while the radiation inside the heat insulator was neglected.

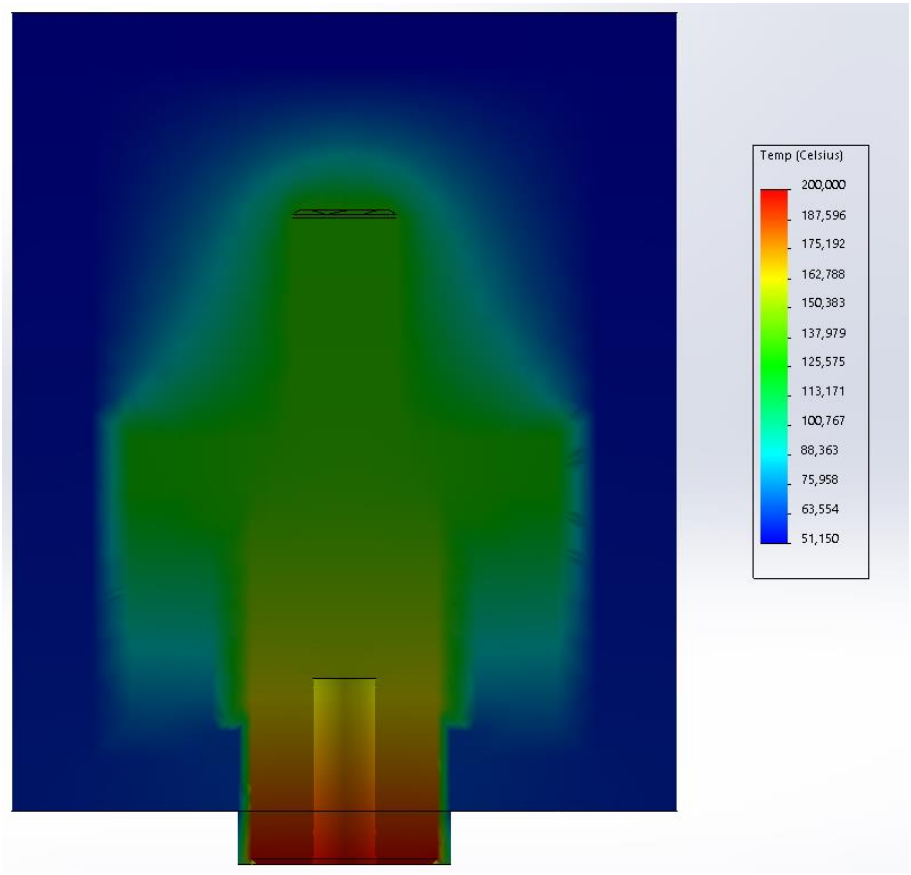

Figure 27 – Results of the thermal simulation made for the heat insulator's initial design.

As shown in Figure 27, there was a significant reduction in the temperature towards an acceptable range. Despite not being finished, the tested model for the heat insulator showed promising results.

Before making the necessary modifications to the heat insulator, it is important to calculate the minimum thickness of the cylindrical ceramic insulator required to hold the forces at stake. The upper rod extension has a diameter of 35 mm and the base plate needs to have a gap for centering the ceramic insulator, as shown in Figure 26. Thus, an interior diameter of 50 mm was established for the ceramic. The main purpose here is to ensure that the compressive strength of the material is higher than the compressive stress that it will be subjected to, as expressed in the following equation

$$\sigma_{comp} > \frac{F}{A} \tag{3.5}$$

where the area (A) is equal to $\frac{\pi}{4} \cdot [d_{external}^2 - d_{internal}^2]$, the maximum force ($F$) is 3000 N and the compressive strength of the ceramic insulator is 600 MPa, as described in Table 5; all the variables are known except for the external diameter, which was calculated to be 50.064 mm. Therefore, there are no significant restrictions for the minimum thickness of the ceramic insulator.

After the calculations of the minimum thickness of the ceramic insulator, some modifications were implemented in the heat insulator, which are shown in Figure 28. The top and bottom lids increased in thickness to avoid major displacements when the components are under load. The diameter of the casing also increased, allowing more space for the ceramic insulator and the rock wool. The top part of the upper rod extension was also modified. The top and bottom parts of the modified component are attached by nuts to the top lid and the base plate, respectively (not in the figure).

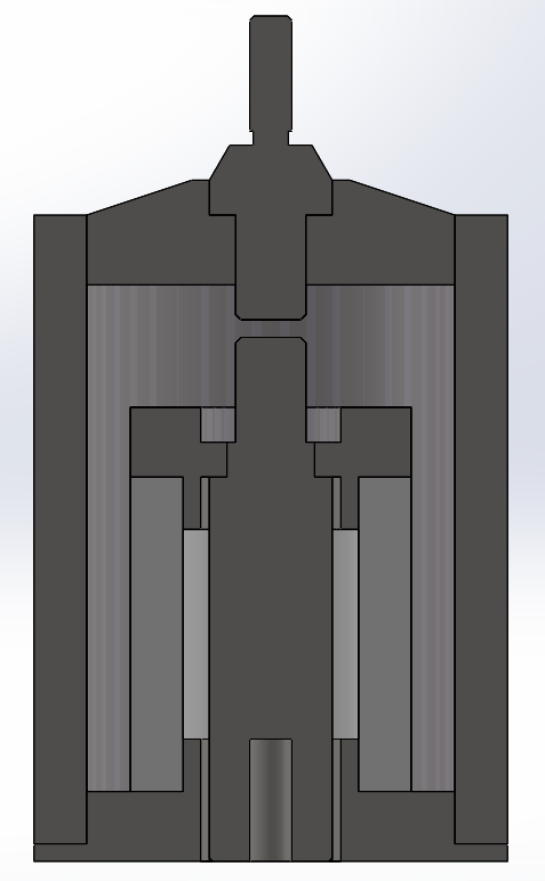

Figure 28 – Modified heat insulator.

With this new configuration, another thermal simulation was run. The applied thermal loads were the same as in the previous simulation and the results are shown in Figure 29. Another simulation with similar thermal loads was also run, but a value of -100 ºC was used instead of 200 ºC – Figure 30.

The results show that the temperature values that reach the load cell are in the range of its admissible service temperature. Despite being acceptable results, it would have been better to reach the temperature's nominal range, which is the temperature at which the manufacture performs the thermal compensation during production. Another inconvenience of this design was the oversized diameter of the casing which made the heat insulator of each station very close. This allows significant heat change, not predicted in the thermal simulations which were run. Because the external casing needs to be reduced, both the ceramic insulator and the rock wool should be reduced as well.

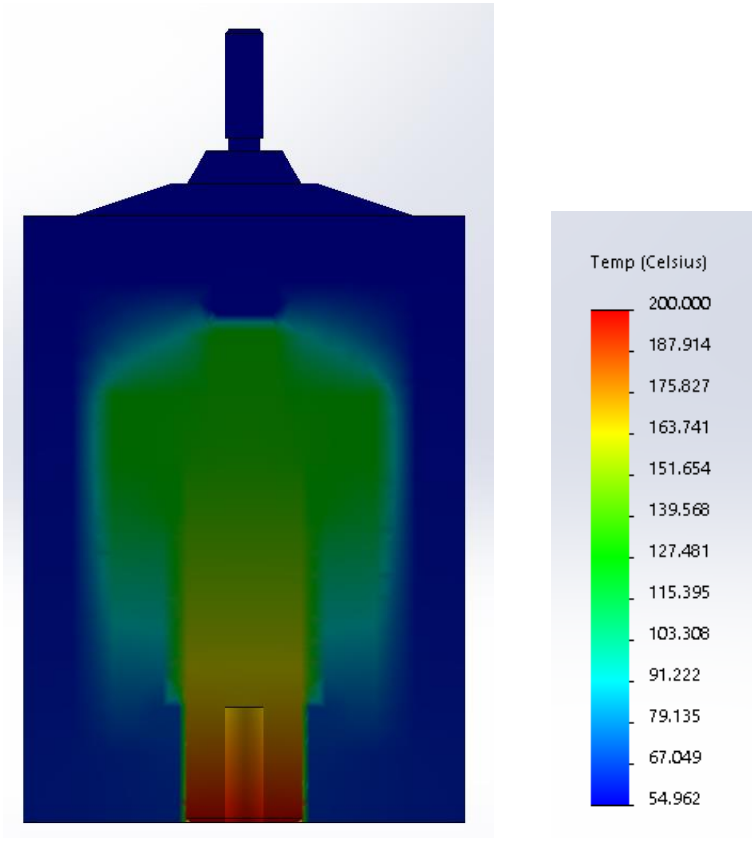

Figure 29 – Results of thermal simulation with a temperature load of 200°C.

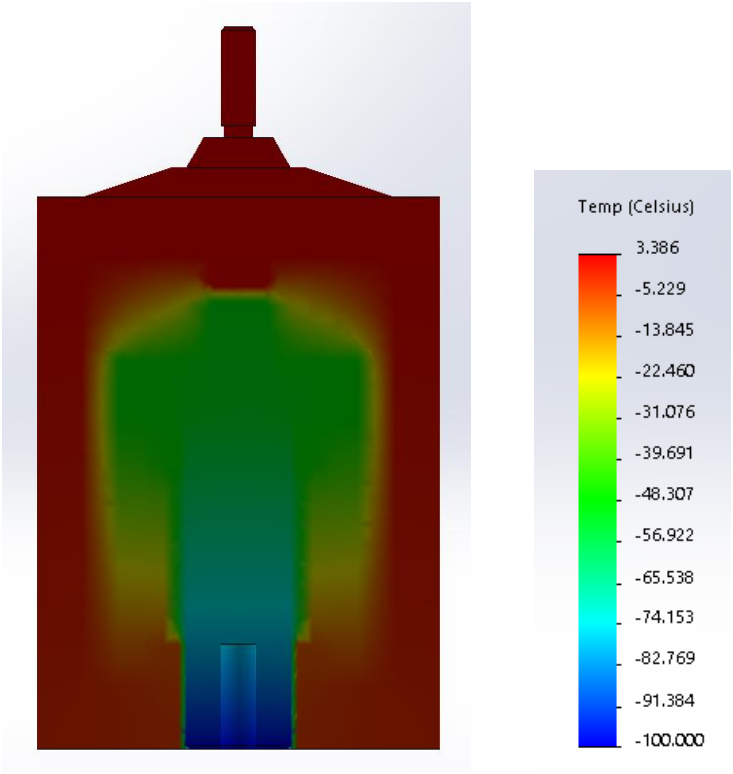

Figure 30 – Results of thermal simulation with a temperature load of -100°C.

Both the casing and the ceramic insulator's diameter were reduced, along with the volume of rock wool inside the equipment. The results were slightly worse, as the temperature that reached the top of the insulator was around 60 ℃, when the heating system is at its maximum temperature. When using the cooling system in its extreme temperature, 0 ℃ reached the top of the equipment. Minor changes in the thickness of the ceramic insulator were made, but without significant impact. The height of the insulator could not suffer major changes, in order to maintain the dimensions of the original upper rod extension. The reduction of the bottom lid – it would give the ceramic more room to grow – was not a good idea either, because it could promote the displacement when the equipment is under a load. Instead, the heat insulator was extended along the upper rod, maintaining the original height of the upper rod extension. This can be observed in Figure 31.

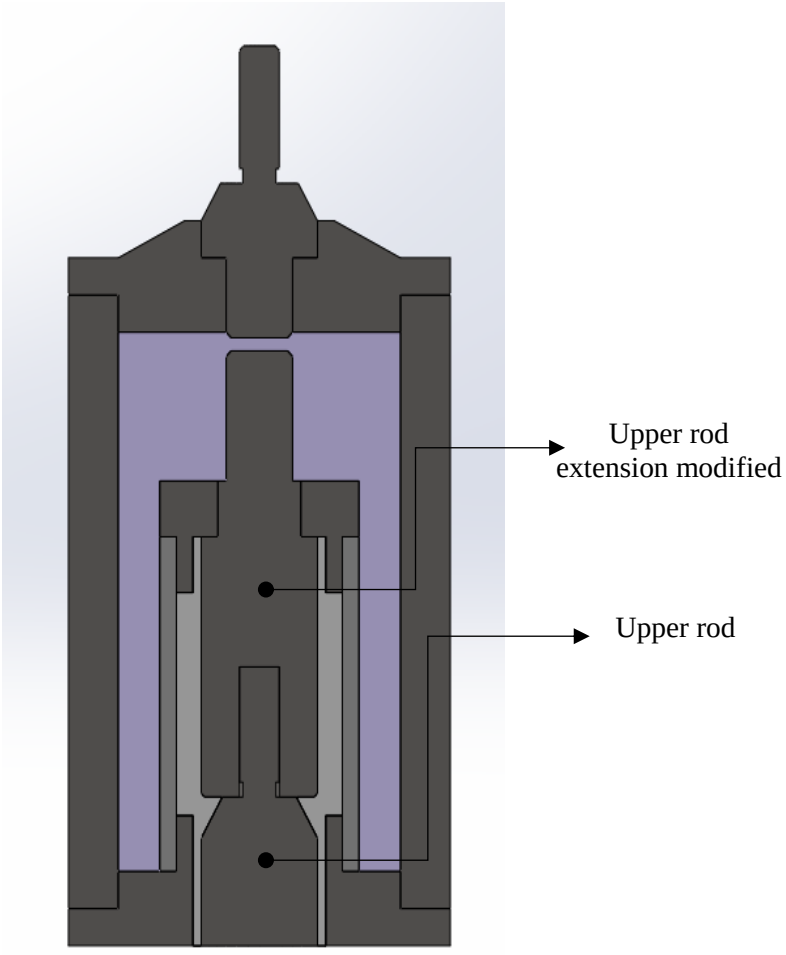

Figure 31 – Heat insulator final design.

The final design showed in Figure 31 was achieved after some iterations. Besides increasing as a whole the heat insulator, the base plate was modified, since in the prior design the gap on the top of the base plate that allowed the nut to be placed did not enable the screwing of the nut. This modification forced the top part of the modified upper rod extension to screw directly on the top lid.

Setting the thermal loads for this new approach requires a special caution of where to put the temperature load. During the first thermal simulations, the temperature load was placed at the bottom of the modified upper rod extension, so in this one, the same thing needed to be done. If the temperature load was defined at the end of the equipment, where is now part of the upper rod, the results could not be compared with the previous ones, due to heat transfer by conduction along the upper rod. The rest of the thermal loads were maintained, leading to the results presented in Figure 32 and Figure 33.

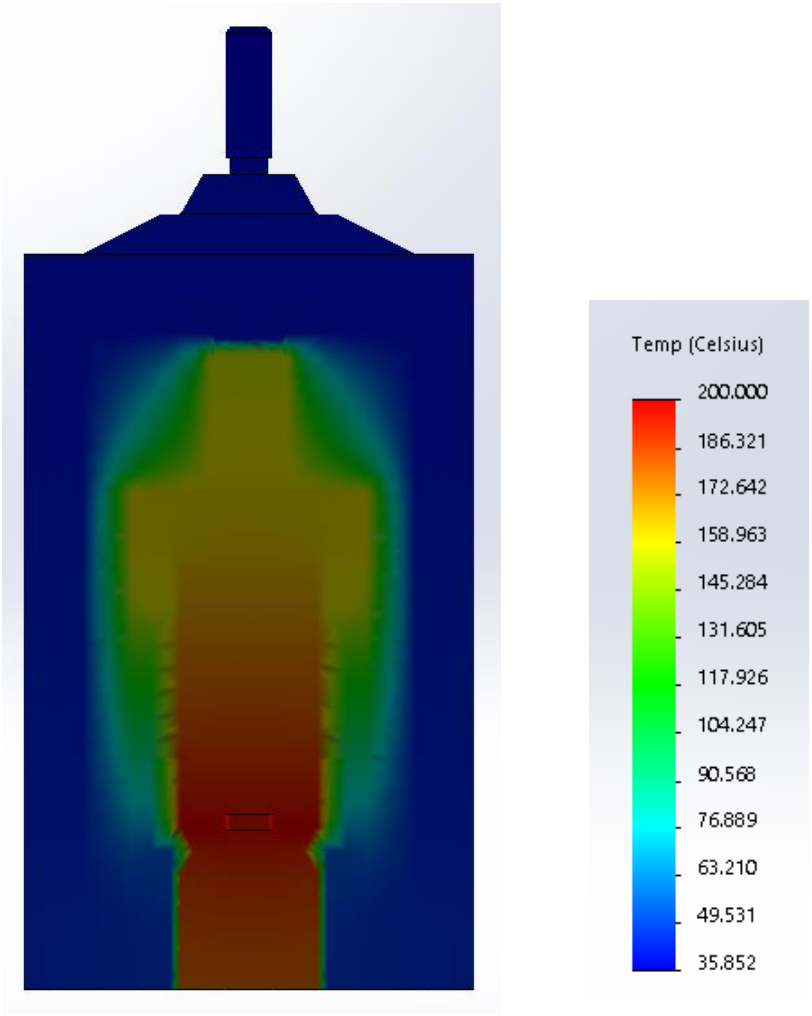

Figure 32 – Thermal simulation for the final design of the heat insulator, with a temperature load of 200°C.

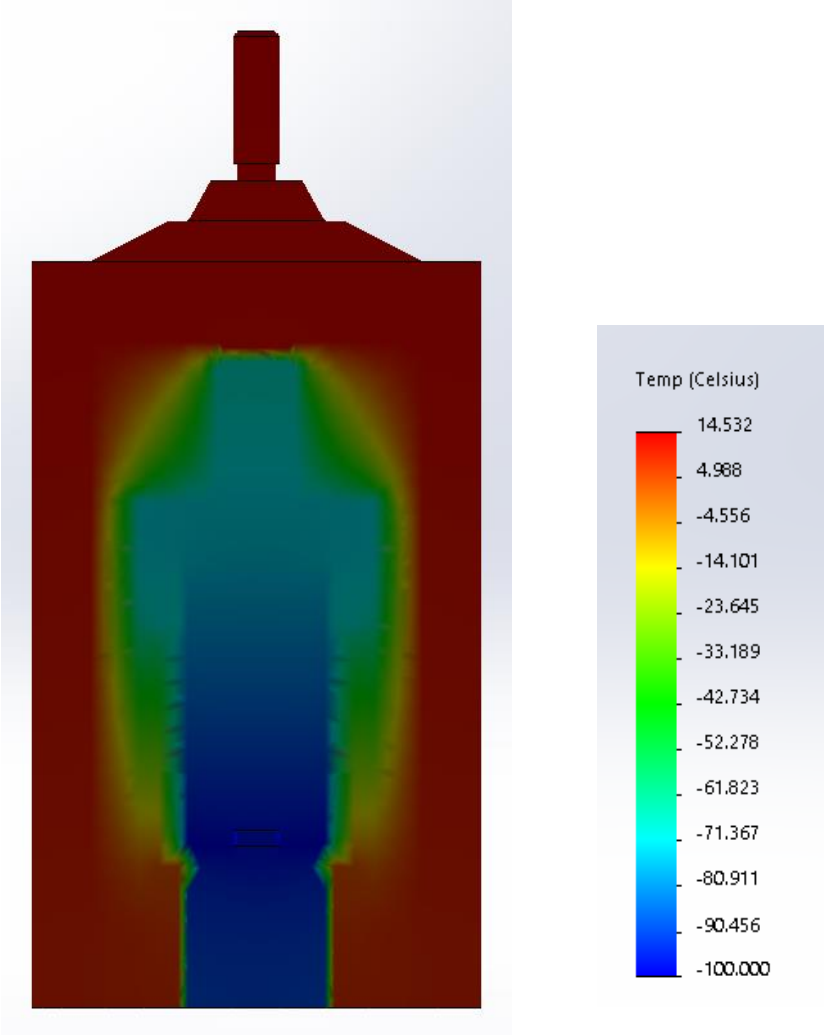

Figure 33 – Thermal simulation for the final design of the heat insulator, with a temperature load of -100°C.

The results obtained after these two thermal simulations were in the temperature nominal range of the load cells, validating the design of the heat insulator. It was important trying to reach these values not only because the load cells behave better within this range, but also due to some uncertainty associated with the numerical simulations. The software requires the definition of the convection coefficient, which calculation is complex and varies with the length and shape of the object. To counteract this, the values defined in Figure 20 were lower than the ones obtained in the QuickField.

Now that the design of the heat insulator is validated in terms of temperature it is necessary to evaluate how it behaves mechanically. For this, a static simulation was run. To set this simulation it is necessary to define a static point, in this case, the tip of the heat insulator, where the load cell will be attached. Then, a static load is defined in the upper rod, more specifically the maximum force of the creep testing machine (3000 N). Similarly to the thermal simulation, it is also required to establish a mesh that can be refined to obtain a more reliable solution. The achieved results are shown in Figure 34 and Figure 35.

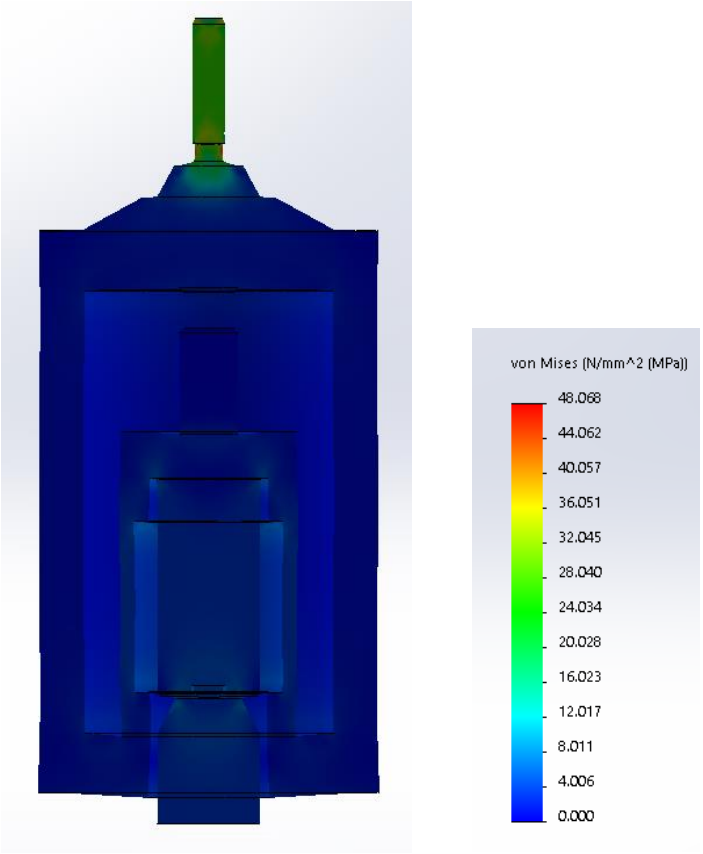

Figure 34 – Stress results of the static load simulation.

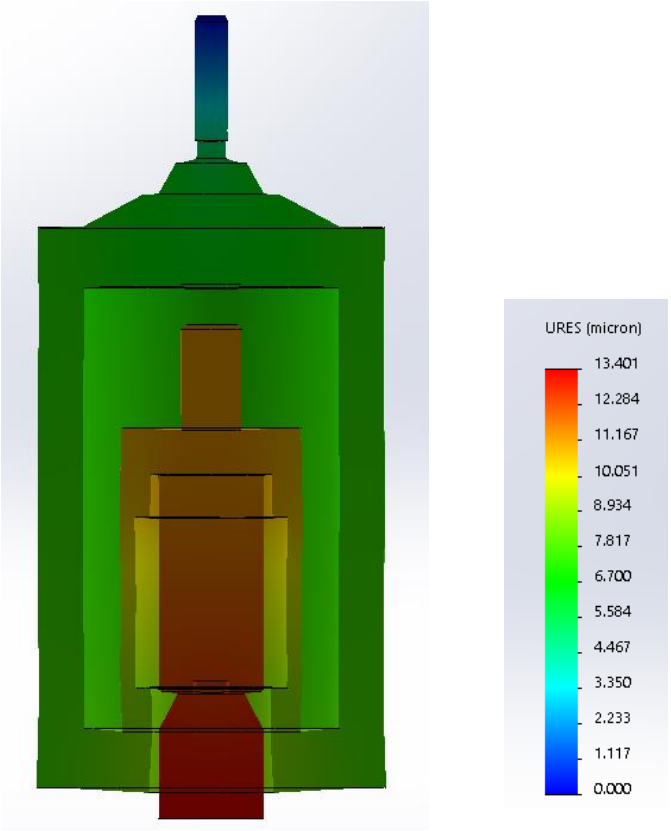

Figure 35 – Displacement results of the static load simulation.

It is possible to verify that the stress along the heat insulator is very low. The maximum values of stress occur on the top of the component and are not significant. In terms of displacement, the values are perfectly acceptable. In the exterior casing, the displacement is between 5 and 8 microns, the maximum displacement is around 13 microns in the upper rod, which does not influence significantly the measures of creep.

Now, having performed the thermal and mechanical validations of the heat insulator, its design is concluded.

3.4 Structural design of the chamber

As said in chapter 2, the thermal chambers have at least one insulation layer. The layer function is to preserve the heat inside the chamber and to protect the operator of the equipment. Although this is a thermal concern, the number of insulation layers will affect the structural design of the chamber. Having more layers will improve the thermal behavior of the chamber, but the total size of these layers is conditioned by the available space and each additional layer implies an increase of the total cost of the thermal chamber.

The most interesting solution for the insulation layers is to have a shell involving the internal volume, constituted by a low conductivity material and a second layer where air flows at RT. Thus, the heat is contained within the internal volume and at the same time, the outer skin of the chamber is being cooled.

The first idea to design the chamber was to conceive a structure easy to assembly. This way, the construction and maintenance of the equipment are simplified. Two main design concepts were sketched. One similar to the thermal chambers of Figure 12, with a small door and the rest of the equipment as one piece. In this type of configuration, a removable wedge port allows the chamber to be removed from the test area. Although this solution is interesting when used in single-station machines, applying it to a three-station machine implies having three removable wedge ports, which compromises the structure of the chamber. Alternatively, it is possible to have just one big removable wedge port, which is executable but brings many concerns in terms of rigidity of the chamber. In the other design, the chamber is split vertically, resulting in two halves. From here, two different possibilities are available on how to attach the back half of the chamber to the creep testing machine. It can be mounted in rail mounts, which allows it to roll back, exiting the test area. Alternatively, it can be attached to one of the columns of the load frame as the front half will be. This way both halves swing around the axis of a different column, opening space in the test area.

After some discussion, was adopted the design in which the two chambers are vertically split and attached to the columns of the load frame.

According to Pina's [3] initial drawings, there is some space limitation that should have to be taken into consideration during the design of the chamber. The distance between the outside stations and the inner wall has to be at least 75 mm. The internal height should have a value between 700 and 750 mm, to accommodate a 300 mm stroke, that should be taken into

consideration with the total height of the heat insulator. In terms of depth, there is not a rigid value that forces a limitation.

3.4.1 Chamber shells

Now that the main lines of the design are defined, the basic concept of the structural elements that constitute each half of the chamber needs to be determined. In order to create the two insulation layers, it is necessary to put a wall between the inner volume wall and the external casing. Achieving this with three independent shells that do not need to be physically attached allows the chamber to be easy to assemble and disassemble.

To produce the shells, 0.5 mm austenitic stainless steel sheets were used. The stainless steel is a reasonably cheap and easy to get material that can resist to temperature variations without corrosion. This material also has a relatively low thermal conductivity, which is advantageous for containing the heat in the inner volume of the chamber. Using 0.5 mm sheets makes the bending fabrication process easy and not expensive.

First, the exterior shell was designed, constituted by a metal sheet bent in a U shape and two metal sheets in L shapes – Figure 36 – that act as the top and bottom lids. The lids have three semicircle cuts giving space for the three rods of the creep testing machine. The extra bends in the exterior casing have two functions. The first is to allow the attachment between the bottom lid and exterior casing, and the second is to weld nuts where fasteners will screw to close the front frame of the chamber.

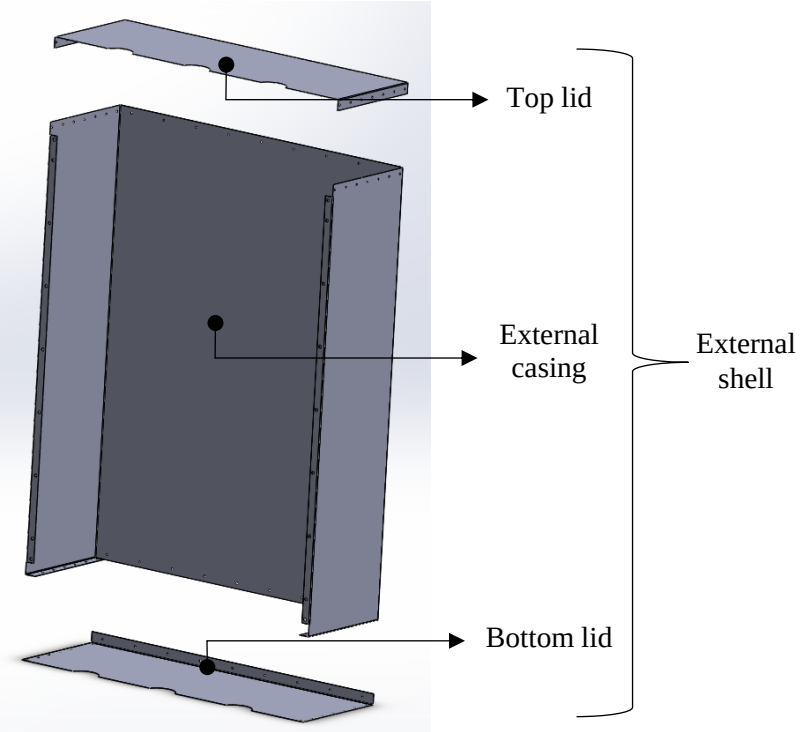

Figure 36 – Exterior casing and lids.

The next two shells need to have a similar design to fit inside of the exterior casing and its lids. The major concern is to do it creating the necessary gaps for the insulation layers. In Figure 37 (a) it is possible to visualize the middle casing. On the top and bottom of this U shape sheet, an extra bend was made, allowing the middle casing to lean against the exterior casing creating the wanted air gap – Figure 37 (b). Therefore, the first insulation layers of the lateral walls of each half are defined, but it is still needed to create the gap between the lids and the shell in the middle. In order to achieve this, two extra sheets were attached to the middle casing by 3 mm pop rivets, as shown in Figure 38 (a). To ensure that air flows through the entire insulation layer, it is necessary to make small slots in the middle casing, creating air channels, as depicted in Figure 38 (b).

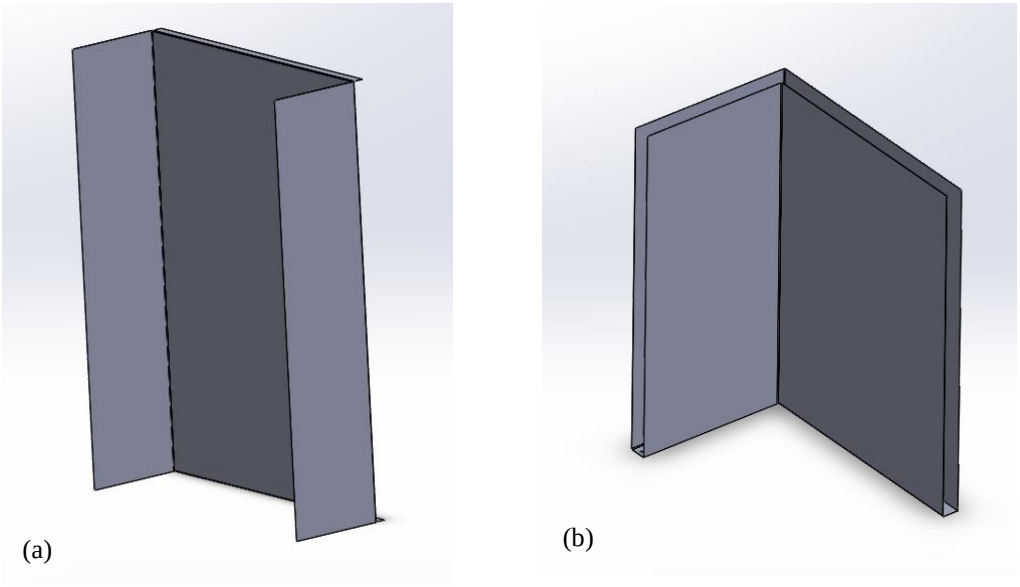

Figure 37 – (a) Middle casing; (b) Section view of the exterior and middle casing forming the insulation layer.

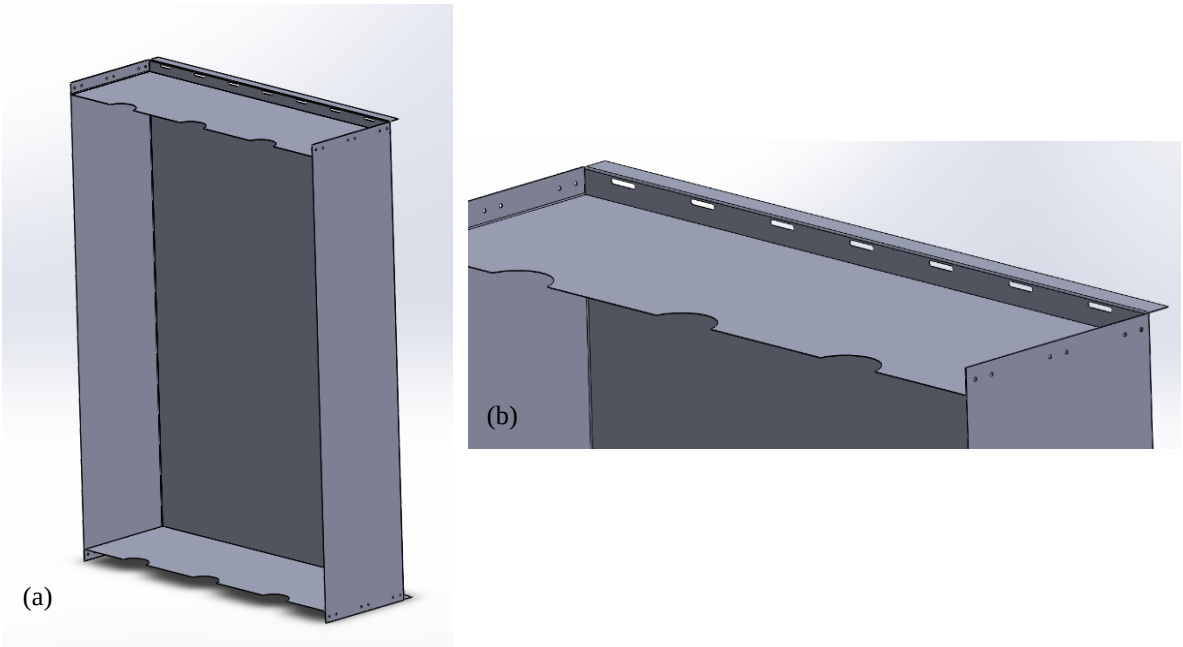

Figure 38 – (a) Middle shell; (b) Detail of the middle shell, where the slots for the air channels were made.

The internal shell that defines the inner volume of the chamber has a very similar design to the previous one. A stainless steel sheet is bent in U shape and two bent sheets are joined by 3 mm pop rivets – Figure 39. The extra bends on the top and the bottom create the second insulation layer. The bends on the side seal the front frame of each half of the chamber with the help of fasteners that screw on the nuts welded in the exterior casing. Additional slots were made to ensure the air flow when the two halves are closed together.

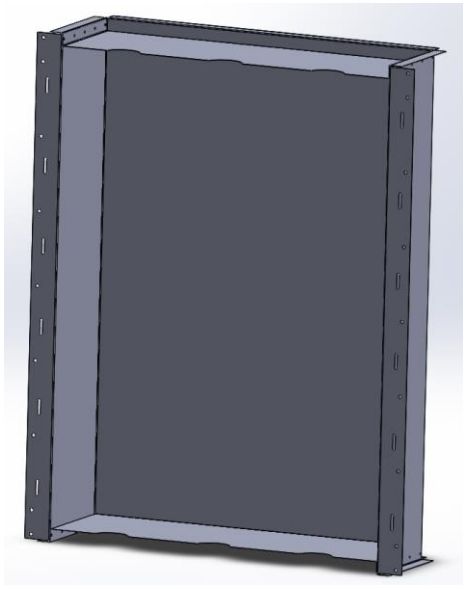

Figure 39 – Internal shell.

At this moment, the basic design of the three shells is defined. Figure 40 shows how the shells are assembled and in Figure 41 it is possible to understand how the three shells are assembled inside each one.

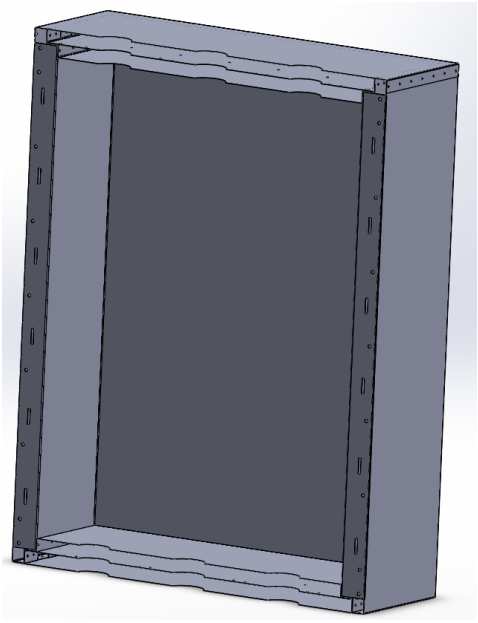

Figure 40 – The three structures assembled.

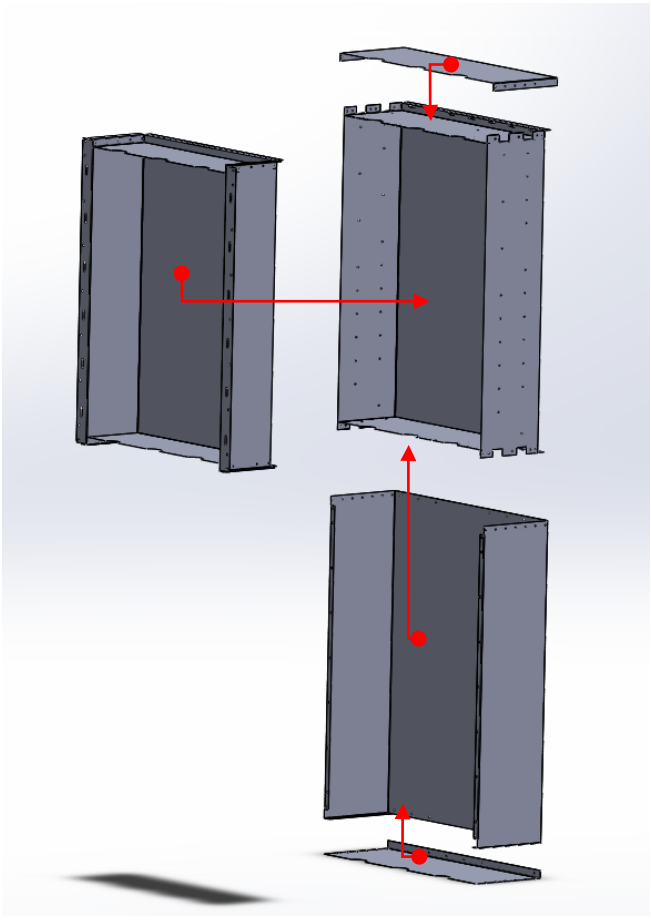

Figure 41 – Exploded view of the assembly of the three shells.

To give rigidity to the chamber, structure profiles need to be joined to the middle shell. The U shaped profiles are attached around the middle shell by 3 mm pop rivets. The lateral structure profiles are joined to the ones on the top and the bottom with the help of a steel angle and a fastener – Figure 42. To allow the described assembly, some extra cuts were made in the original stainless steel sheet – Figure 43. The components that give rigidity to the chamber are made from carbon steel, so they need to be coated for protection against corrosion.

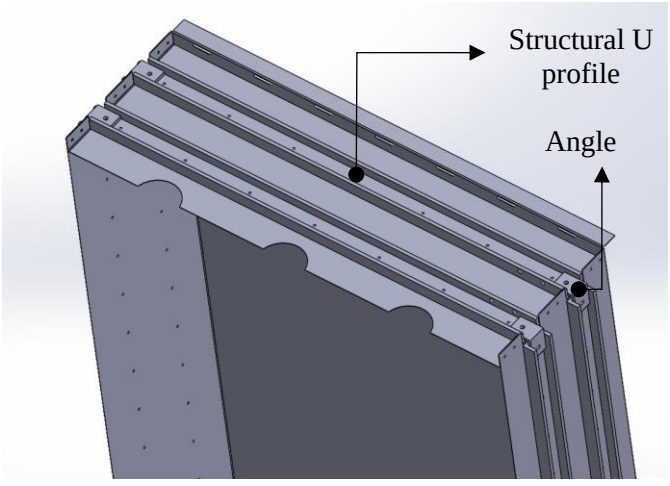

Figure 42 – Middles shell with the U structure profiles.

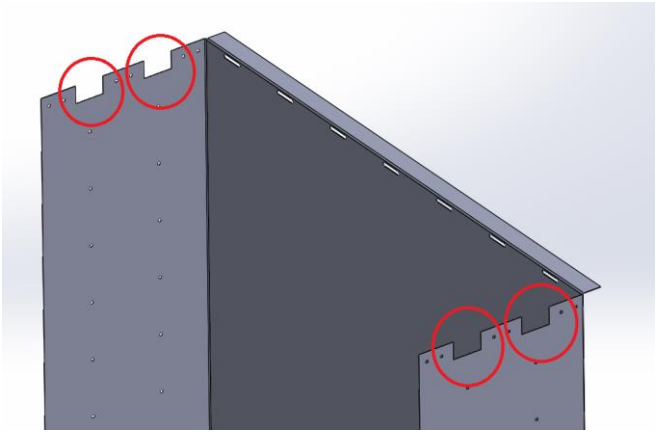

Figure 43 – Extra cuts made in the middle casing.

Some parts of the shells ensure guidance when assembled. Nevertheless, cylindrical Teflon spacers were glued to the different structures with RTV silicon, guaranteeing a perfect alignment/centering between the three shells and forming the two insulation chambers. In Figure 44 it is depicted a detail of the middle shell where a few spacers were glued. In this example, the spacers lead against the exterior casing, ensuring the alignment/centering. The RTV silicone was used due to its high resistance to extreme temperatures. Table 7 shows some proprieties of the RTV silicon.

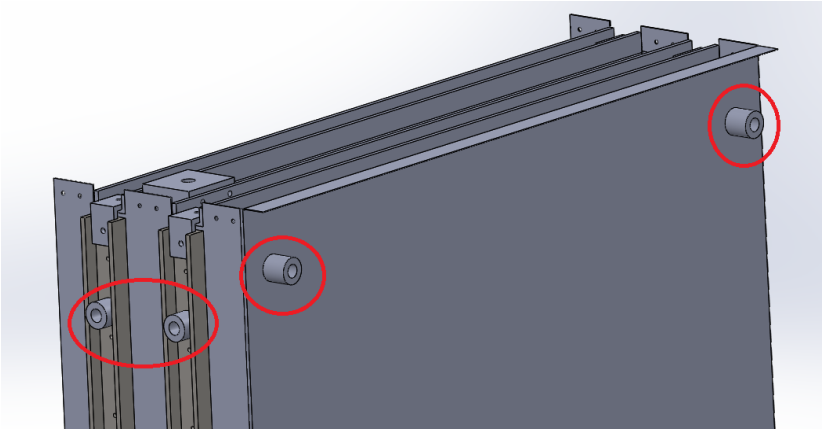

Figure 44 – Detail of the middle casing with the spacers glued.

Table 7 – Proprieties of the RTV silicon.

Characteristic	Value
Temperature range	-110 to 180 [°C]
Tensile strength range	2 to 10 [MPa]

Figure 40 showed that the front frame was open. Therefore, a component constituted by four rectangles and three semi-circles of 5 mm stainless steel sheets welded together, close the top and bottom front frame. These components are attached to the middle shell by several steel angles and countersunk head fasteners. To finalize the front frame, two more side stainless steel sheets were attached to the assembly with countersunk head fasteners that screw to the nuts welded in the exterior casing. It is also planned to glue all around the front frame of the chamber stripes of cork to improve the thermal insulation.

Figure 45 shows an image of the assembly of the chambers shells and the components of the front frame.

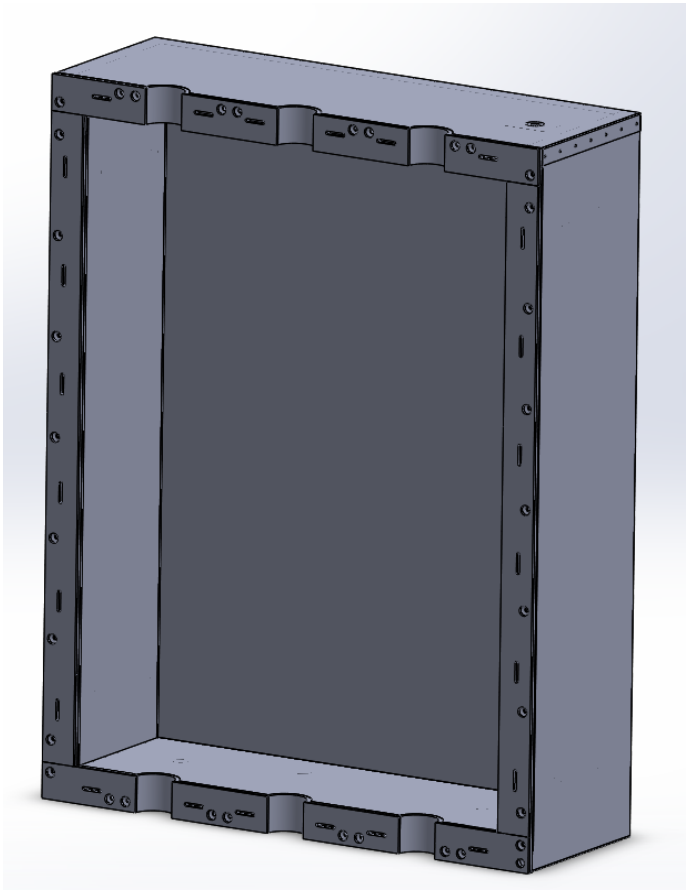

Figure 45 – Assembly of the chamber shell and the front frame components.

3.4.2 Insulations layers

In the previous section, a description was provided on how the insulation layers were designed. Now, it is necessary to define their dimensions. To do this, it is necessary to know the power of the heating elements first. After analyzing the chambers available in the market, it was concluded that for volumes similar to the chamber in development, 5,000 W is enough to reach 200 ℃.

During the design of the chamber, a length of 20 mm was established for each insulation layer. This value was defined due to its convenience for the design, and also having in mind the

thermal insulation. To verify if the value of the length of the insulation layers is acceptable, a simple analysis was made resorting to the concept of thermal resistance. In the same way that an electric resistance may be associated with the conduction of current, a thermal resistance can be associated with heat transfer by conduction and convection. The equation for the thermal resistance in conduction is

$$r_{cond} \equiv \frac{\Delta T}{q_x''} = \frac{L}{k} \tag{3.6}$$

where r_{cond} is the thermal resistance for conduction, expressed in $m^2 \cdot K/W$, ΔT is the difference of temperature between two points, expressed in K and q_x'' is the conduction heat flux, expressed in W/m^2. The thermal conductivity is represented by k, expressed in W/m·K. and L is the length of the material, expressed in meters. The equation for the thermal resistance for convection is

$$r_{conv} \equiv \frac{(T_\infty - T_s)}{q''} = \frac{1}{h} \tag{3.7}$$

where r_{conv} is the thermal resistance for convection, expressed in $m^2 \cdot K/W$, $(T_\infty - T_s)$ is the difference of temperature between the fluid and surface, expressed in K and q'' represents the convection heat flux, expressed in W/m^2. The convection coefficient is represented by h and is expressed in $W/m^2 \cdot K$.

To calculate the heat flux transfer through the walls of the chamber it is possible to associate all the thermal resistance, thus obtaining the total heat flux transfer to the outside of the chamber, as the next equation demonstrates

$$q'' = \frac{\Delta T}{\Sigma\, r} \tag{3.8}$$

where $\Sigma\, r$ is the sum of all the thermal resistances. Dividing the heat flux by the total area of the chamber the heat transfer rate is obtained, which is the transfer of heat from the chamber to its surroundings.

The shells that make the insulation layers are of stainless steel, the material that provides insulation in one of the layers is rock wool and the other layer is where air flows. The conductivity of the material and the convection coefficient of the air are represented in Table 8.

Table 8 – Values of conductivity and convection coefficient.

	Characteristic	**Value**
Stainless steel	Conductivity	16 [W/m·K]
Rock wool		0.04 [W/m·K]
Air	Natural convection coefficient	5 [$W/m^2 \cdot K$]
	Forced convection coefficient	100 [$W/m^2 \cdot K$]

The equation used to calculate the heat transfer rate is

$$q = \frac{\Delta T}{\frac{1}{A} \cdot \left(\frac{1}{h_e} + 3\frac{L_s}{k_s} + \frac{L_r}{k_r} + 2\frac{1}{h_i}\right)} \tag{3.9}$$

where q represents the heat transfer rate, expressed in W and ΔT is the difference of temperature between the chamber at its maximum value (200 ℃) and RT (≈25 ℃). The total area of the chamber is represented by A, expressed in m^2. The exterior convection coefficient is represented by h_e and the internal by h_i, both expressed in $W/m^2 \cdot K$. The conductivity of the stainless sheets and the rock wool are represented by k_s and k_r respectively and are expressed in W/m·K. The length of the sheets and the rock wool are expressed in meters and are represented by L_s and L_r [24].

Oversized dimensions for the chamber were considered in the calculations in order to ensure an acceptable value of heat transfer to its surroundings. Thus, the dimensions assumed for the chamber were 810 mm of height, 610 mm of width and 420 mm of depth, resulting in a total area of 2.181 m^2. The calculated heat transfer rate is about 530W, being this value is a little bit more than 10% of the power of the heating elements. Meaning that 10% of the heat used to reach the maximum values of temperature in the chamber is transferred to the atmosphere. A 10% loss is acceptable, which validates the size of the insulation cases.

3.4.3 Front window

A window was designed on the front side of the chamber, allowing the visualization of the specimens that are being tested. Initially, a cut was made in the three independent shells providing the space to the implementation of the window, as depicted in Figure 46.

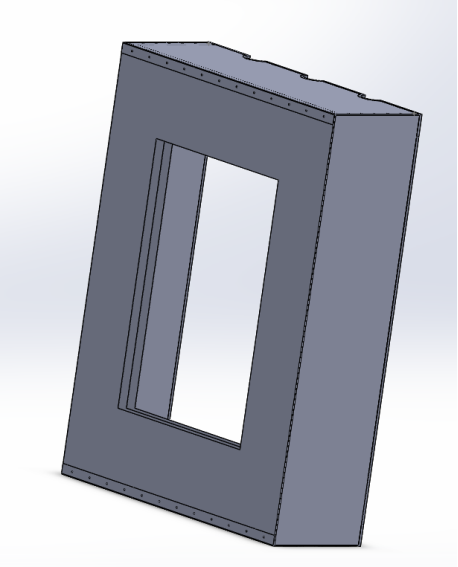

Figure 46 – Window hole for the front half of the chamber.

In order to create a rigid frame to mount the glass panels and the window spacers, stainless steel angles were placed around the opening of the window. These angles also make the front frame of the window. Then smaller stainless steel angles were glued to the first angle, creating a surface where the rest of the components can lean on. Between the out glass panel and the angle, there is a rubber band to seal the window. After the first glass panel, there is a window spacer followed by another glass panel. There is one more window spacer and one glass panel, before another stainless steel angle holds together all the components. The last angle screws to the angle used to create a rigid frame and to a 5 mm stainless sheet that is placed around the window interior frame.

Figure 47 (a) shows a section view of the front half of the chamber and Figure 47 (b) shows an exploded view of the components of the window. Observing Figure 47 is possible to understand how all the components are assembled.

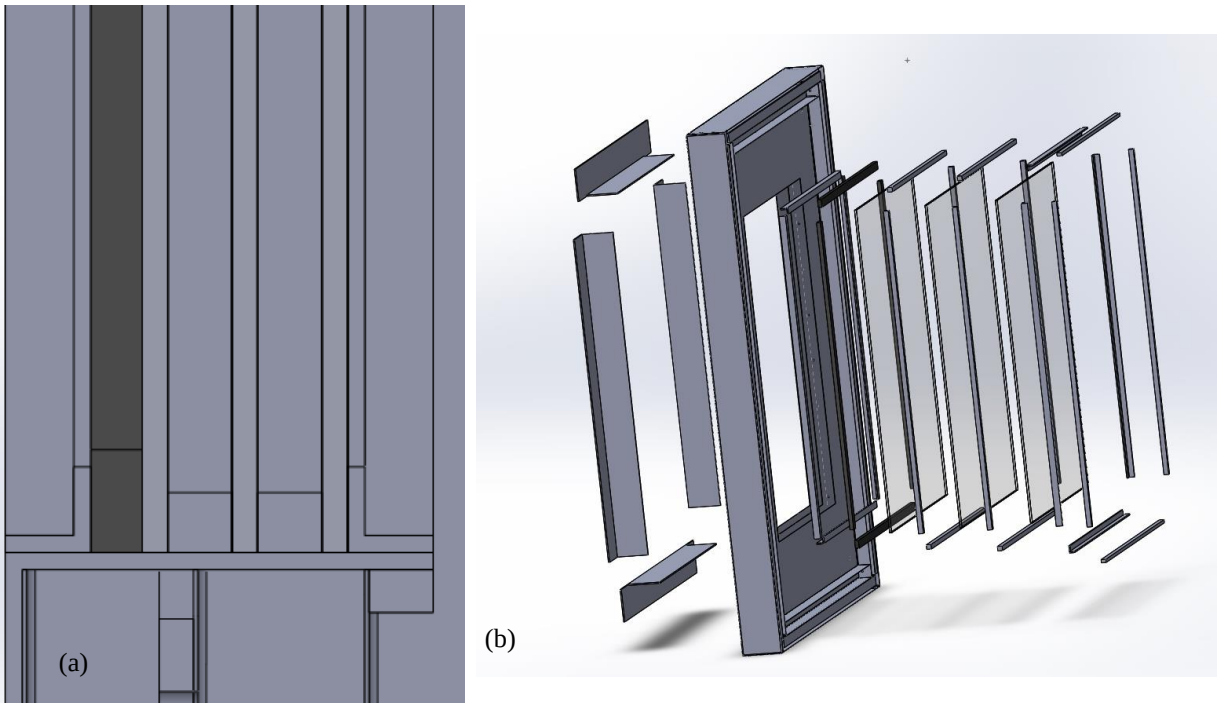

Figure 47 – (a) Section view of the window; (b) Exploded view of the window.

Adding a window also adds a new area where the heat transfer for the exterior is different from the one calculated in section 3.4.2. Thus, it is necessary to calculate the heat flux that occurs through the window and compares it with the heat flux that occurred when there was no window. To calculate the heat flux that goes through the window, equation (3.8) was considered. The parameters used to obtain the thermal resistances are expressed in Table 9. The thickness of the glass is 3 mm and between each glass panel, there is an air case of 7.5 mm.

Table 9 – Parameter used to calculate the thermal resistances.

	Characteristic	Value
Glass	Conductivity	1.6 [W/m·K]
Air	Conductivity	0.023 [W/m·K]
	Natural convection coefficient	5 [W/m^2·K]
	Forced convection coefficient	100 [W/m^2·K]

The calculated heat flux obtained was 146.6 W/m^2. In section 3.4.2 was said that the heat power rate was 530 W and the total area of the chamber was 2.181 m^2. Therefore, dividing the heat power rate by the area the value of 243 W/m^2 of heat flux that goes through the chamber is obtained. Comparing the two values of the heat flux it was concluded that the window does not add any heat losses to the exterior, validating its design and materials.

3.4.4 Connections between the thermal chamber and the creep testing machine

The components that attach the chamber to the creep testing machine need to be designed. Figure 48 shows how each half of the chamber is attached to the columns of the load frame.

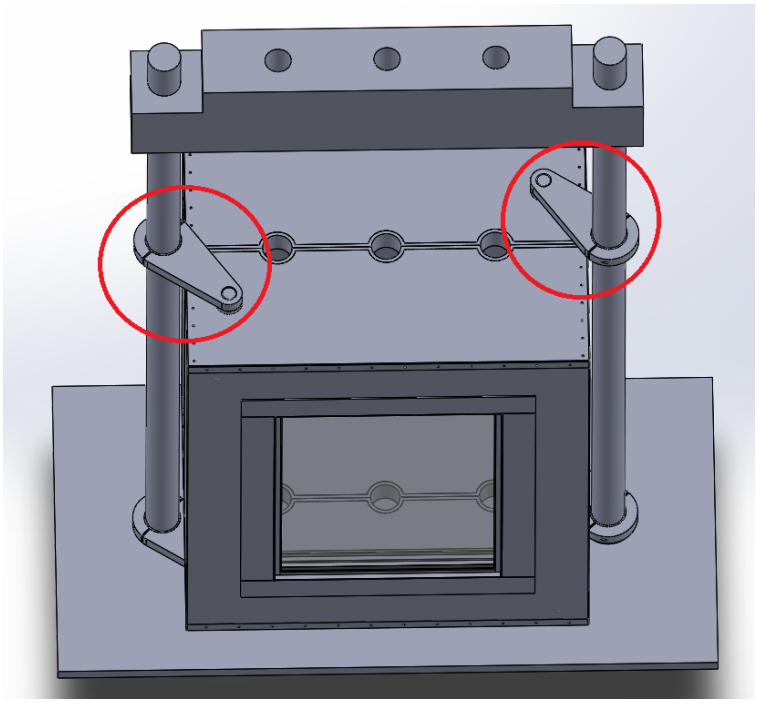

Figure 48 – Components responsible for the attachment between the chamber and the creep testing machine.

To create this mechanical connection, a base plate (made of a machined block of aluminum) was screwed to the structural profiles on the top and the bottom of each half of the chamber, as is depicted in Figure 49 (a). Then, a custom made shaft – Figure 49 (b) – is screwed to the base plate, ensuring that the chamber and the cranks pivot together. The other end of the crank involves around the column of the load frame, also ensuring that they pivot.

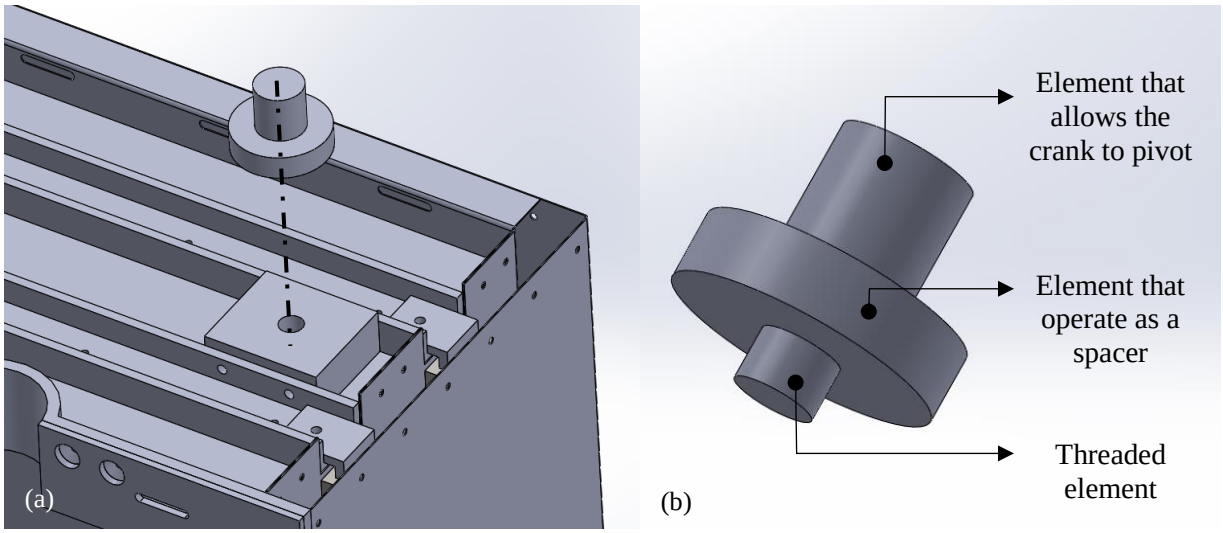

Figure 49 – (a) Base plate screwed to the structural profile; (b) Scheme of the custom made shaft.

Figure 50 shows an exploded view of the different elements that compose the crank. The elements 1 and 2 of Figure 50 are bushings, elements 3 are spacers to ensure that when the element 4 and 5 (the crank itself) are screwed together around the column this component can pivot. The bushing 2 needs to have a slot to be placed around the column.

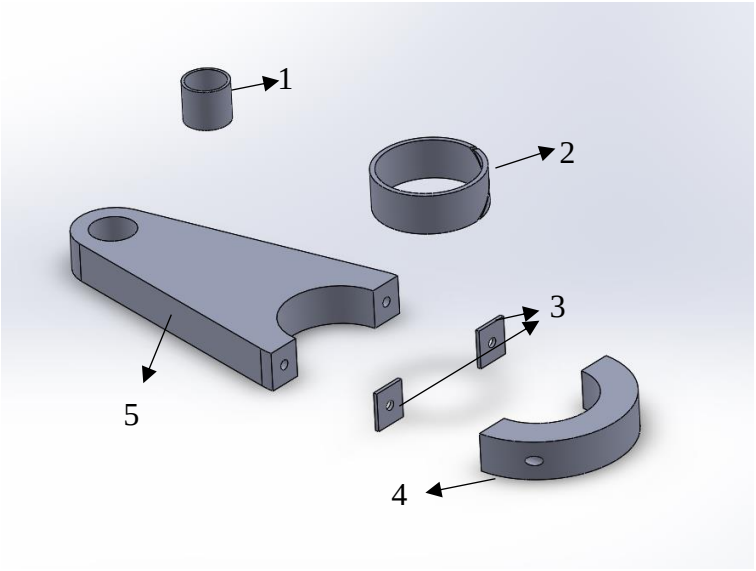

Figure 50 – Component of the crank.

On the bottom of the load frame, there is a table where two spacers (one for each half of the chamber) hold both halves of the chamber, as depicted in Figure 51 (a). Figure 51 (b) shows an exploded view of one of the spacers. The spacers have two halves that are screwed to each other and a washer that creates a smooth surface for the chamber pivot. This washer also needs to have a slot to be placed around the column.

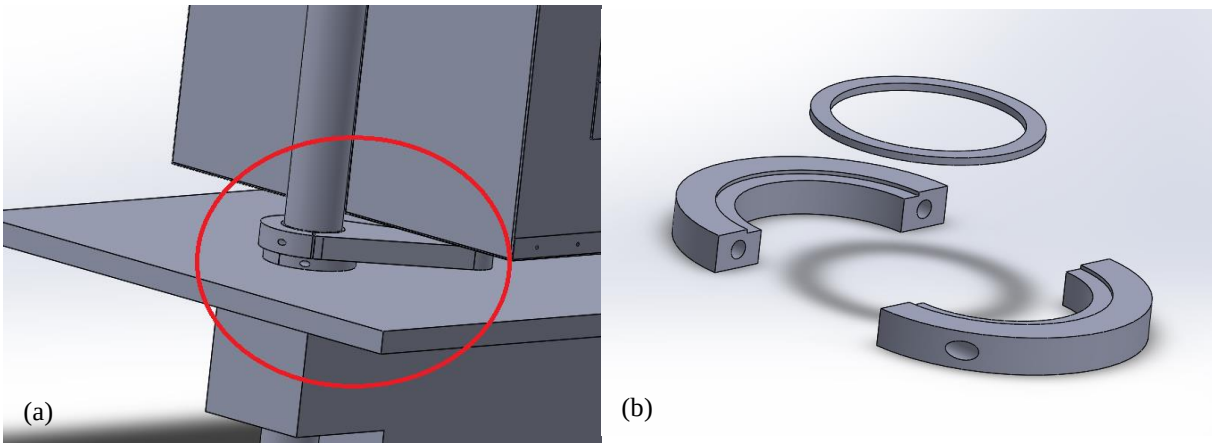

Figure 51 – (a) Detail of the spacer; (b) exploded view of the spacer.

3.4.5 Back half

In the back half of the chamber a panel, where some components were installed, namely the motors of the fans for the heating elements, the valves of the cooling system, the protective equipment, the temperature controller and the switches was created. At the same time, three holes in all shells of the back half of the chamber were made. Two are needed to allow the shaft of the fans of the heating elements to go through the shells, while the other, in the center, is to exhausts the coolant. In the exterior casing, two holes from where two fans blow air to one of the insulation layers were also made. An electrical enclosure was also predicted to accommodate the temperature controller and the switches.

Figure 52 depicts the back panel and some of the holes made in the back half of the chamber.

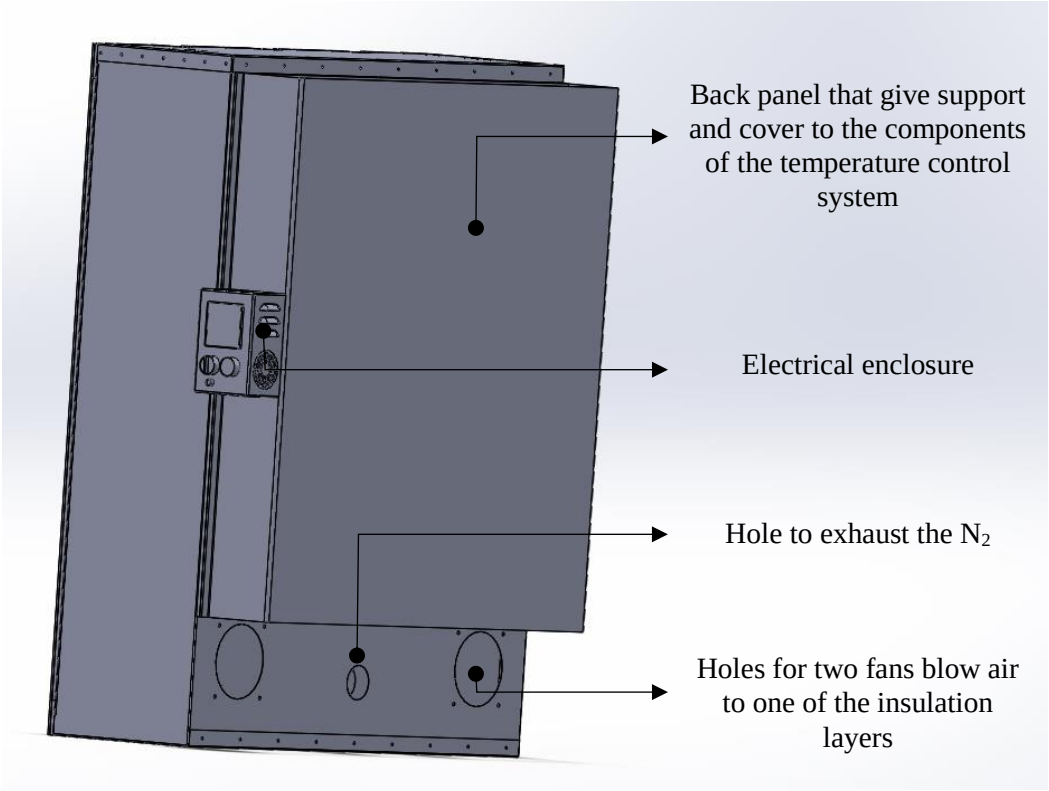

Figure 52 – Back panel.

In Figure 53 It is shown the electrical enclosure where the temperature controller and the switches were placed. Putting these components in an enclosure makes it easy to operate by the user.

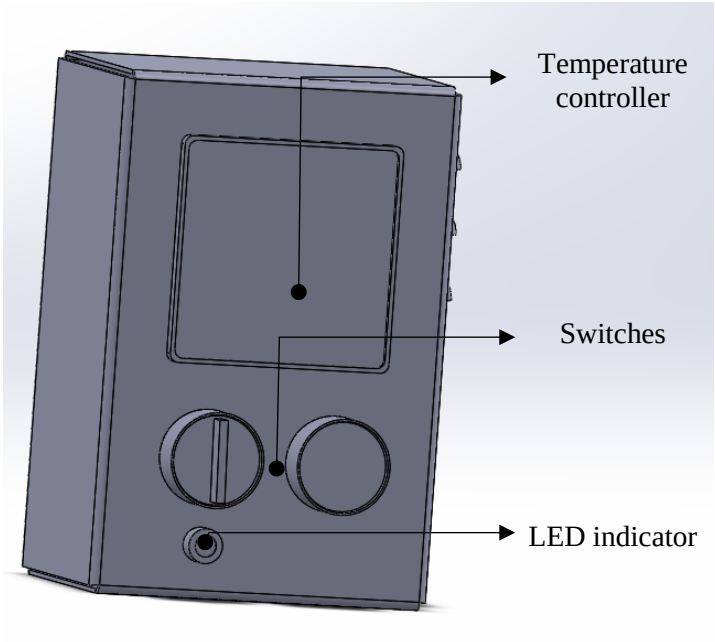

Figure 53 – Electrical enclosure.

3.5 Discussion

Chapter 3 presented the design of the thermal chamber and the heat insulators. The main goal of the heat insulators is to reduce the temperature that reaches the load cells. To achieve this, two distinct designs were explored and several iterations were made before achieving the final solution, which was validated by a thermal simulation run in SolidWorks. The results obtained showed that the temperature that reaches the load cells is in their nominal range.

Subsequently, the different solutions for the design of the thermal chamber were presented, as well as their advantages and limitations. The design that splits vertically the chamber into two halves was adopted. Then, a description of the different stages that lead to the final designed was presented. When convenient, a mathematical explanation supporting some configurations of the chamber was presented. Also, the mechanical connections that allow the chamber to pivot were made and explained.

Finally, a panel was designed to be attached to the back half of the chamber to assemble various components and an electrical enclosure for the temperature controller and for the switches was created.

4 Control and command

In this chapter, the necessary elements to control the temperature in the thermal chamber are presented. Then, the electric components are selected and the control circuit is designed.

4.1 Temperature control

For controlling the temperature in the thermal chamber the following elements are used:

- Temperature controller;
- Cooling and heating elements;
- Interface temperature controller/cooling and heating elements;
- Temperature sensor;

Figure 54 depicts the way the components are connected. The temperature controller receives a temperature setpoint from the user and information about the real temperature in the chamber, measured by the temperature sensor. Based on these data and some suitable control law, it generates a control action that is then applied to the heating and cooling elements through some appropriate interface. These elements actuate over the chamber by cooling or heating the volume of air inside it [27].

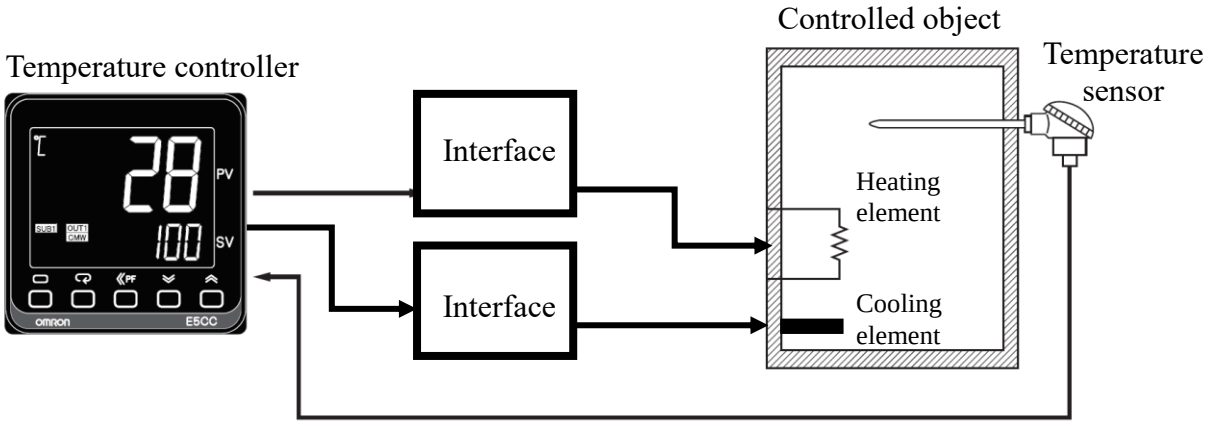

Figure 54 – Scheme of the typical components of a temperature control system [27].

The temperature sensor must be compatible with the temperature controller. Generally speaking, the sensors can be divided into two categories: contact and non-contact. Examples of contact sensors are the thermocouples, resistance thermometers (normally made of platinum) and thermistors. Non-contact sensors are the irradiation thermometers.

The main purpose of the interface is to connect the controller and the cooling and heating elements. Therefore, depending on the type of heating and cooling devices, the interface can be a magnetic switch, a valve, a relay, namely an SSR, a power controller or a cycle controller.

In the temperature controller, the user defines the setpoint, meaning the temperature value intended for the chamber. The performance of the temperature control depends on the control law used (e.g., ON/OFF, proportional, integral or derivative types) and the characteristics of the controlled object (i.e., the chamber). Typical behaviors are shown in Figure 55 that depict the evolution of the temperature versus time. Figure 55 (1) illustrates an over/undershooting transient, where the temperature response oscillates before it settles at the setpoint value. One way to eliminate this problem is to reduce the ramp slope, but this may result in a slow response, as shown in Figure 55 (3). Figure 55 (2) represents a good response, where the temperature evolves, reaching the set point as quickly as possible without overshooting [27] [28] [29].

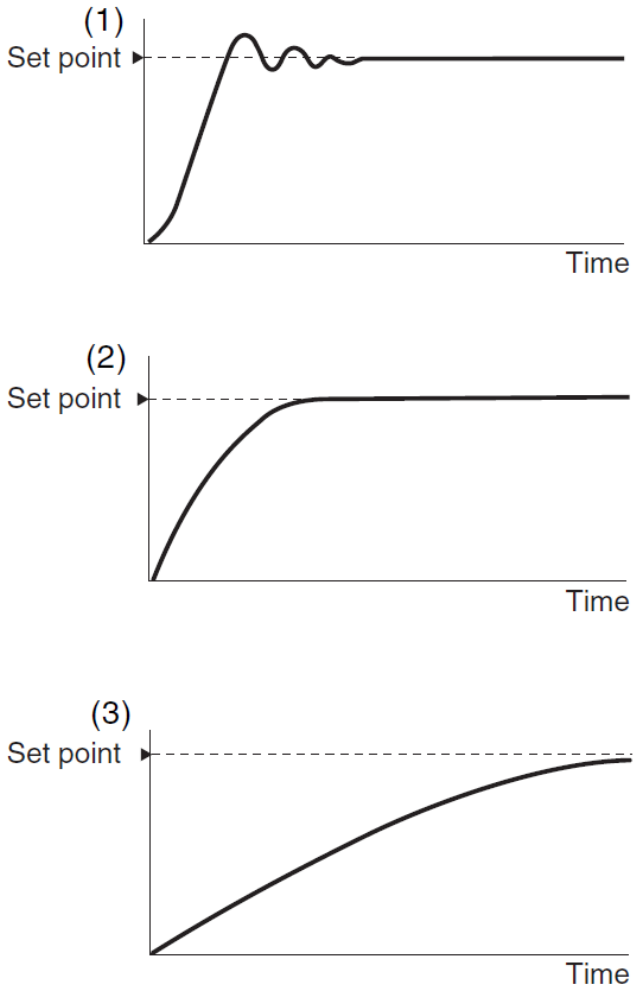

Figure 55 – Different temperature responses of the controlled system [27].

Figure 56 shows two other examples of poor control. On the left, the response has an offset, or steady-state error which means that the controlled variable never reaches the set point. Normally, this occurs when a proportional controller is used. To mitigate this problem, an integral control action is normally introduced. On the right, the response takes too long to reach the setpoint when an external disturbance occurs. Usually, this is due to the effect of the proportional and integral control actions. To improve the response, a derivative component is also included [27] [30].

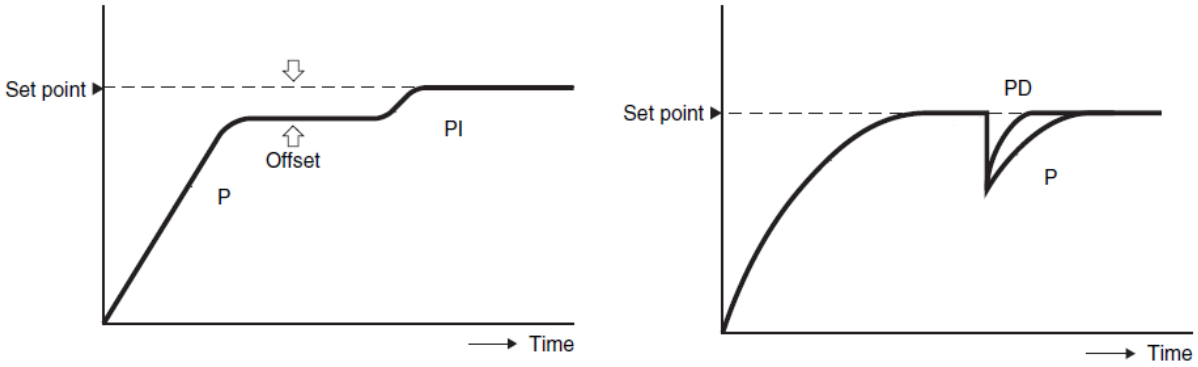

Figure 56 – Responses of the controlled system with different control actions [27].

4.1.1 Heating control

Industrial temperature controllers implement some kind of feedback control. Figure 57 shows a generic configuration, where the main parts of the feedback control are built into the temperature controller itself. Temperature controller's from most manufacturers implement ON/OFF and PID control. Figure 58 illustrates the configuration of such control type [27] [28].

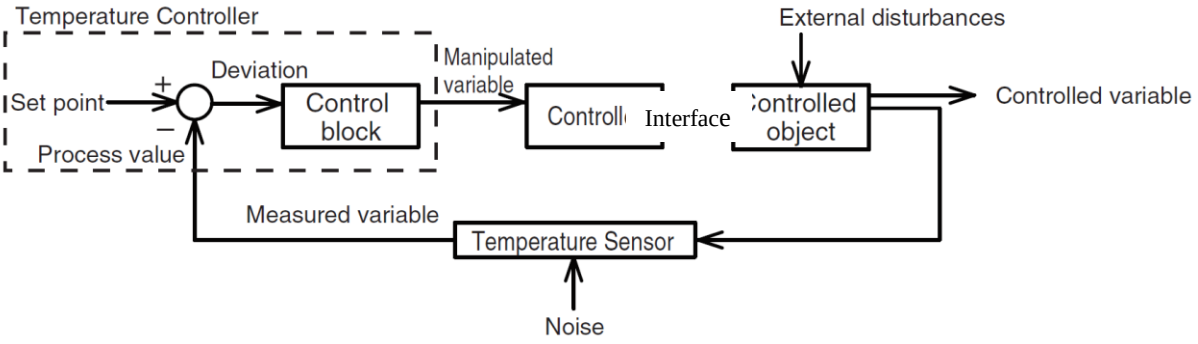

Figure 57 – Configuration of a feedback control system [27].

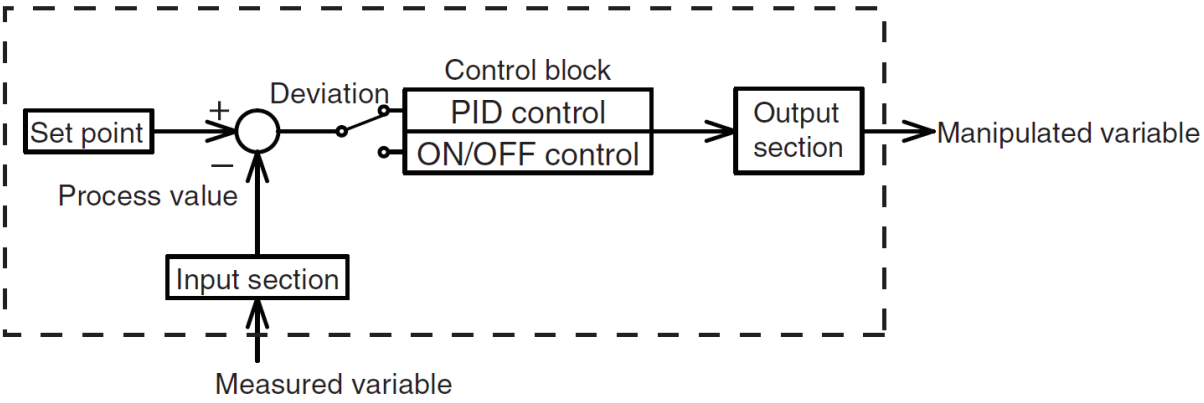

Figure 58 – Temperature controller configuration [27].

As defined in chapter 3, heating elements are used to heat the thermal chamber. Those will be controlled using PID control. The heating of the chamber is based on forced convection to ensure a low temperature gradient. Therefore, two fans operate along with the heating elements. Thus, the temperature controller needs to have an auxiliary relay output to operate the fans. Moreover, there are two fans that ensure the air circulation in one of the chamber insulation layers, which the temperature controller also needs to actuate.

As mentioned in section 4.1, there is a variety of temperature sensors. The selection of the temperature sensor is based on its price, range of temperatures and other specific characteristics. The platinum resistance thermometers have very high precision, but are expensive. In addition, they are easily influenced by lead wires, have a slow thermal response, and are affected by shock and vibrations. Although, the thermistors have fast thermal responses and small errors, their temperature range is limited. Therefore, thermocouples are chosen for

measuring the chamber temperature, since they have a broad measurement range, have high resistance to shock and vibrations, and have a fast thermal response [27].

4.1.2 Cooling control

Although the cooling and heating elements are different, the cooling control relies on the same principle of the heating control: a feedback control system – Figure 57. The cooling of the chamber uses a cryogenic coolant and a cryogenic solenoid to control the injection of the coolant in the chamber. The valve has two positions: totally open and totally closed. Hence an ON/OFF control action is necessary to command the valve.

Figure 59 shows the typical response to an ON/OFF control action. Interpreting the Figure 59 as the cooling control, when the control action is set to ON, the cryogenic solenoid valve is totally open, letting the coolant enter the chamber. As soon as the temperature sensor detects a temperature value lower than the setpoint, the controller sets the control action to OFF, closing the cryogenic solenoid valve. At this point, no more coolant enters in the chamber. The remaining coolant in the chamber is slowly exhausted and the temperature inside the chamber starts to rise until and then exceeds the set point. When the temperature sensor detects that the effective temperature is higher than the setpoint, it sends again a signal to the controller, which sets once more the control action to ON. These cycles perpetuate for as long as needed.

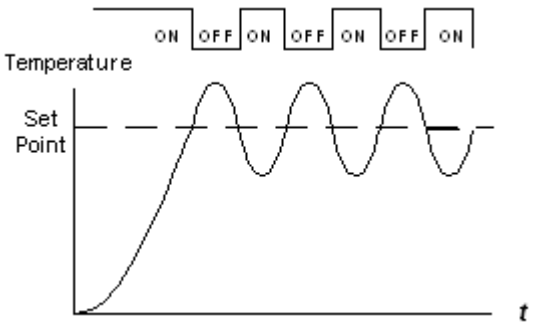

Figure 59 – Response to an ON/OFF control [31].

The fans used in the heating control to homogenize the temperature inside the chamber are also used in the cooling. To ensure reduced temperature gradients, the entry points of the coolant in the inner volume of the chamber are distributed.

The temperature sensor used for the heating control is the same as for the cooling control, since thermocouples have a wide range of temperatures they can operate.

Figure 60 shows a scheme of the main components of the cooling method. At the end of the vessel containing L-N_2, is a pressure reducer valve that controls the pressure in the pipes. Then, a directional control valve (in this case a cryogenic valve), commanded by a solenoid, allows or blocks the passage of the coolant to the injectors inside the chamber. At the derivation

from the directional control valve is a safety valve that ensures a pressure relief in case certain levels of pressure are achieved.

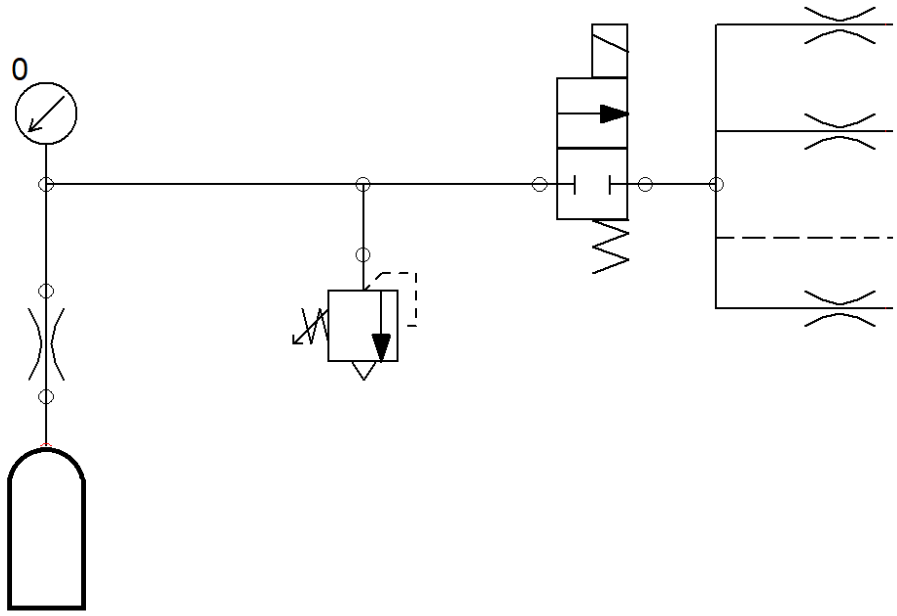

Figure 60 – Scheme of the cooling method.

4.2 Selection of the temperature controller

There are different temperature controllers' manufacturers that offer a variety of equipment with a diversity of characteristics. To narrow down the search, a specific manufacturer was selected: OMRON. This choice was due to the reliability of the brand, the wide range of temperature controllers they offer, and the availability of an OMRON's department nearby.

4.2.1 Characteristics of OMRON temperature controllers

The OMRON temperature controllers can operate with a double PID control – Figure 61 (3). This feature appears to respond to the limitations of conventional temperature controllers and yields good performance to both set point and disturbance inputs. In typical PID control, a single PID block is used to control the system response to a set point and to external

disturbances. Therefore, if good response to external disturbances is desired, then poor response to the setpoint may be obtained – Figure 61 (1). On the other hand, if good response to the setpoint is intended, then bad response to external disturbances can result – Figure 61 (2) [27].

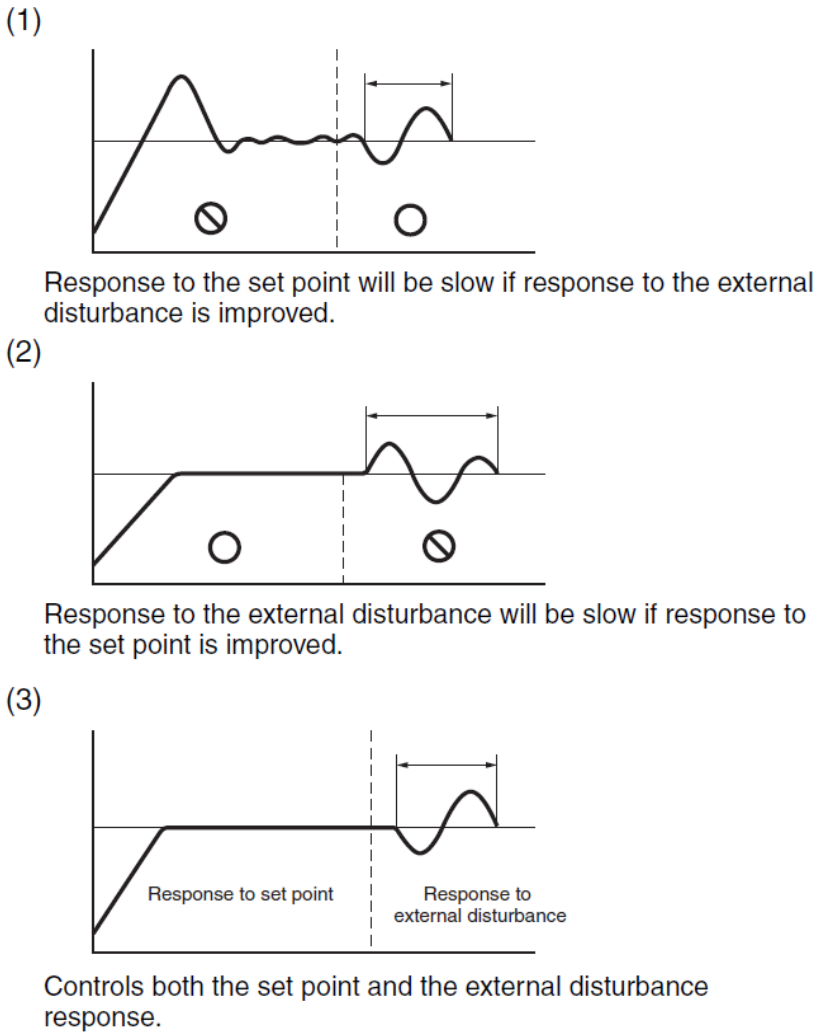

Figure 61 – System response with one PID and two PID controllers [27].

Whatever the case, to ensure good temperature control, the PID constants need to be adjusted properly. This can be done manually or automatically, through auto-tuning and self-tuning. The most common methods used for auto-tuning are the step response and the limit cycle methods.

A PID controller outputs a continuous control action between 0% and 100% of its signal range, contrasting with the ON/OFF control mode that outputs just 100% (ON) or 0% (OFF). The OMROM temperature controllers can implement both control modes. To implement PID control, the temperature controller uses time-proportional control action, which allows control output values between 0% and 100%. The controller output is then applied to the actuation elements via a relay or SSR.

When using time-proportional control a time parameter has to be defined, denoted by control period. Generically, it is necessary to set the control action to ON during a certain

percentage of the control period and set the control action to OFF for the rest of the control period. Figure 62 exemplifies how to achieve a value of 80% for the output signal, using two different control periods. As can be seen, the output turns ON and OFF only once during the control period, so that long control periods delay the response and short ones speed it up. OMRON recommends a control period of 20 s for relay outputs and 2 s for SSR outputs [27] [32].

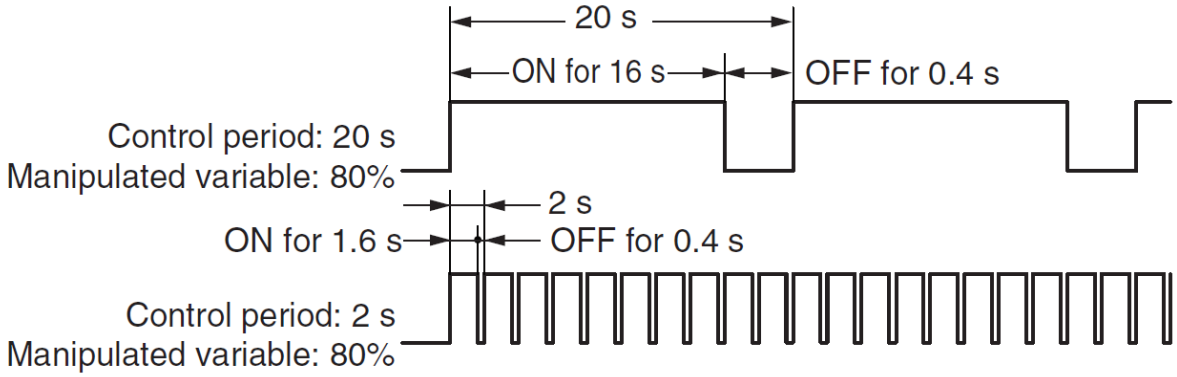

Figure 62 – Response with a time-proportional control [27].

In Table 10, the various types of control outputs available in the temperature controllers from OMRON are summarized. The contact relay outputs are suited for control methods with relatively low switching frequencies and can drive a load directly. The non-contact SSR outputs can only function at a maximum load of 1A. The voltage outputs from the ON/OFF control action can drive an external SSR with a large capacity, using a 12-VDC ON/OFF pulse outputs. The linear control output in current is a continuous 4-20 mA or 0-20 mA output, used for driving power controllers and electromagnetic valves. Finally, the linear control in voltage has a continuous 0-5 VDC or 0-10 VDC output used for driving pressure controllers [27] [32].

Table 10 – Types of outputs.

ON/OFF output	Linear output
Relay	Current
SSR	Voltage
Voltage	

OMRON's temperature controllers accept feedback through analog current or voltage inputs. The inputs can also be from a temperature sensor, such as a thermocouple (all types), platinum resistance thermometer, thermistor, and infrared temperature sensor.

The configuration of the control profiles, alarms, or any other feature provided by the temperature controller can be done directly in the controller or through a computer, since an open serial communication protocol RS-485 is available. With this, it is possible to create a

custom user interface based on free software. An alternative is to use the OMRON software (CX_Thermo) that contains all the features needed to define all the parameters of the temperature controller. Together with a USB-serial conversion cable, the OMRON software is an easier and more intuitive way of configuring the controller than defining the parameters directly on the controller [32] [33].

Now that all the characteristics of the temperature controllers were presented it is possible to define the type of control for the heating system. PID control is more appealing in terms of response than ON/OFF control. Therefore, time-proportional is the type of control that is used in the heating control method.

Using time-proportional control implies a high frequency commutation, so it is necessary to use an SSR instead of a normal relay. Some temperature controllers already have one incorporated, but it can only work at a maximum current load of 1 A. To power the two heating elements used in the thermal chamber with 2500 W each, it is necessary a much higher current than 1 A. According to Ohm's Law the current (I) is directly proportional to the voltage (V) and inversely proportional to the resistance (R)

$$I = \frac{V}{R} \tag{4.1}$$

where the current is expressed in A, the voltage is expressed in V and the resistance is expressed in Ω.

It is also known by Joule's Law that the heat power generated (P), when an electric current flows through a conductive material (in this case the heating elements) is equal to the resistance times the square of the current

$$P = R \cdot I^2 \tag{4.2}$$

where the heat power is expressed in W.

Combining the two equations it is possible to obtain

$$I = \frac{P}{V} \tag{4.3}$$

Knowing that each heating element has 2500 W and the voltage is 230 V, the current needed is around 21,7 A. Thus, an external SSR needs to be implemented in the heating system.

4.2.2 SSR precautions

The use of an SSR raises some concerns in terms of the proper functioning of the electric system. The SSR operates with small amounts of power, which obliges to shut out any electrical noise in the input terminals, because it can lead to the malfunction of the SSR. To absorb the noise caused by a pulse signal, a combination of a capacitor (C) and a resistor (R) is enough. Figure 63 illustrates an example of how to eliminate the pulse noise. The values of (C) and (R)

should be carefully chosen. If (R) is too large, the voltage supply (E) will not match the required input voltage, and the bigger the value of C the longer the release time will be. Inductive noise can also be a problem in the input terminals of the SSR. If the noise is electromagnetic, then a twisted-pair wire should be used. If the problem is static noise, a shielded cable must be applied. The noise originated by a high frequency device can be eliminated with a filter composed by a capacitor and a resistor, similar to the one in Figure 63.

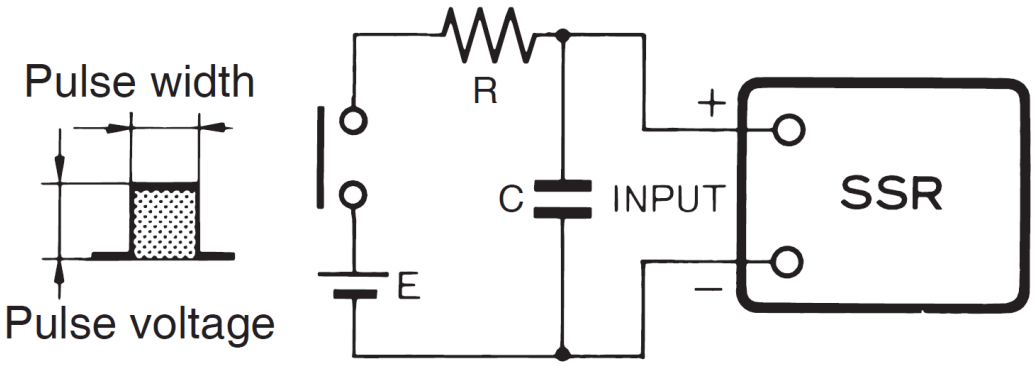

Figure 63 – Circuit to eliminate the pulse noise at the input terminals of an SSR [34].

Now, the precautions to take into consideration for the output terminals are presented. First, in the event of a large voltage surge in the AC current that is being used by the SSR, the built in snubber circuit (resistor and capacitor) will not be enough to avoid damaging the SSR. Therefore, it is necessary to include a surge absorbing varistor to protect the SSR. If DC current is being applied to the output terminals of the SSR, a counter electromotive force may occur, when driving loads such as a solenoid or an electromagnetic valve. If this exceeds the withstand voltage of the SSR output element, it could damage it. The solution is to place a diode in parallel with the load, as shown in Figure 64.

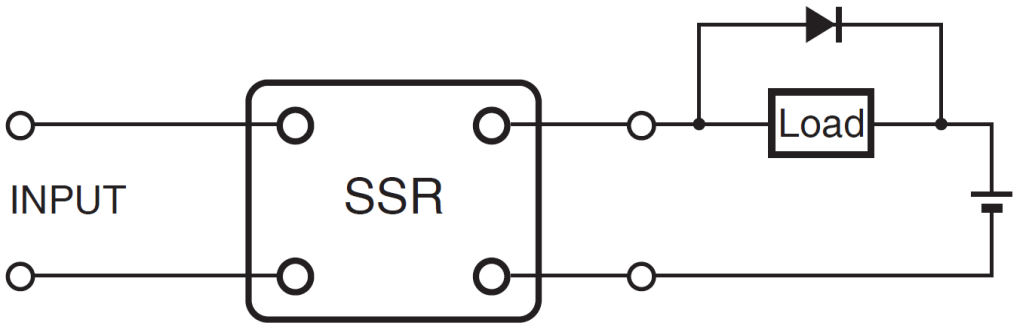

Figure 64 – Circuit to eliminate DC switching noise with inductive load [34].

Inrush currents are common when powering a load. According to the type of load connected to the output terminals of the SSR, different inrush current values will appear. Figure 65 gives an approximated idea of the inrush currents for several loads [34].

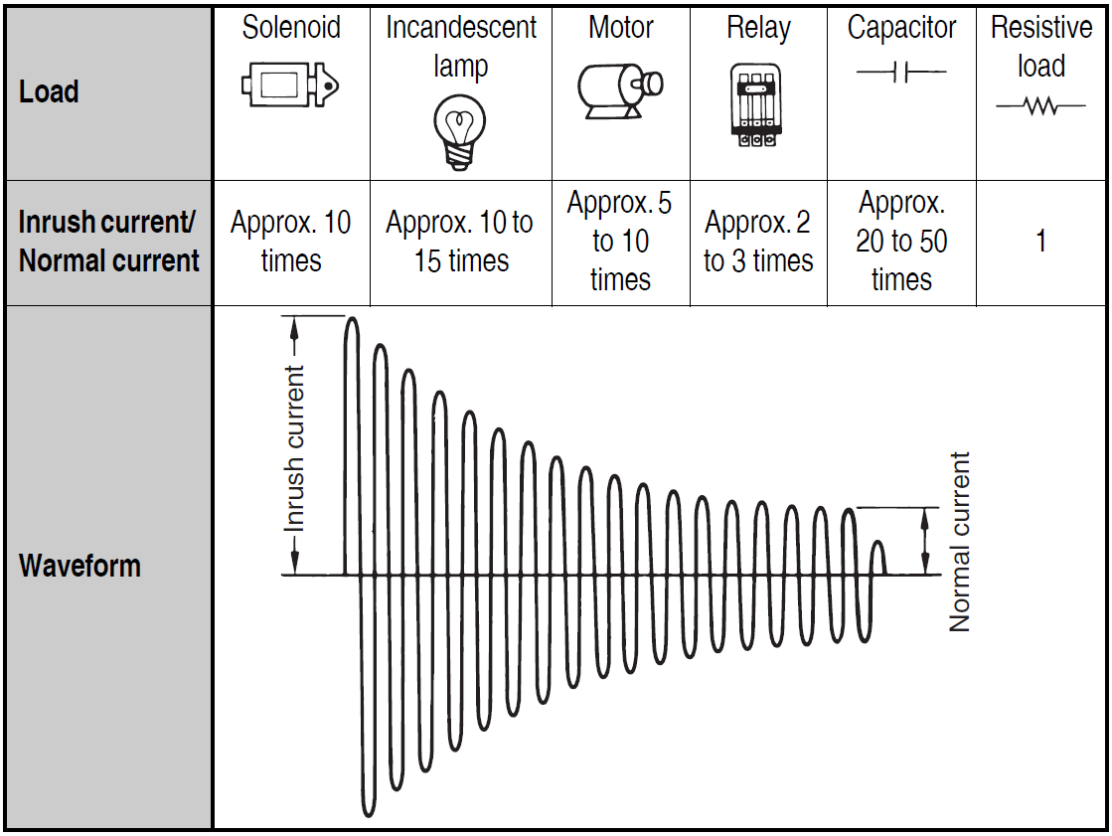

Figure 65 – Inrush current values compared with their normal current for different loads [34].

4.2.3 Selection of the OMRON controller

The temperature controller required for this system needs to fulfill the following conditions:

- Universal input for a thermocouple ;
- Relay output control to command the cryogenic valve;
- Voltage output control for driving an SSR;
- Auxiliary relay output control for the fans;
- Able to define set points and heating/cooling curves;
- Compatible with 220-240 VAC, 50 Hz power supply;

The device selected is the industrial temperature controller E5CC-TQX3 A5 M-000, because it complies with all the requested conditions. It has a universal input for different temperature sensors, including for thermocouples. The control output #1 is a voltage output for driving an external SSR, the control output #2 is an auxiliary relay output. The other two auxiliary outputs are used to command the fans. The temperature controller has the ability to define set points and heating/cooling curves and operates between 100-240 VAC [32].

4.3 Electronic components

Figure 66 illustrates the electric components that have been implemented. The first block is the power switch to turn on and off the system. The next block shows the protective equipment, which is essential to guarantee that the system is protected against overloads or short-circuits and that people are protected against electric shock in case there is a leakage current. A reed contact, placed in the chamber ensures that the system only operates when the two halves of the chamber are closed together. There are two lights to illuminate the specimens and one indicator light to alert the user that the system is powered on. Then, it is visible the thermocouple that gives the input signal to the temperature controller. From the temperature controller, there is an output signal to an SSR, which commends the two heating elements, another output control to the cryogenic solenoid valve, and one more output control to command the fans.

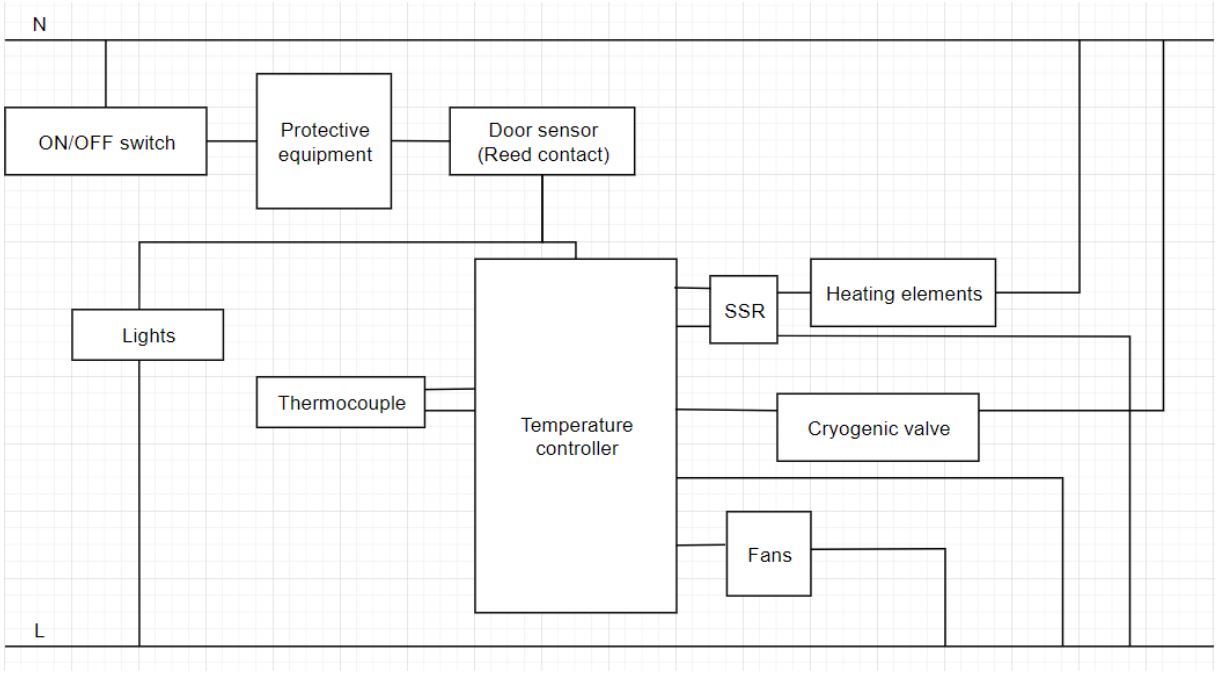

Figure 66 – Scheme of the command circuit.

4.3.1 Temperature controller

The temperature controller was selected in section 4.2.3. It is a temperature controller from OMRON with the model number E5CC-TQX3 A5 M-000, that fulfills all the necessary requests. Figure 67 shows an image of the selected device.

Figure 67 – Temperature controller from OMRON E5CC-T series [35].

4.3.2 Temperature sensor

As previously said, the chamber has to operate between -100 ℃ and 200 ℃, so the temperature sensor needs to be able to operate in this range of temperatures. In section 4.1.1, the reasons that led to the choice of a thermocouple were pointed out. Table 11 shows various types of thermocouples and their range of temperatures.

Table 11 – Temperature ranges of thermocouples [36].

Type	Temperature range [℃]
B	0 to 1820
E	-270 to 1000
J	-210 to 1200
K	-270 to 1372
R	-50 to 1767
S	-50 to 1767
T	-270 to 400

The thermocouple type T is the one that better suits the needs of this system – Figure 68. There are innumerous options to buy this type of equipment in RS Components, for example, at a wide range of prices. The selected thermocouple is from RS Pro, can operate between -200 and 350 ℃ and has the RS Code number 621-2209 [37].

Figure 68 – Thermocouple type T [37].

4.3.3 SSR

The SSR needs to have an input voltage of 12 VDC. The two heating elements are powered at 220-240 VAC, so the output voltage of the SSR has to be the same. It is also necessary to ensure that the current load admissible at the SSR terminals is superior to the one that powers the heating elements. The calculations of the current load were made in section 4.2.1, resulting in a value of around 21.7 A.

The G3NA-225B-UTU DC5-24 from OMRON – Figure 69 – was selected. This SSR has an input operating voltage range of 5-24 VDC and a load voltage range of 24-240 VAC. Finally, the maximum load current admissible is 25 A, therefore all the requirements for the SSR are fulfilled.

As said in section 4.2.2, there are some concerns that should not be overlooked when using an SSR. In the input terminals, no additional equipment is required, since the SSR has a built-in snubber. This relay also has a built-in surge absorbing varistor. So, there is no extra equipment needed to protect the output terminals. Since the load that is being powered is a resistive one, no inrush currents appear [38].

Figure 69 – SSR from OMRON G3NA series [39].

4.3.4 Heating elements and fan

The variety of heating elements in the market is very large. There are several manufacturers and each one has a wide range of heating elements for different applications. To narrow down the search, the option followed was to search the heating elements of domestic ovens, since ovens are a reasonable approximation to the chambers and they can reach the necessary temperature values.

Figure 70 – Heating element from AEG [40].

Therefore, two circular heating elements from AEG were selected, with original part number 3116448006 – Figure 70. Two heating elements were chosen to better spread the heat in the chamber. The main characteristics of each one are described in Table 12.

Table 12 – Heating element characteristics [40].

Characteristic	Value
Power	2500 W
Voltage	230-240 V
Height	225 mm
Width	195 mm
Bracket	145 mm
Tags width	90 mm

Another reason to select a heating element from a domestic oven is the facility to find a fan with an incorporated motor that fits the heating element. So, a motor and fan assembly from Belling was selected, with original part number 082603745 – Figure 71. The main characteristics of the assembly are described in Table 13.

Figure 71 – Motor and fan assembly from Belling [41].

Table 13 – Motor and fan assembly characteristics [41] [42].

Characteristic	Value
Power	24-28 W
Voltage	220-240 V
Frequency	50/60 Hz
Class	CL.180
Diameter of the motor mounting plate	130 mm
Depth of motor mounting plate	60 mm
Diameter of the fan blade	150 mm
Depth of fan blade	22 mm

4.3.5 Cryogenic solenoid valve and cryogenic safety valve

The injection of the coolant occurs through a series of rigid pipes located inside the chamber. The cryogenic valve ensures the flux of the coolant or ceases it according to the difference between the temperature in the chamber and the setpoint defined in the temperature controller.

Based on the consumption of the coolant of the INSTRON chambers and their volume, a consumption of 30 l/h was estimated to maintain a temperature of -100 °C inside the designed chamber. Therefore, the cryogenic solenoid valve has to ensure a flow superior to the one mentioned. The valve selected is from Alcon 68 series – Figure 72 – and the main characteristics are presented in Table 14.

Table 14 – Characteristics of the cryogenic solenoid valve [43].

Characteristic	Value
Coil voltage AC	24 V, 110 V, 120 V, 230 V
Power	14.5 W
Pressure range (for AC voltage)	5-55 bar
Pipe size	1/4 "
Orifice size	4.5 mm
Flow	0.43 m^3/h

Figure 72 - Cryogenic solenoid valve [43].

When using cryogenic cooling, normally, a cryogenic safety valve is used, providing protection against thermal expansion in the pipeworks and other parts of the facility. The valve from HEROSE type 06001 was selected. Its main characteristics are presented in Table 15.

Table 15 – Characteristics of the cryogenic safety valve [44].

Characteristic	Value
Nominal size	1/4 "
Orifice size	6 mm
Set pressure range	5-55 bar

4.3.6 Fans

The fans that ensure a constant flow in the external insulation case were selected from SUNON. This manufacturer has a vast offer of equipment, including fans that are AC powered. The SF23092A 2092HSL.GN fan – Figure 73 – was selected, which has the main characteristics displayed in Table 16.

Figure 73 – SUNON's AC fan [45].

Table 16 – Fan characteristics [46].

Characteristic	Value
Power	14.5/14 W
Voltage	220-240 V
Current	0.07/0.06 A
Frequency	50/60 Hz
Speed	2250/2750 rpm
Air flow	29/36 CFM

4.3.7 Protective equipment

The protective equipment is of paramount importance, because it protects the system and the people who operate it. First of all, it is necessary to know the current required by all the electric components in order to define the appropriate protective equipment. The heating elements, the motor and fan assemblies, the cryogenic solenoid valve and the two other fans are the components that require more power, as is possible to observe in Table 12, Table 13, Table 14 and Table 16. The total power is 5,098.5 W. Using the equations (4.1), (4.2) and (4.3), the total current in the circuit was calculated, resulting in the value of 22.2 A. The rest of the components require low power, so the current that they absorb is negligible.

LOVATO Electric has a Residual Current circuit Breaker with Overcurrent protection (RCBO) that incorporates protection for the circuit and for the users. The model P1 RB 1N C25 AC030 was selected. The main characteristics are presented in Table 17.

Table 17 – RCBO characteristics [47].

Characteristic	Value
Insulation voltage	400 V
Impulse withstand voltage	4 kV
Operating voltage	230 V
Residual operating current	30 mA
Short-circuit capacity	10 kA
Current	25 A
Number of poles	1P+N

4.3.8 Reed contact

The reed contact, along with its magnet, will act as a door sensor, preventing the thermal chamber from start to work when the two halves are not joined together. This type of contact was adopted due to its reliability, even in the eventuality of frost or ice formation. A reed contact model SRA200G from Cynergy was selected.

4.3.9 Switches

To activate and deactivate the equipment it is indispensable to have switches. To power up the circuit, a two position switch was selected. The model number is XB5AD25 from SCHNEIDER and has the contact block already included, as shown in Figure 74.

Figure 74 – Two position switch [48].

Another switch is necessary to turn on and off the lights inside the chamber. Therefore, a pushbutton with a normally open and a normally closed contact was selected from SCHNEIDER, that has the contact block already incorporated. The model number is XB4BW3165 – Figure 75 – and has a LED light incorporated.

Figure 75 – Pushbutton.

4.3.10 Lights

The indicator lights give a visual feedback that the equipment is working. There is a big variety of these components with different possibilities of color, type of operating current, type of terminals and so on. A green light indicator that can operate with 220-240 VAC was selected from RS Pro, with the RS Stock No 700-1946 – Figure 76.

Figure 76 – RS Pro green indicator [49].

Although all the manufacturers offer LED lights in the interior of their thermal chambers, no information is given about what protection against the extreme temperatures is applied. The information given by the companies about the service temperatures of their lights is few, or when it is given, does not fit the necessary requests.

4.4 Electric circuit

4.4.1 Power circuit

The power circuit is presented.

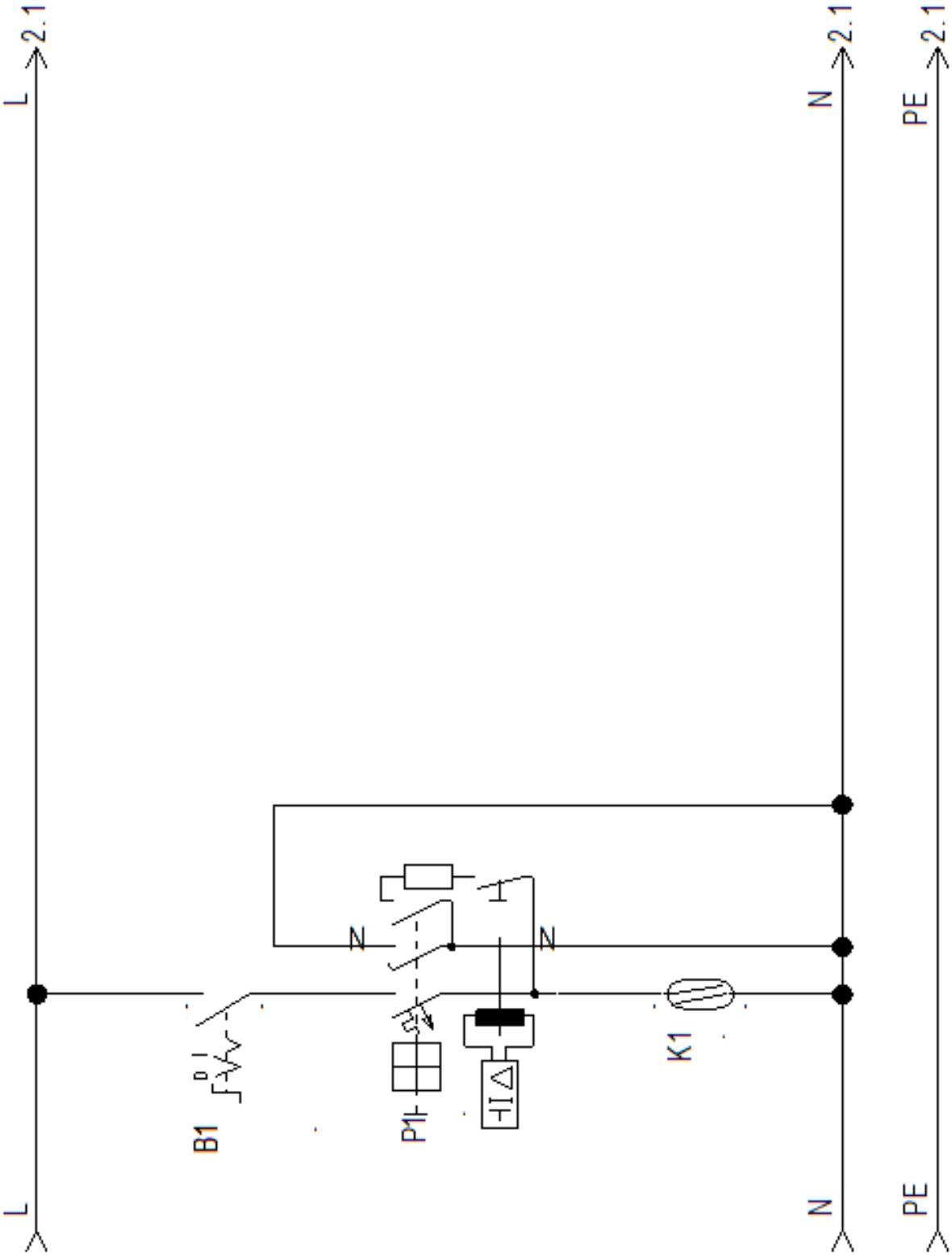

4.4.2 Command circuit

The command circuit is presented.

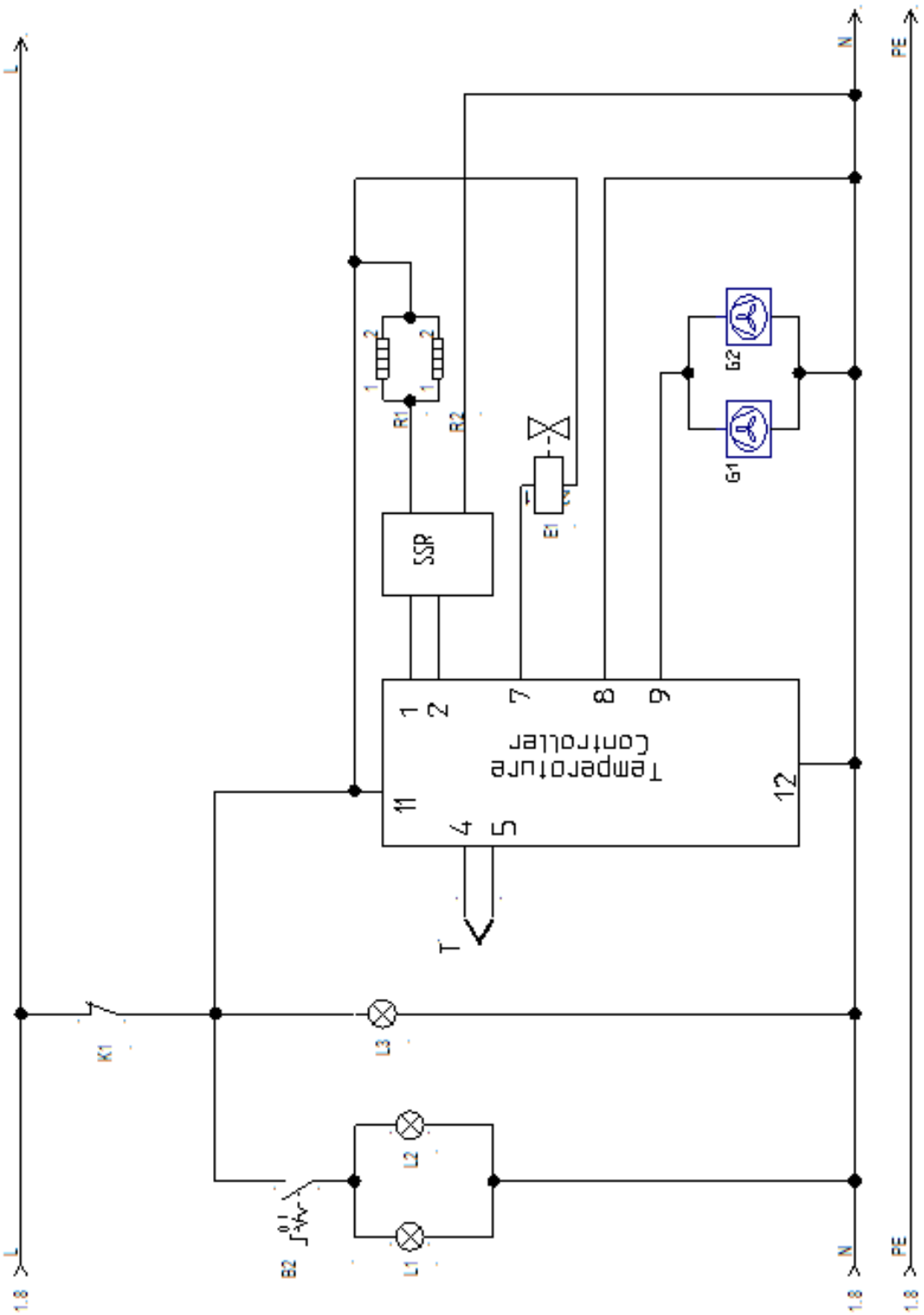

4.5 Discussions

Chapter 4 presented the control of the temperature chamber. When designing a system like this, it is important to define how the heating and cooling is going to be performed. From there, it is possible to define the appropriate type of control that is going to be adopted. At the same time, it is fundamental to know the limitations and advantages of each type of control and to implement the one that better suits the needs of the system.

Selecting the temperature controller is a critical step, because this device is the core of the system. It has to fulfill all the needs of the heating and cooling functions and also accommodate the complementary components that compose the system.

The selection of all the components was made, trying to find the best solution for the equipment in terms of quality and performance. The command circuit was completely defined

5 Conclusions

5.1 Conclusions

The market demand for thermal chambers for multi-station creep testing machines is very low. Therefore, the few solutions that some manufacturers offer are expensive and not suitable for models different from those they commercialize. This raised the need for designing a thermal chamber for the three-station creep testing machine of the AJUP.

The main goal of this dissertation was to design a thermal chamber that operates between -100 and 200 ℃. The chamber has to be capable of performing temperature tests automatically.

In a first stage, the commercial solutions of thermal chambers for creep testing machines were analyzed and the designs that enable its incorporation were understood. The heating and cooling solutions were studied to better perceive how the thermal chambers operate.

On the top of the creep testing machine of the AJUP, there are three load cells that have a service temperature of -20 and 70 ℃. The temperature values that reach the load cells when the chamber is operating in its extreme values exceed the range of the service temperature. Thus, it was necessary to develop a heat insulator, which reduces the temperature values applied to the load cells. Two different designs were explored, trying not only to reach the service temperature values, but also the temperature nominal range. Along with the development of the heat insulator, the designs suffered several iterations that discredited or validated alternative solutions after thermal simulation in SolidWorks.

The next step was to design the chamber. There were different approaches on how to design it, but the followed solution was the one in which the chamber is split vertically in two halves and each half is attached to one of the columns of the load frame. This attachment is made by a crank that allows the chamber to pivot with the column. The evolution of the design was presented and mathematical justifications were given for some relevant options in terms of thermal efficiency of the chamber. In the back half of the chamber, a panel was designed to accommodate several components of the temperature control system.

In the last stage, the temperature control system was presented and the heating and the cooling methods were described. Then, the temperature controller was selected. After selecting

the controller the different electric components were defined based on the needs of the chamber and the temperature controller. At the end, the power and command circuit were defined.

The chamber was designed and its temperature control system was defined concretizing the main goals of the dissertation.

The article “Thermal chamber for adhesives multi-station creep testing machine” was submitted to the U.Porto Journal of Engineering.

5.2 Future development

A thermal simulation with all the components of the chamber should be run to confirm the calculations made in terms of thermal efficiency. Ideally, the thermal simulation should also have incorporated the creep testing machine. Since the chamber was designed in SolidWorks and the creep testing machine in SolidEdge there is no recommendation for which software use.

The LED lights that illuminate the specimens need to be defined. It is also interesting to incorporate a resistance in one of the glass panels of the window. This way during the cooling, the air on the glass panel does not condensate.

6 References

1. Da Silva, L.F., A. Öchsner, and R.D. Adams, *Handbook of adhesion technology*. 2011: Springer Science & Business Media.
2. Freire, H.M., *Desenvolvimento de um dispositivo experimental para medir a resistência à fluência de ligações adesivas.* 2015.
3. Pina, L.P.L., *Development of a multi-station creep testing machine for adhesive joints.* 2016.
4. Silva, E.D.R., *Development of a Three-station Creep Machine for Adhesive Joints Testing.* 2018.
5. Kinloch, A.J., *Adhesion and adhesives: science and technology*. 2012: Springer Science & Business Media.
6. Adhesives&Selants. *Types of Adhesives*. 2019; Available from: https://www.adhesives.org/adhesives-sealants/science-of-adhesion/design-of-adhesives-bonds/types-of-adhesives.
7. Handbook, M.S., *Adhesive Bonding*. 1987, MIL-HDBK-691B, US Department of Defense.
8. Dowling, N.E., *Mechanical behavior of materials: engineering methods for deformation, fracture, and fatigue*. 2012: Pearson.
9. Da Silva, L.F., et al., *Testing adhesive joints: best practices*. 2012: John Wiley & Sons.
10. ZWICK, *Creep Testing MachineKappa Multistation for Plastics*. 2019.
11. INSTRON, *Multi Station Systems 5900 series*. 2018.
12. Associação de Laboratórios Acreditados de Portugal, *Guia 19.* 2004.
13. Pombeiro, A.J.L.O., *Técnicas e operações unitárias em química laboratorial*. 1983: Fundação Calouste Gulbenkian.
14. Lefcourt, A., B. Buell, and U.J.A.E.i.A. Tasch, *Large environmental chamber: Design and operating characteristics.* 2001. **17**(5): p. 691.
15. Leskinen, A., et al., *Characterization and testing of a new environmental chamber.* 2015.
16. INSTRON, *Enviromental Chambers 3119 600 Series*. 2017.
17. Berryman, J.G. and W.D. Daily, *Optimal joule heating of the subsurface*. 1994, Google Patents.

18. WATTCO. *Electric Heating Elements Wattco*. 2019; Available from: https://www.wattco.com/electric-heating-elements/.

19. Handbook, K.J.K.A., *Heating Alloys for Electric Household Appliances.* 2013.

20. WATTCO, *Tubular heaters*. 2017.

21. SIGMA, *Cryogenic Coling for Temperature Chambers and Thermal Platforms*. 2000.

22. Hashmi, S., *Comprehensive materials processing*. 2014: Newnes.

23. ZWICK, *Temperature chambers for AllroundLine*. 2019.

24. Bergman, T.L., et al., *Fundamentals of heat and mass transfer*. 2011: John Wiley & Sons.

25. AEP Traducers, *TS-TSA*. 2018.

26. QuickField. *Natural convection*. 2019; Available from: https://quickfield.com/natural_convection.htm.

27. OMRON, *Techical Guide for Temperature Controllers*. 2019.

28. Broutin, S.L. and J.W. Stayt Jr, *Automatic closed-looped gain adjustment for a temperature tuned, wavelength stabilized laser source in a closed-loop feedback control system*. 2002, Google Patents.

29. Dobkin, B. and J. Williams, *Analog circuit design volume 2: immersion in the black art of analog design*. Vol. 2. 2012: Newnes.

30. Ogata, K. and Y. Yang, *Modern control engineering*. Vol. 5. 2010: Prentice hall Upper Saddle River, NJ.

31. UNITRONICS. *General background How PID Works*. 2019; Available from: https://unitronicsplc.com/Download/SoftwareHelp/UniLogic_Knowledgebase/Imports/How_PID_Works.htm.

32. OMRON, *Digital Temperature Controller E5_C/E5_C-T*. 2019.

33. OMRON, *Digital Temperature Controllers Communications Manual E5CC, E5EC*. 2019.

34. OMRON, *Solid State Relays Common Precautions*. 2019.

35. OMRON. *E5CC-T*. 2019; Available from: http://www.ia.omron.com/products/family/3288/download/catalog.html.

36. Powell, R.L., *Thermocouple reference tables based on the IPTS-68*. Vol. 125. 1974: US National Bureau of Standards.

37. RS Pro, *Cable Thermocouple Type T*. 2019.

38. OMRON, *Solid State Relay G3NA*. 2016.

39. Mouser. *G3NA-240B-UTU DC5-24 Omron Automation and Safety*. 2020; Available from: https://pt.mouser.com/ProductDetail/653-G3NA240BUTUDC524.

40. Sussex, C. *AEG: Fan Oven Element 2500W - 3116448006*. 2019; Available from: https://www.sussexcookers.com/foe003-aeg-fan-oven-element-2500w-3116448006?search=2500w.

41. Cooker, S. *Belling: 142 Oven Fan Motor Assembly*. 2019; Available from: https://www.sussexcookers.com/fom010-belling-142-oven-fan-motor-assembly.

42. Belling. *Belling Fan Motor*. 2019; Available from: https://www.bellingspares.co.uk/product.pl?pid=268482.

43. ALCON Solenoid Valves, *68 Series*. 2019.

44. HEROSE, *Safety Valves Type 06001*. 2019.

45. Mouser. *SF23092A-2092HSL.GN Sunon*. 2020; Available from: https://pt.mouser.com/ProductDetail/369-SF23092A2092HSL.

46. SUNON, *AC Axial Fan & Blower*. 2018.

47. LOVATOEletric, *Modular devices*. 2019

48. SCHNEIDER, *Product datasheet XB4BW33M5*. 2019.

49. RS Pro, *Datasheet RS Pro Flush indicator Panel Mout.* 2019.

Appendix A: Table

			TABLE MODELS				FLOOR MODELS					
			3119-605	3119-606	3119-609	3119-615	3119-607	3119-608	3119-610	3119-616	3119-617	3119-618
External Height	A	mm	635	710	810	1010	710	710	810	1050	910	1150
		in	25.0	27.9	31.9	39.8	27.9	27.9	31.9	41.3	35.8	45.3
Internal Height	B	mm	485	560	660	860	560	560	660	900	760	1000
		in	19.1	22.0	26.0	33.9	22.0	22.0	26.0	35.4	29.9	39.4
External Width	F	mm	350	350	350	350	550	550	550	550	550	550
		in	13.8	13.8	13.8	13.8	21.7	21.7	21.7	21.7	21.7	21.7
Internal Width	E	mm	240	240	240	240	400	400	400	400	400	400
		in	9.4	9.4	9.4	9.4	15.7	15.7	15.7	15.7	15.7	15.7
External Depth	G	mm	590	590	590	590	930	930	930	855	855	855
		in	23.2	23.2	23.2	23.2	36.6	36.6	36.6	33.7	33.7	33.7
Internal Depth	H	mm	230	230	230	230	400	400	400	400	400	400
		in	9.0	9.0	9.0	9.0	15.7	15.7	15.7	15.7	15.7	15.7
Pull Rod Port Diameter	J	mm	67	67	67	67	90[1]	90[1]	90[1]	90[1]	135	135
		in	2.6	2.6	2.6	2.6	3.5	3.5	3.5	3.5	5.3	5.3
Pull Rod Port Center to Inside Rear	K	mm	120	120	120	120	200	200	200	200	200	200
		in	4.7	4.7	4.7	4.7	7.8	7.8	7.8	7.8	7.8	7.8
Pull Rod Port Center to Inside Front	L	mm	110	110	110	110	200	200	200	200	200	200
		in	4.3	4.3	4.3	4.3	7.8	7.8	7.8	7.8	7.8	7.8
Window Height	C	mm	350	350	460	640	350	350	460	460	460	460
		in	13.8	13.8	18.1	25.2	13.8	13.8	18.1	18.1	18.1	18.1
Window Width	D	mm	125	125	125	125	125	125	125	125	125	125
		in	4.9	4.9	4.9	4.9	4.9	4.9	4.9	4.9	4.9	4.9
Weight	-	kg	65	65	75	85	135	165	165	165	150	173
		lb	143	143	165	187	297	363	363	363	330	382

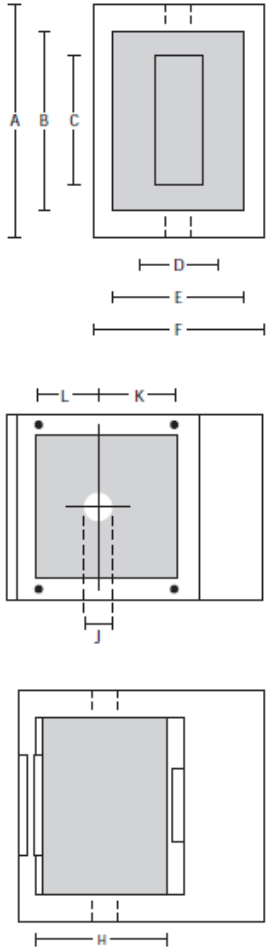

Notes:
1. Includes reducer to 67 mm

Overall System Accuracy

		TABLE MODELS			FLOOR MODELS		
		3119-605	3119-606	3119-609	3119-607	3119-608	3119-610
Temperature	°C	-150	-100	-40	+200	+350	+600
	°F	-240	-150	-40	+390	+660	+1110
Accuracy	°C	±5.5	±5.0	±4.5	±3.5	±4.5	±5.5
	°F	±10.0	±9.0	±8.1	±6.5	±8.1	±10.0

Carbon Dioxide (CO_2) - Pipe thread 3/8 inch BSP male.
Instron® reserves the right to change specifications without notice.

Specifications

	TABLE MODELS		FLOOR MODELS				
	3119-605/-606/-609	3119-615	3119-607/-610	3119-608	3119-616	3119-617	3119-618
Maximum Temperature	+350°C (660°F)	+350°C (660°F)	+350°C (660°F)	+600°C (1112°F)	+350°C (+660°F)	+350°C (+660°F)	+350°C (+660°F)
Minimum Temperature (Requires Cooling Option)	-100°C (-150°F) - LN_2 -70°C (-95 °F) - CO_2	-100°C (-150°F) - LN_2 -70°C (-95 °F) - CO_2	-150°C (-238°F) - LN_2 -70°C (-95 °F) - CO_2	-150°C (-238°F) - LN_2 -70°C (-95 °F) - CO_2	-80°C (-112°F) - LN_2	-80°C (-112°F) - LN_2	-80°C (-112°F) - LN_2
Heat-Up Time to Maximum or Stated Temperature from Ambient Including Typical Load String	Better than 50 Minutes (120/240V) Better than 100 Minutes (100/200V)	Better than 50 Minutes (120/240V) Better than 100 Minutes (100/200V)	Better than 25 Minutes (240V) Better than 35 Minutes (200V)	Better than 60 Minutes (240V)	Typically 120 Minutes to 250°C (Depending on load string)	Typically 120 Minutes to 250°C (Depending on load string)	Typically 120 Minutes to 250°C (Depending on load string)
Heating Method	Forced Convection	Forced Convection	Forced Convection	Forced Convection	Forced Convection	Forced Convection	Forced Convection
Cool Down Time to Minimum or Stated Temperature from Ambient Including Typical Load String	Better than 20 Minutes (LN_2 to -100°C) Better than 15 Minutes (CO_2 to -70°C)	Better than 20 Minutes (LN_2 to -100°C) Better than 15 Minutes (CO_2 to -70°C)	Better than 40 Minutes (LN_2 to -150°C) Better than 30 Minutes (CO_2 to -70°C)	Better than 40 Minutes (LN_2 to -150°C) Better than 30 Minutes (CO_2 to -70°C)	Typically 120 Minutes to -70°C (Depending on load string)	Typically 120 Minutes to -70°C (Depending on load string)	Typically 120 Minutes to -70°C (Depending on load string)
Typical LN_2 Consumption to Achieve Specified Temperature at Grip from Ambient	3 Liters to -30°C (-22°F) 7 Liters/Hr Steady State 7 Liters to -100°C (-150°F) 12 Liters/Hr Steady State[1]	3 Liters to -30°C (-22°F) 7 Liters/Hr Steady State 7 Liters to -100°C (-150°F) 12 Liters/Hr Steady State[1]	7 Liters to -30°C (-22°F) 10 Liters/Hr Steady State 25 Liters to -150°C (-238°F) 20 Liters/Hr Steady State[2]	7 Liters to -30°C (-22°F) 10 Liters/Hr Steady State 25 Liters to -150°C (-238°F) 20 Liters/Hr Steady State[2]	See note 4	See note 4	See note 4
Temperature Stability	±2°C (±3.6°F)	±2°C (±3.6°F)	±2°C (±3.6°F)	±2°C (±3.6°F)	±2°C (±3.6°F)	±2°C (±3.6°F)	±2°C (±3.6°F)
Temperature Gradient	±1% of Set Point after 10 Minutes Stability Time, or ±2°C (±3.6°F) Whichever is Greater[3]	±1% of Set Point after 10 Minutes Stability Time, or ±2°C (±3.6°F) Whichever is Greater[3]	±1% of Set Point after 10 Minutes Stability Time, or ±2°C (±3.6°F) Whichever is Greater[3]	±1% of Set Point after 10 Minutes Stability Time, or ±2°C (±3.6°F) Whichever is Greater[3]	±1% of Set Point after 10 Minutes Stability Time, or ±2°C (±3.6°F) Whichever is Greater[3]	±1% of Set Point after 10 Minutes Stability Time, or ±2°C (±3.6°F) Whichever is Greater[3]	±1% of Set Point after 10 Minutes Stability Time, or ±2°C (±3.6°F) Whichever is Greater[3]
Max Temperature Overshoot	2°C (3.6°F)	2°C (3.6°F)	2°C (3.6°F)	2°C (3.6°F)	2°C (3.6°F)	2°C (3.6°F)	2°C (3.6°F)
Power Requirements	100-120V (30A) or 200-240V (16A) 50/60Hz Single Phase	200 - 240V 50/60Hz Single Phase	200-240V (30A) 50/60Hz Single Phase	240V (30A) 50/60Hz Single Phase	200 - 240V (30A) 50/60Hz Single Phase	200 - 240V (30A) 50/60Hz Single Phase	200 - 240V (30A) 50/60Hz Single Phase

Notes

1. Based on chamber containing typical 12 kg grips and pull rods such as 2732-008. Total gas consumption will be affected by the duration and frequency of door opening. It will also vary according to the size of the load string and specimen.
2. Based on chamber containing typical 25 kg grips and pull rods such as 2716-002. Total gas consumption will be affected by the duration and frequency of door opening. It will also vary according to the size of the load string and specimen.
3. Temperature measured at the specimen (steel) over a 50 mm (2 in) gauge length. Not applicable within 15°C of ambient.
4. LN2 consumption will be dramatically affected by the load string and testing conditions. Consumption is likely to be at least twice that of 3119-610.

Cryogenic fittings:

Liquid Nitrogen (LN_2) – Pipe thread 1/2 inch BSP male.
Carbon Dioxide (CO_2) - Pipe thread 3/8 inch BSP male.
Instron® reserves the right to change specifications without notice.

We are also able to supply custom variants of our chambers; please contact us if our standard chambers do not meet your requirements.

Appendix B: Technical drawings

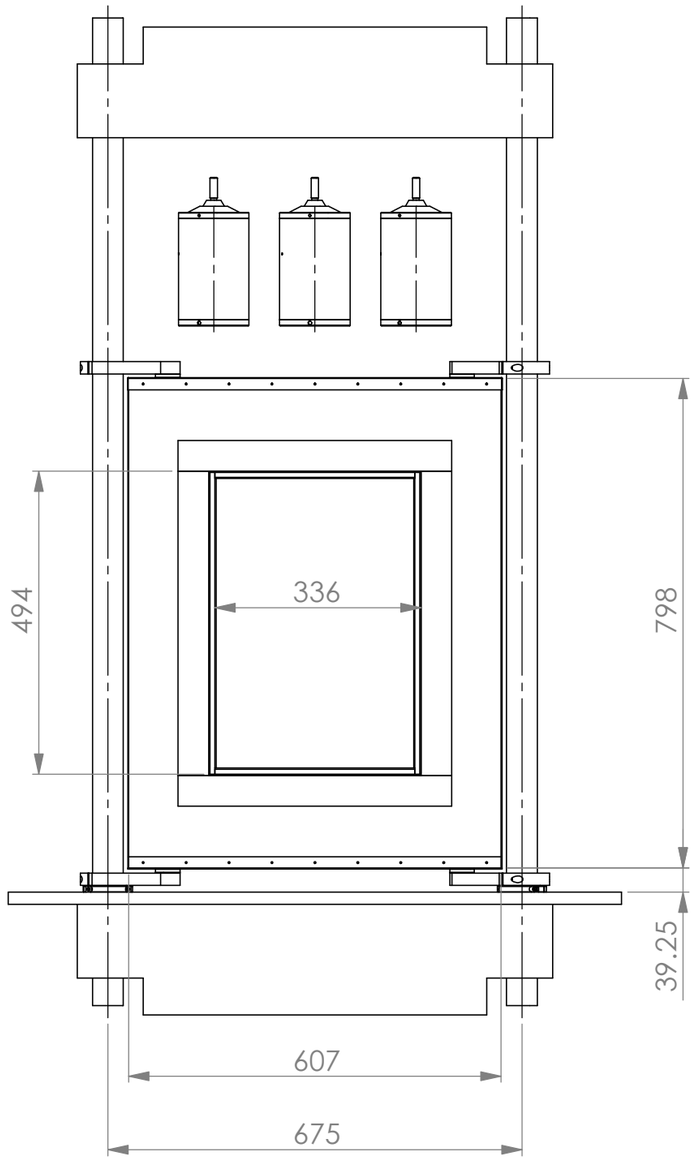

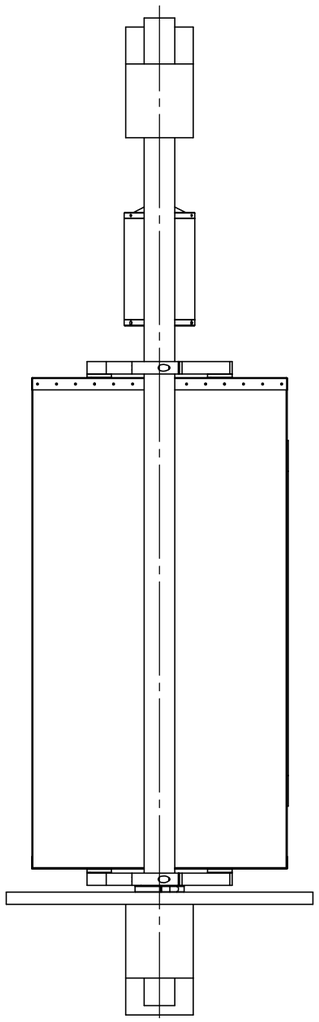

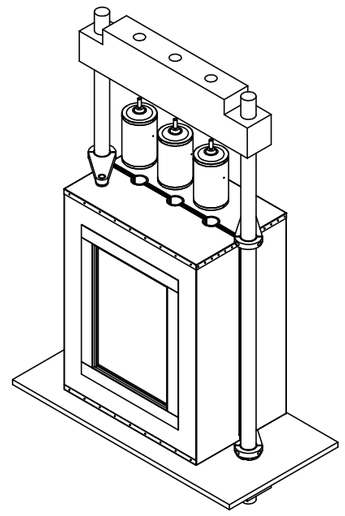

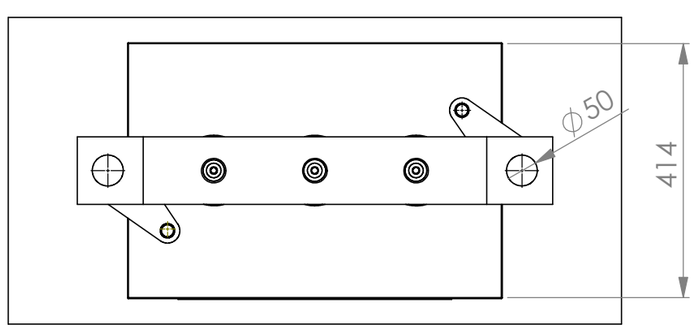

UNLESS OTHERWISE SPECIFIED: DIMENSIONS ARE IN MILLIMETERS SURFACE FINISH: TOLERANCES: LINEAR: ANGULAR:		FINISH:		DEBURR AND BREAK SHARP EDGES		DO NOT SCALE DRAWING	REVISION
	NAME	SIGNATURE	DATE			TITLE: Thermal chamber	
DRAWN							
CHK'D							
APPV'D							
MFG							
Q.A				MATERIAL:		DWG NO. 2020012701	A3
				WEIGHT:		SCALE:1:20	SHEET 1 OF 1

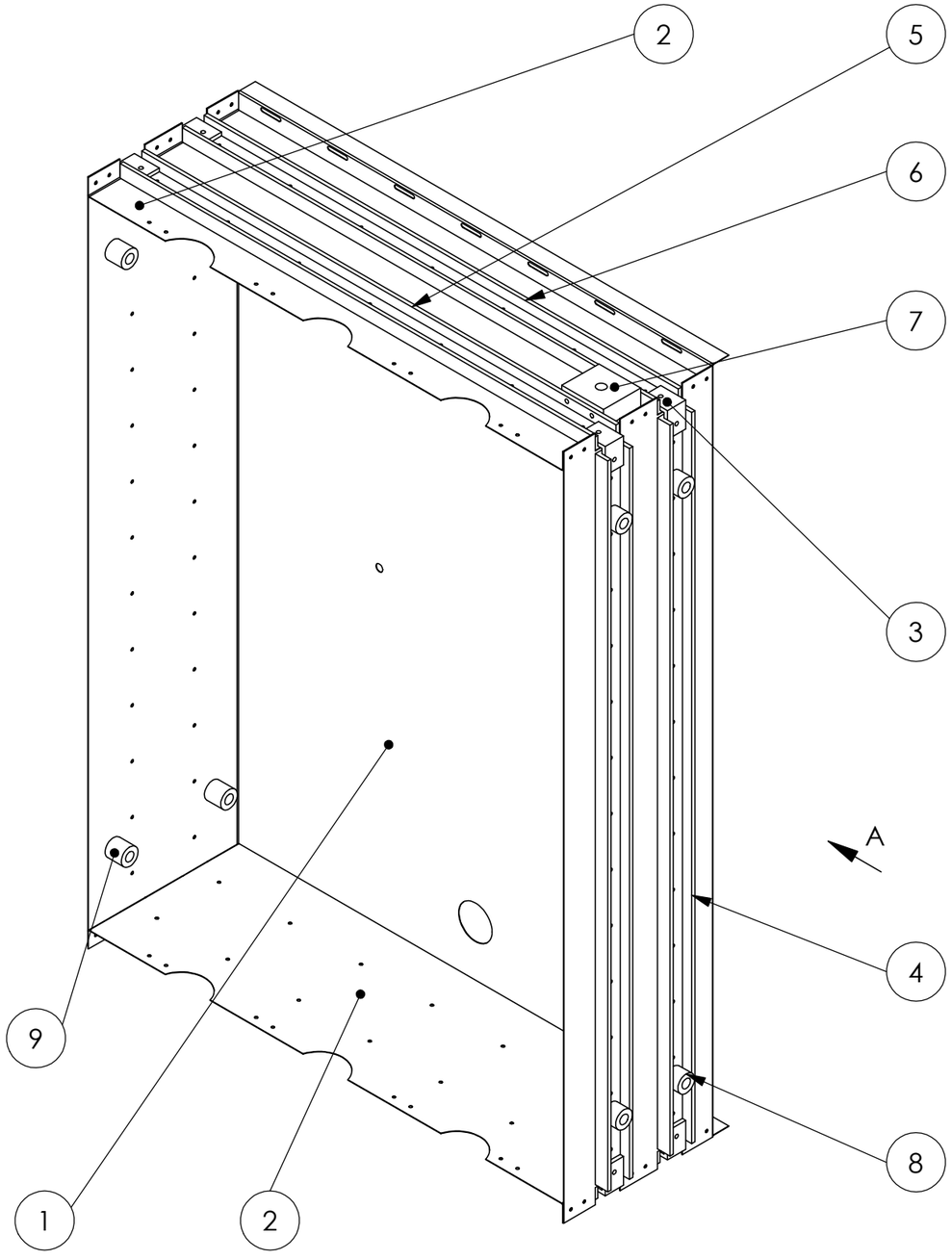

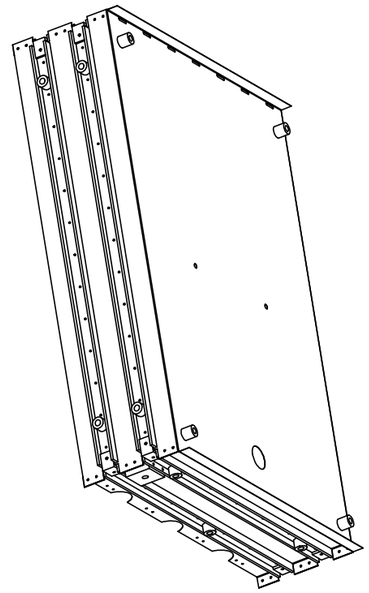

A

ITEM NO.	PART NUMBER	DESCRIPTION	QTY.
1	Des 2020013002	chapa_media_1_bh	1
2	Des 2020013003	chapa_media_2_bh	2
3	Des 2020013004	cantoneira_L	8
4	Des 2020013005	U_20_40_5_vert	4
5	Des 2020013006	U_15_40_5_hor_furo_2	2
6	Des 2020013007	U_15_40_5_hor_furo_1	2
7	Des 2020013008	apoio_suporte	2
8	Des 2020013009	batente_L15.5	11
9	Des 2020012903	batente_L19.5	12

UNLESS OTHERWISE SPECIFIED:
DIMENSIONS ARE IN MILLIMETERS
SURFACE FINISH:
TOLERANCES:
LINEAR:
ANGULAR:

FINISH:

DEBURR AND BREAK SHARP EDGES

DO NOT SCALE DRAWING | REVISION

	NAME	SIGNATURE	DATE
DRAWN			
CHK'D			
APPV'D			
MFG			
Q.A			

MATERIAL:

WEIGHT:

TITLE:
2.chamber_back_half_medio_rigidez_batente

DWG NO.
Des 2020013001

A3

SCALE:1:10

SHEET 1 OF 9

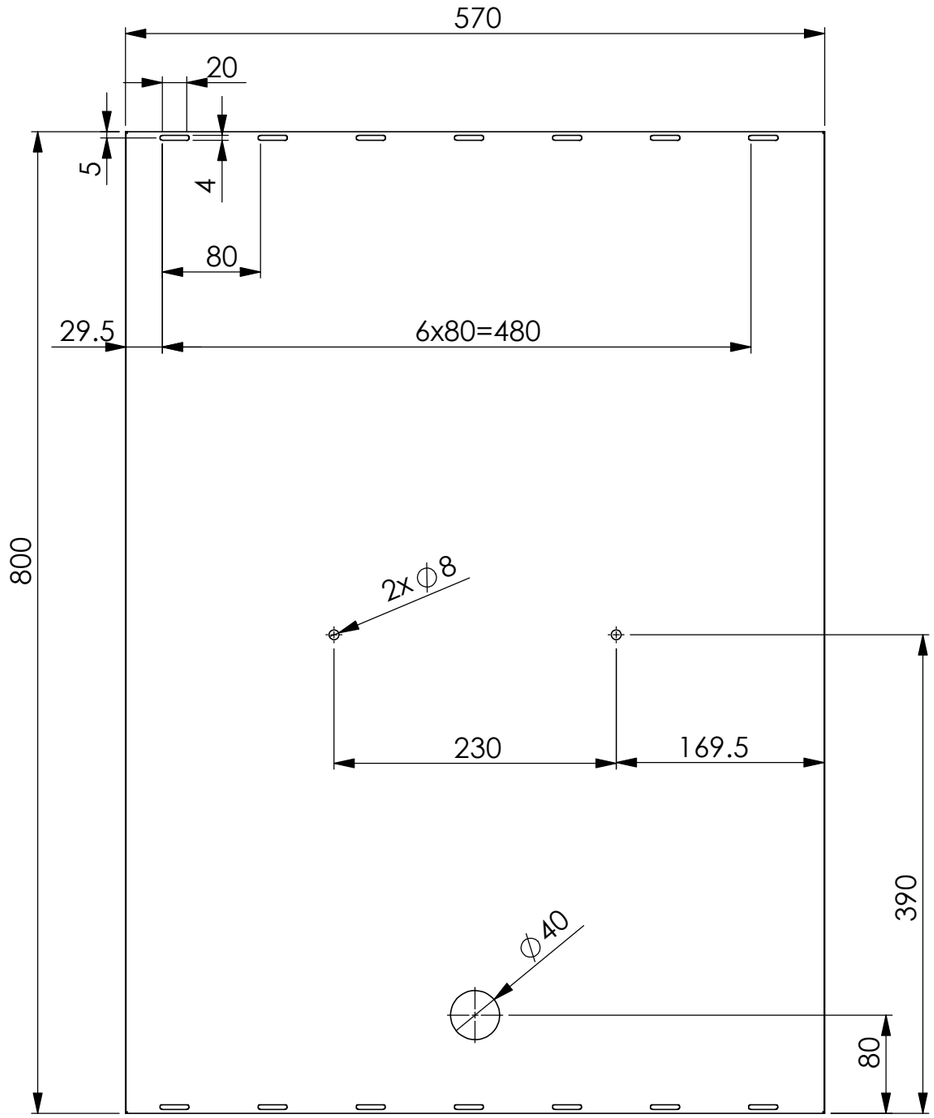

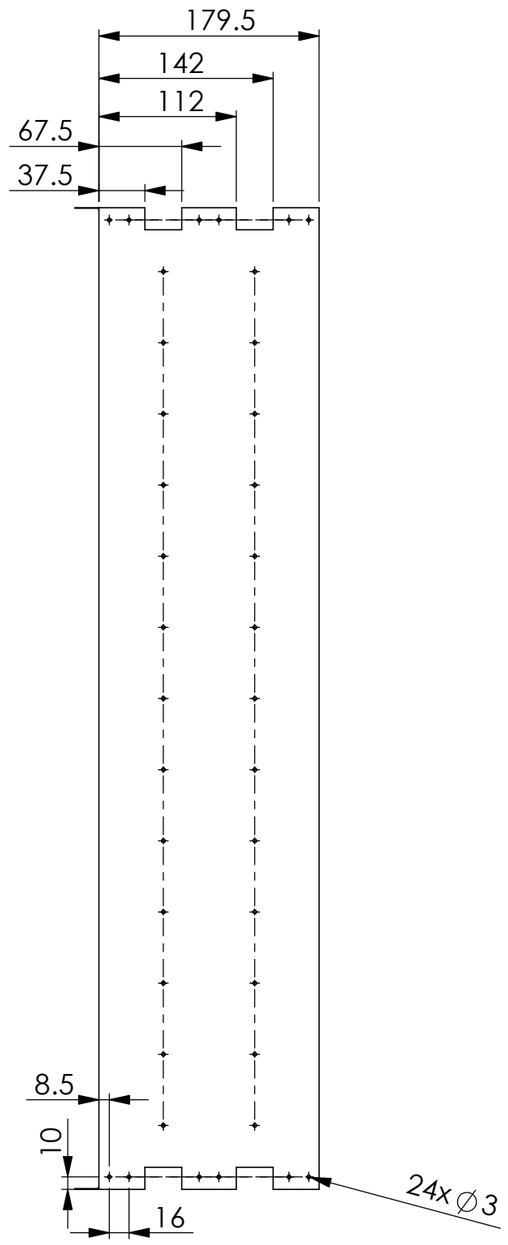

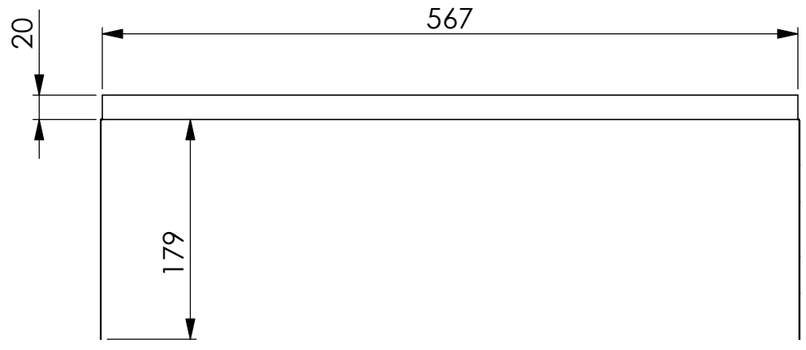

Inox AISI 304

chapa t= 0.5

Furos não cotados a fazer durante a montagem

UNLESS OTHERWISE SPECIFIED: DIMENSIONS ARE IN MILLIMETERS SURFACE FINISH: TOLERANCES: LINEAR: ANGULAR:		FINISH:		DEBURR AND BREAK SHARP EDGES		DO NOT SCALE DRAWING	REVISION
	NAME	SIGNATURE	DATE			TITLE: chapa_media_1_bh	
DRAWN							
CHK'D							
APPV'D							
MFG							
Q.A				MATERIAL:		DWG NO. Des 2020013002	A3
				WEIGHT:		SCALE:1:10	SHEET 2 OF 9

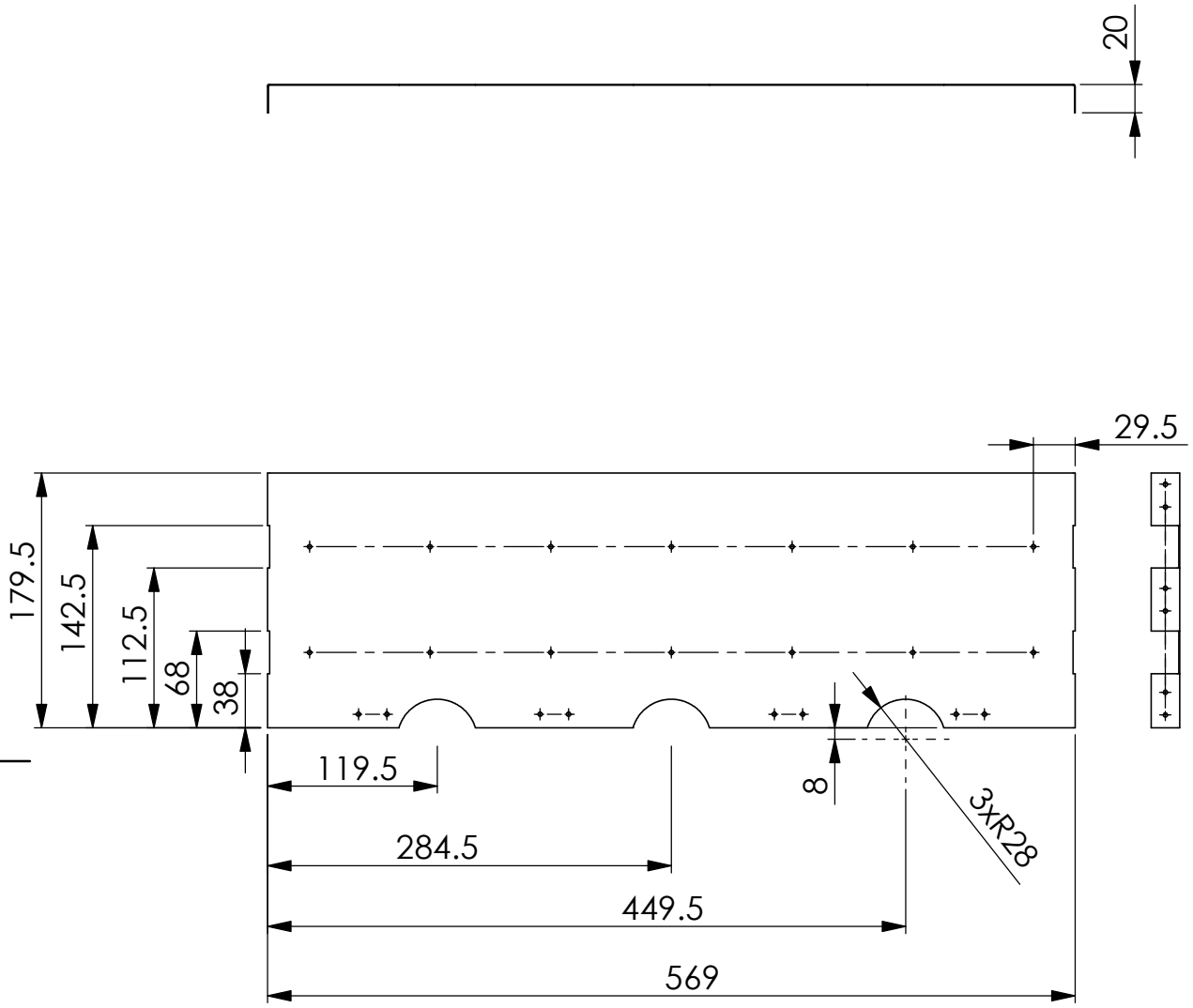

Inox AISI 304

chapa t= 0.5

Furos não cotados a fazer durante a montagem

UNLESS OTHERWISE SPECIFIED: DIMENSIONS ARE IN MILLIMETERS SURFACE FINISH: TOLERANCES: LINEAR: ANGULAR:	FINISH:	DEBURR AND BREAK SHARP EDGES	DO NOT SCALE DRAWING / REVISION

	NAME	SIGNATURE	DATE
DRAWN			
CHK'D			
APPV'D			
MFG			
Q.A			

TITLE:	chapa_media_2_bh
MATERIAL:	
DWG NO.	Des 2020013004
A4	
WEIGHT:	
SCALE:1:10	SHEET 3 OF 9

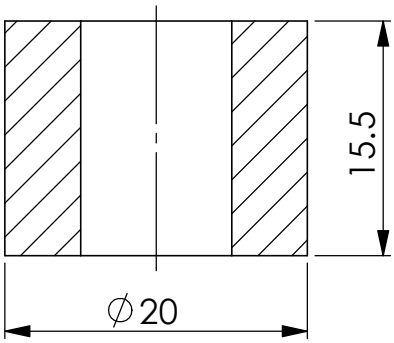

Teflon
26 peças

UNLESS OTHERWISE SPECIFIED: DIMENSIONS ARE IN MILLIMETERS SURFACE FINISH: TOLERANCES: LINEAR: ANGULAR:	FINISH:		DEBURR AND BREAK SHARP EDGES	DO NOT SCALE DRAWING	REVISION	
	NAME	SIGNATURE	DATE	TITLE: batente_L15.5		
DRAWN						
CHK'D						
APPV'D						
MFG						
Q.A				MATERIAL:	DWG NO. Des 2020013009	A4
				WEIGHT:	SCALE:2:1	SHEET 4 OF 9

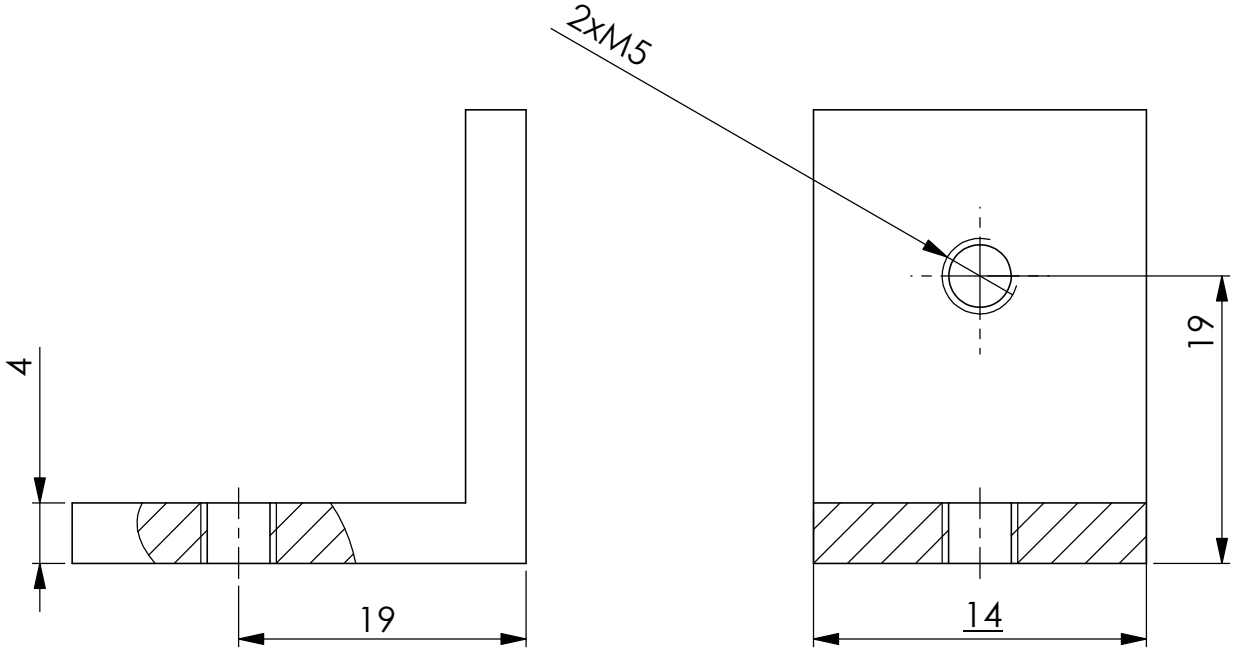

Perfil L 30x30x4

DIN 17100

UNLESS OTHERWISE SPECIFIED: DIMENSIONS ARE IN MILLIMETERS SURFACE FINISH: TOLERANCES: LINEAR: ANGULAR:	FINISH:		DEBURR AND BREAK SHARP EDGES		DO NOT SCALE DRAWING	REVISION
	NAME	SIGNATURE	DATE		TITLE:	
DRAWN					cantoneira_L	
CHK'D						
APPV'D						
MFG						
Q.A				MATERIAL:	DWG NO. Des 2020013004	A4
				WEIGHT:	SCALE:2:1	SHEET 5 OF 9

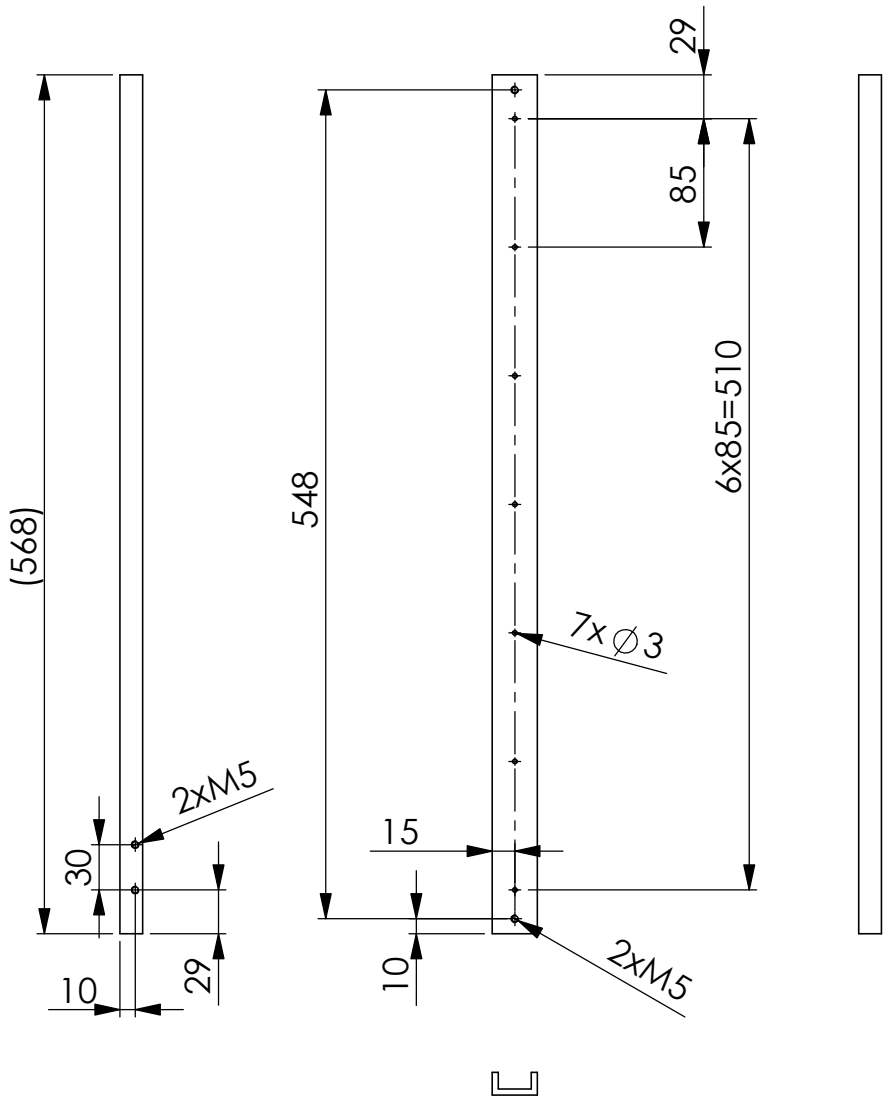

Perfil U 30x15x4

DIN 17100

UNLESS OTHERWISE SPECIFIED: DIMENSIONS ARE IN MILLIMETERS SURFACE FINISH: TOLERANCES: LINEAR: ANGULAR:			FINISH:		DEBURR AND BREAK SHARP EDGES	DO NOT SCALE DRAWING / REVISION
	NAME	SIGNATURE	DATE			TITLE: U_15_40_5_hor_furo_1
DRAWN						
CHK'D						
APPV'D						
MFG						
Q.A				MATERIAL:		DWG NO. Des 2020013007 / A4
				WEIGHT:		SCALE:1:5 / SHEET 6 OF 9

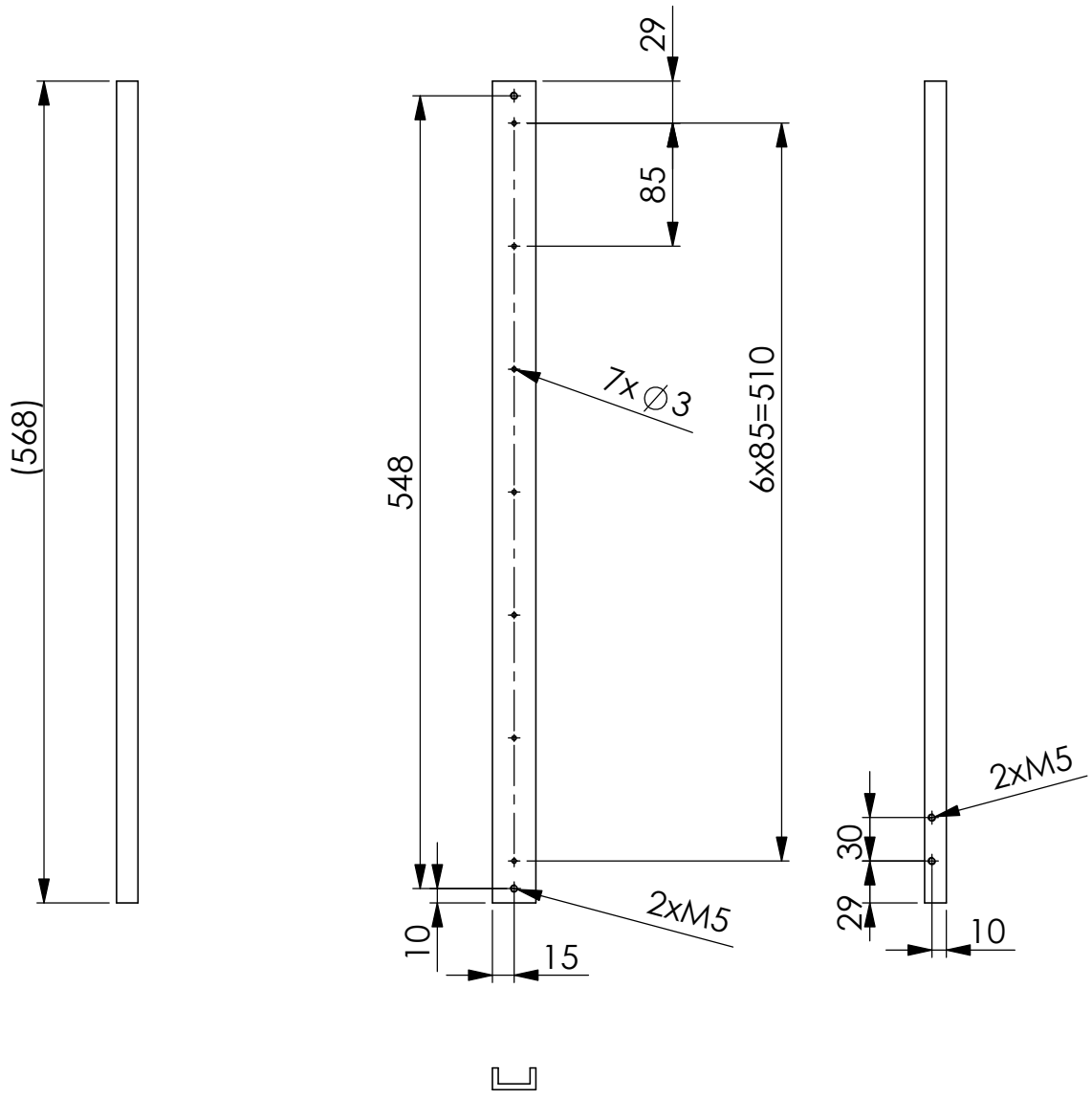

Perfil U 30x15x4
DIN 17100

UNLESS OTHERWISE SPECIFIED: DIMENSIONS ARE IN MILLIMETERS SURFACE FINISH: TOLERANCES: LINEAR: ANGULAR:	FINISH:	DEBURR AND BREAK SHARP EDGES	DO NOT SCALE DRAWING / REVISION

	NAME	SIGNATURE	DATE
DRAWN			
CHK'D			
APPV'D			
MFG			
Q.A			

TITLE: U_15_40_5_hor_furo_2

MATERIAL:

DWG NO. Des2020013006

A4

WEIGHT:

SCALE:1:5

SHEET 7 OF 9

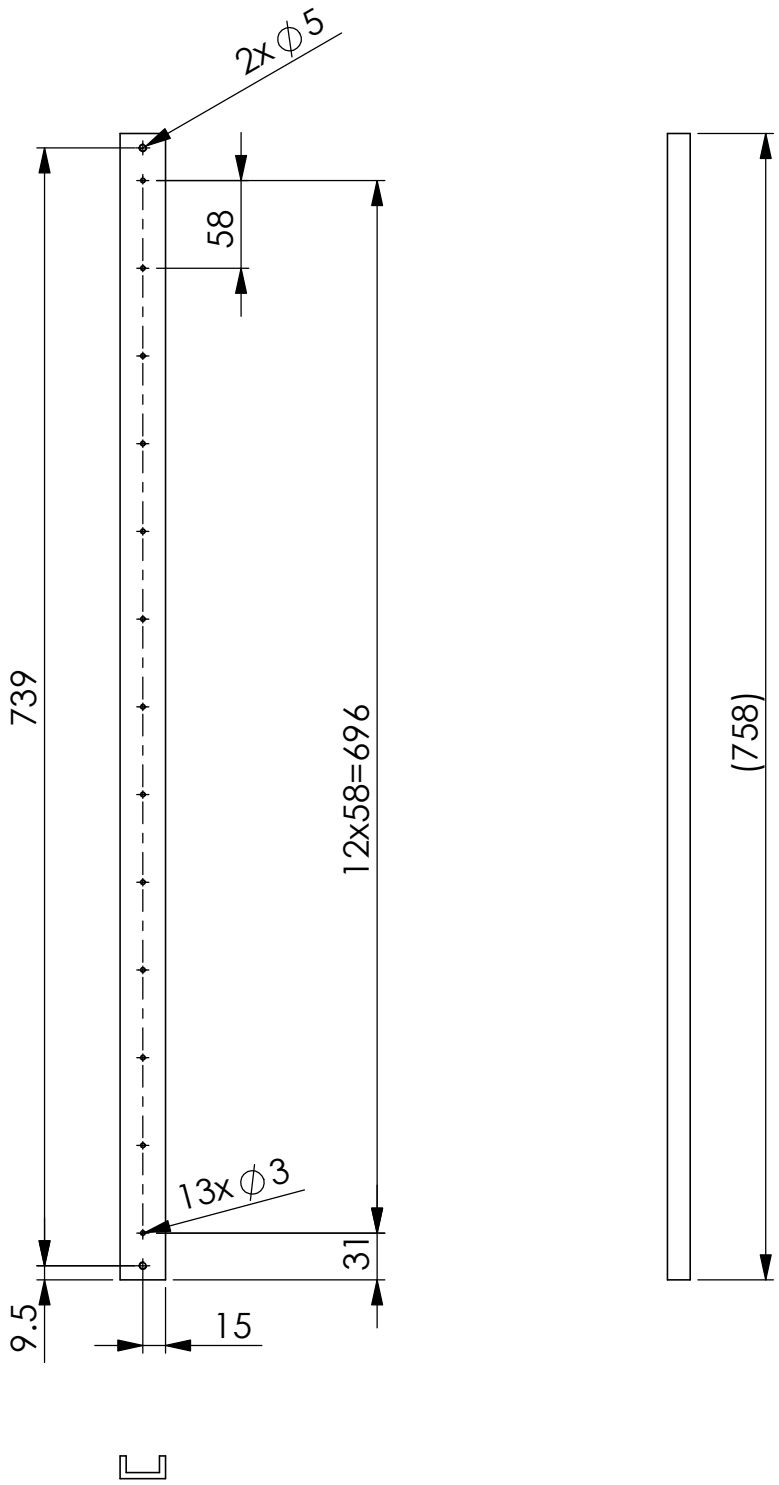

Perfil U 30x15x4

DIN 17100

UNLESS OTHERWISE SPECIFIED: DIMENSIONS ARE IN MILLIMETERS SURFACE FINISH: TOLERANCES: LINEAR: ANGULAR:	FINISH:		DEBURR AND BREAK SHARP EDGES	DO NOT SCALE DRAWING	REVISION	
	NAME	SIGNATURE	DATE	TITLE: U_20_40_5_vert		
DRAWN						
CHK'D						
APPV'D						
MFG						
Q.A				MATERIAL:	DWG NO. Des 2020013005	A4
				WEIGHT:	SCALE:1:5	SHEET 8 OF 9

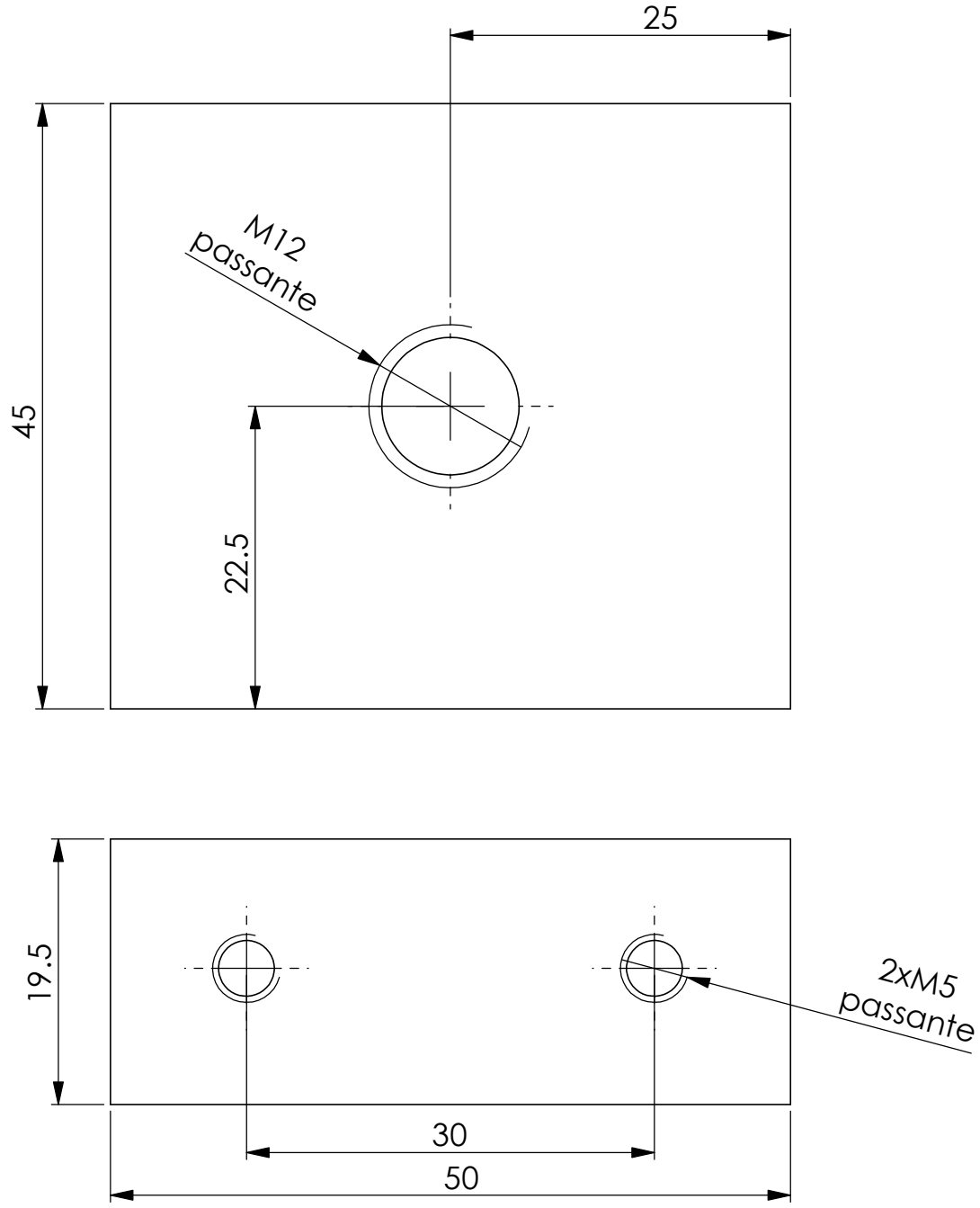

Al 6061 T6

UNLESS OTHERWISE SPECIFIED: DIMENSIONS ARE IN MILLIMETERS SURFACE FINISH: TOLERANCES: LINEAR: ANGULAR:	FINISH:	DEBURR AND BREAK SHARP EDGES	DO NOT SCALE DRAWING / REVISION

	NAME	SIGNATURE	DATE
DRAWN			
CHK'D			
APPV'D			
MFG			
Q.A			

TITLE: apoio_suporte

MATERIAL:

DWG NO. Des 2020013008

A4

WEIGHT:

SCALE:2:1

SHEET 9 OF 9

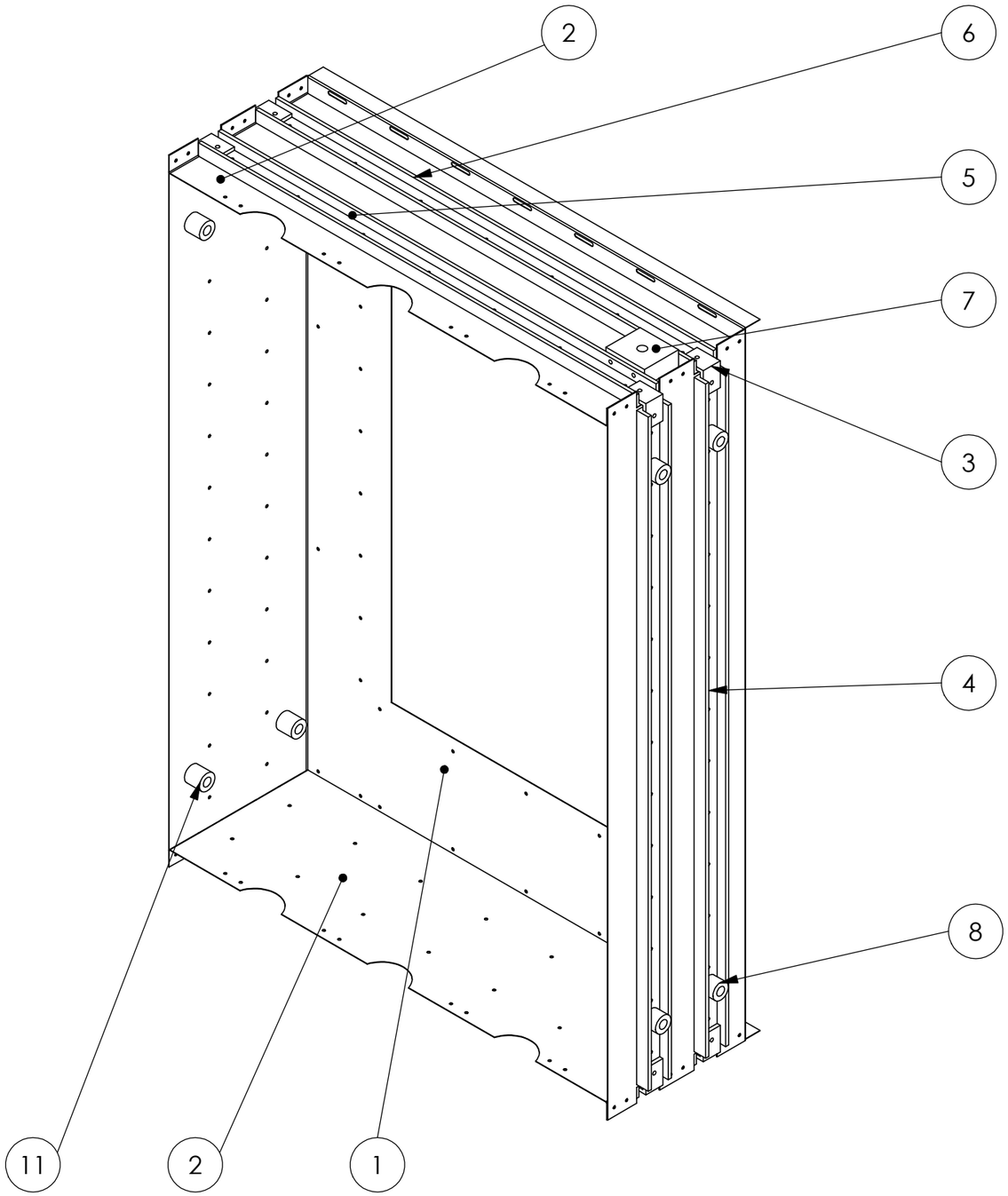

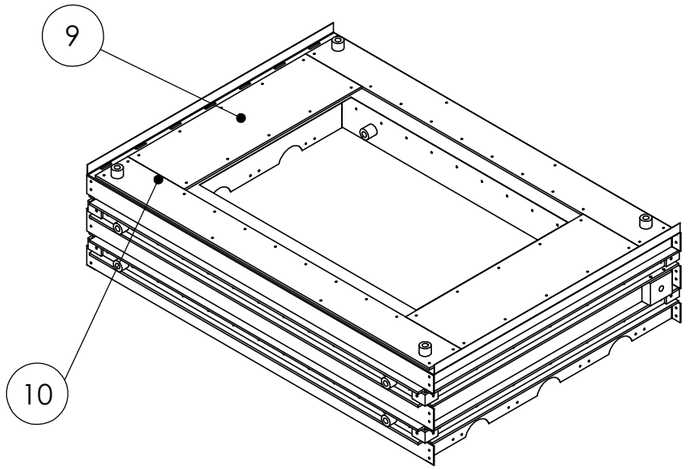

ITEM NO.	PART NUMBER	DESCRIPTION	QTY.
1	Des 2020020101	chapa_media_1_fh	1
2	Des 2020013003	hapa_media_2_bh	2
3	Des 2020013004	cantoneira_L	8
4	Des 2020013005	U_20_40_5_vert	4
5	Des 2020013006	U_15_40_5_hor_furo_2	2
6	Des 2020013007	U_15_40_5_hor_furo_1	2
7	Des 2020013008	apoio_suporte	2
8	Des 2020013009	batente_L15.5	15
9	Des 2020020103	chapa_rigidez_horizontal_fh	2
10	Des 2020020104	chapa_rigidez_vertical_fh	2
11	Des 2020012903	batente_L19.5	8

UNLESS OTHERWISE SPECIFIED:
DIMENSIONS ARE IN MILLIMETERS
SURFACE FINISH:
TOLERANCES:
LINEAR:
ANGULAR:

FINISH:

DEBURR AND BREAK SHARP EDGES

DO NOT SCALE DRAWING

REVISION

	NAME	SIGNATURE	DATE
DRAWN			
CHK'D			
APPV'D			
MFG			
Q.A			

MATERIAL:

WEIGHT:

TITLE:

2.chamber_front_half_medio_rigidez_batente

DWG NO.

Des 2020020101

A3

SCALE:1:10

SHEET 1 OF 4

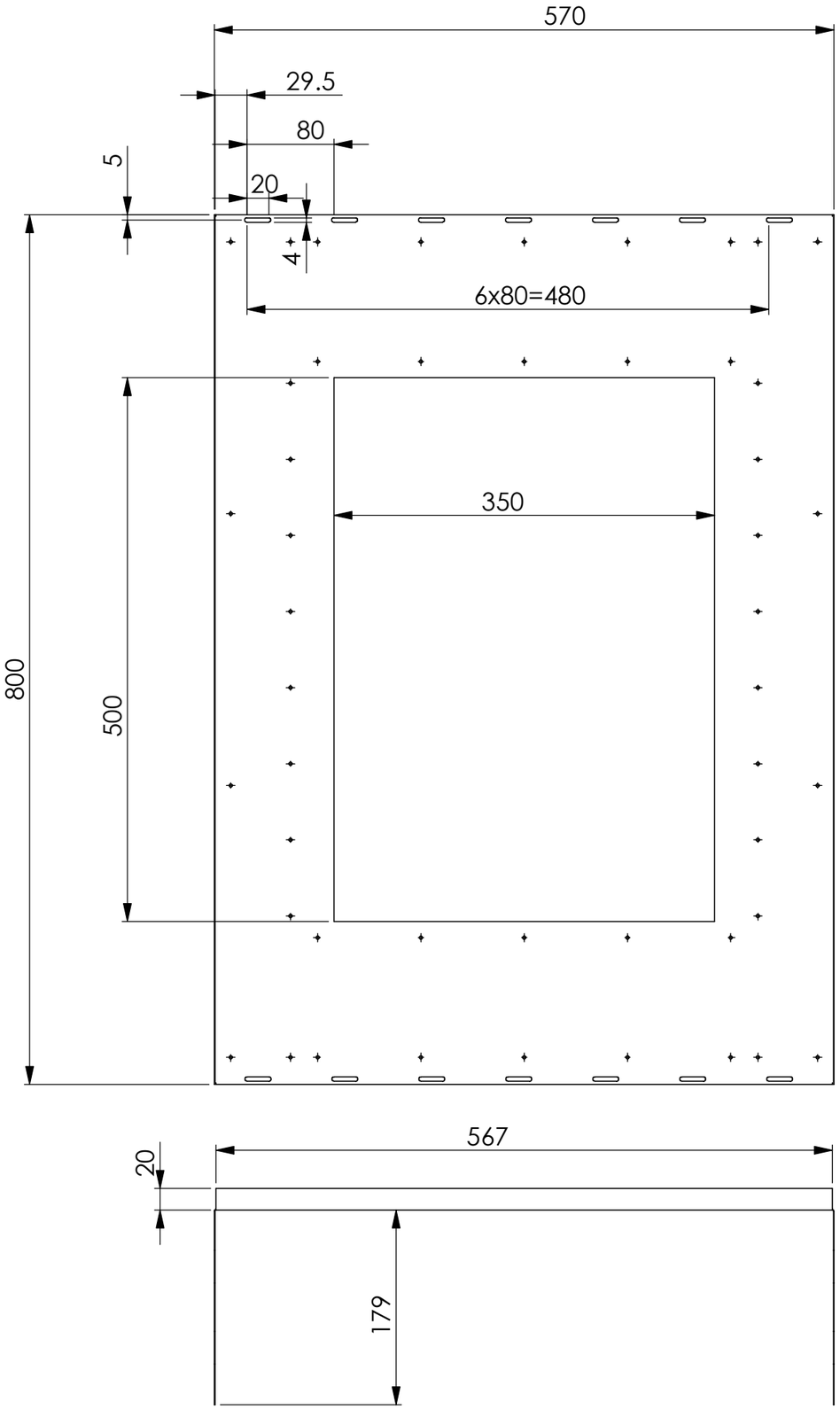

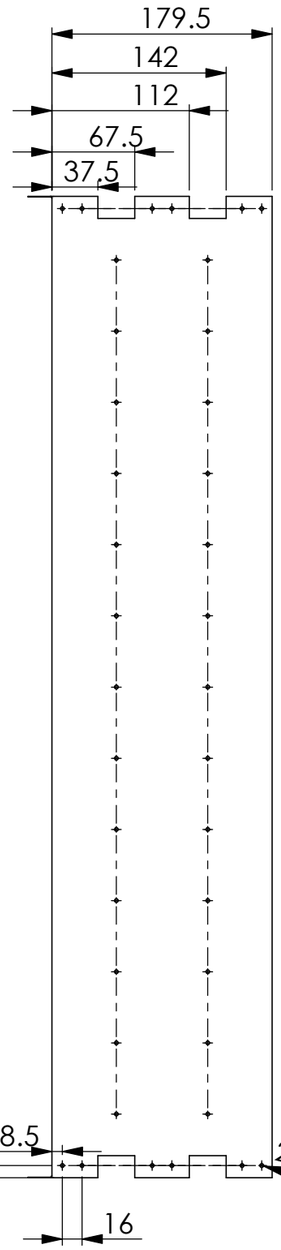

Inox AISI 304

chapa t= 0.5

Furos não cotados a fazer durante a montagem

UNLESS OTHERWISE SPECIFIED: DIMENSIONS ARE IN MILLIMETERS SURFACE FINISH: TOLERANCES: LINEAR: ANGULAR:		FINISH:		DEBURR AND BREAK SHARP EDGES		DO NOT SCALE DRAWING	REVISION
	NAME	SIGNATURE	DATE			TITLE: chapa_media_1_fh	
DRAWN							
CHK'D							
APPV'D							
MFG							
Q.A				MATERIAL:		DWG NO. Des 2020020101	A3
				WEIGHT:		SCALE:1:10	SHEET 2 OF 4

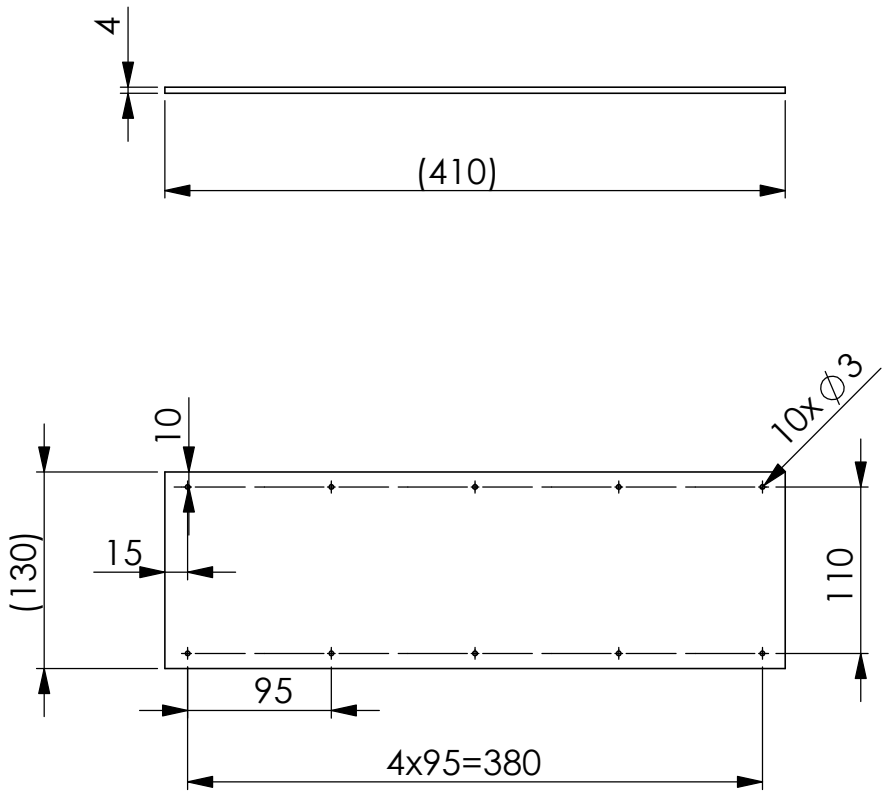

Inox AISI 304

UNLESS OTHERWISE SPECIFIED: DIMENSIONS ARE IN MILLIMETERS SURFACE FINISH: TOLERANCES: LINEAR: ANGULAR:	FINISH:		DEBURR AND BREAK SHARP EDGES	DO NOT SCALE DRAWING	REVISION	
	NAME	SIGNATURE	DATE			
DRAWN						
CHK'D						
APPV'D						
MFG						
Q.A				MATERIAL:	DWG NO. Des 2020020103	A4
				WEIGHT:	SCALE:1:5	SHEET 3 OF 4

TITLE: chapa_rigidez_horizontal_fh

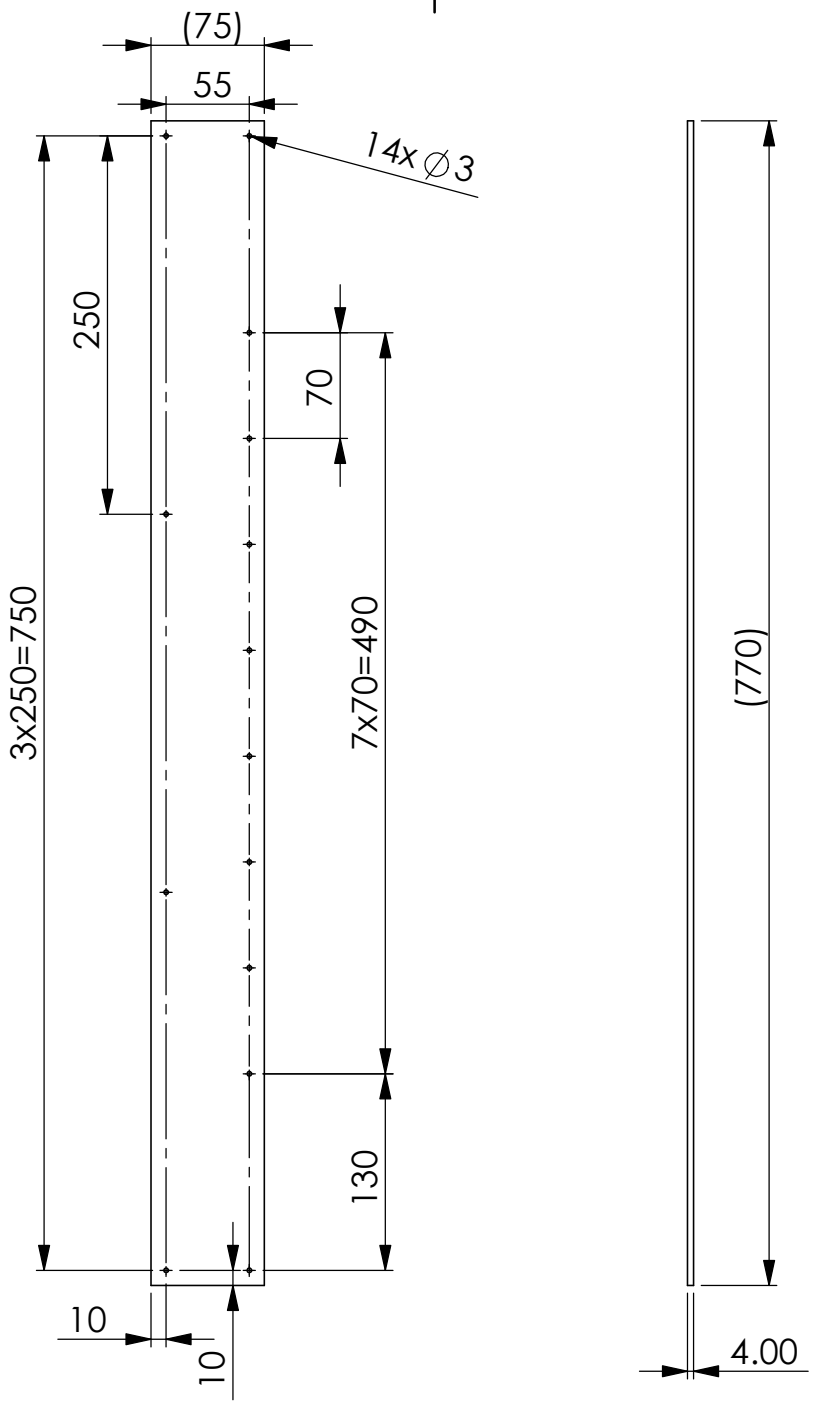

Inox AISI 304

UNLESS OTHERWISE SPECIFIED: DIMENSIONS ARE IN MILLIMETERS SURFACE FINISH: TOLERANCES: LINEAR: ANGULAR:	FINISH:	DEBURR AND BREAK SHARP EDGES	DO NOT SCALE DRAWING / REVISION

	NAME	SIGNATURE	DATE
DRAWN			
CHK'D			
APPV'D			
MFG			
Q.A			

TITLE: chapa_rigidez_vertical_fh

MATERIAL:

DWG NO. Des 2020020104

A4

WEIGHT:

SCALE:1:5

SHEET 4 OF 4

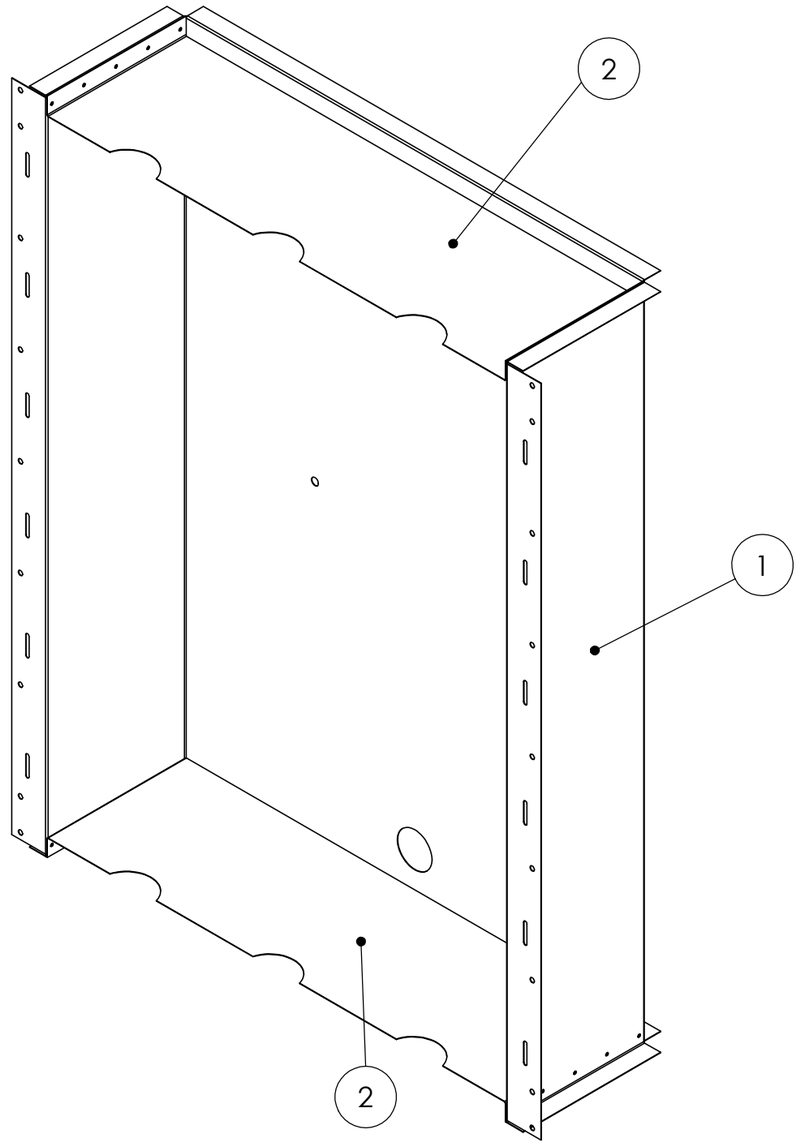

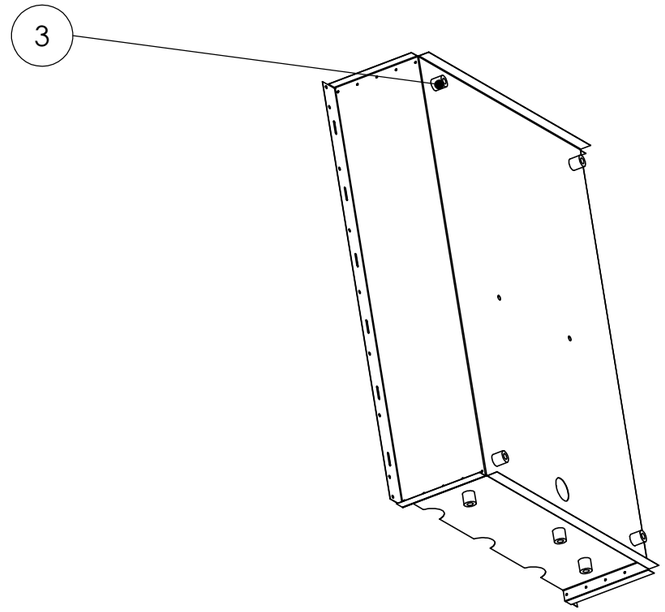

A (1 : 10)

ITEM NO.	PART NUMBER	DESCRIPTION	QTY.
1	Des 2020012901	chapa_interior_1_bh	1
2	Des 2020012902	chapa_interior_2_bh	2
3	Des 2020012903	batente_L19.5	7

UNLESS OTHERWISE SPECIFIED: DIMENSIONS ARE IN MILLIMETERS SURFACE FINISH: TOLERANCES: LINEAR: ANGULAR:		FINISH:		DEBURR AND BREAK SHARP EDGES		DO NOT SCALE DRAWING	REVISION
	NAME	SIGNATURE	DATE			TITLE:	
DRAWN						3.chamber_back_half_interior	
CHK'D							
APPV'D							
MFG							
Q.A				MATERIAL:		DWG NO.	A3
						Des 20202904	
				WEIGHT:		SCALE:1:5	SHEET 1 OF 1

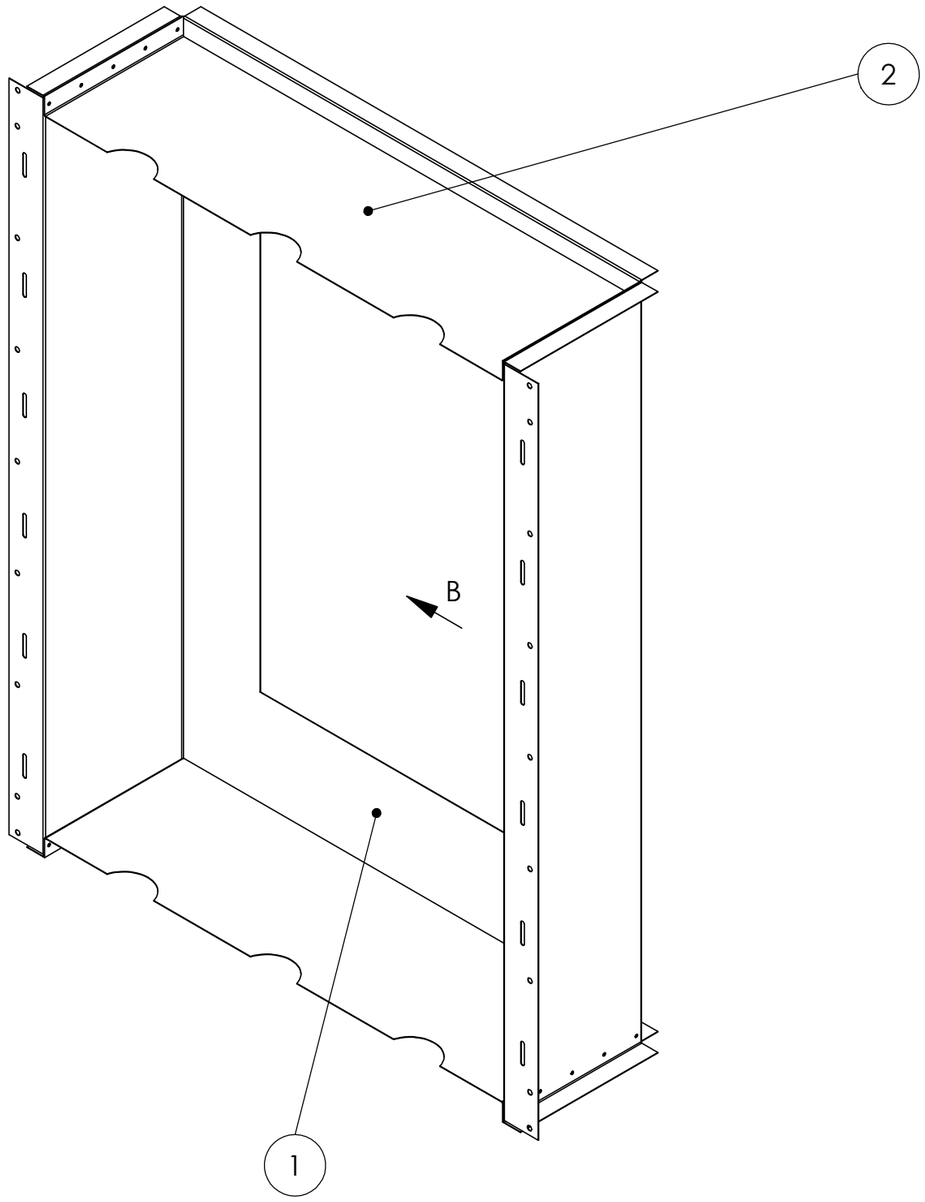

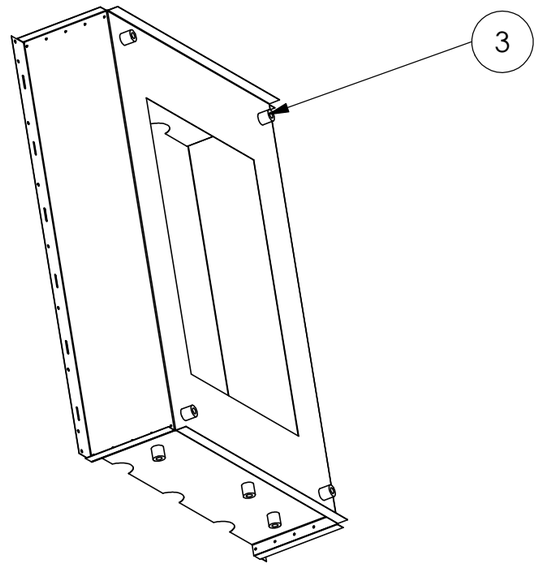

B

ITEM NO.	PART NUMBER	DESCRIPTION	QTY.
1	Des 2020013105	chapa_interior_1_fh	1
2	Des 2020012902	chapa_interior_2_fh	2
3	Des 2020012903	batente_L19.5	7

UNLESS OTHERWISE SPECIFIED: DIMENSIONS ARE IN MILLIMETERS SURFACE FINISH: TOLERANCES: LINEAR: ANGULAR:	FINISH:		DEBURR AND BREAK SHARP EDGES		DO NOT SCALE DRAWING	REVISION	
	NAME	SIGNATURE	DATE				TITLE: 3.chamber_front_half_interior
DRAWN							
CHK'D							
APPV'D							
MFG							
Q.A				MATERIAL:			DWG NO. Des 2020013106 A3
				WEIGHT:		SCALE:1:10	SHEET 1 OF 2

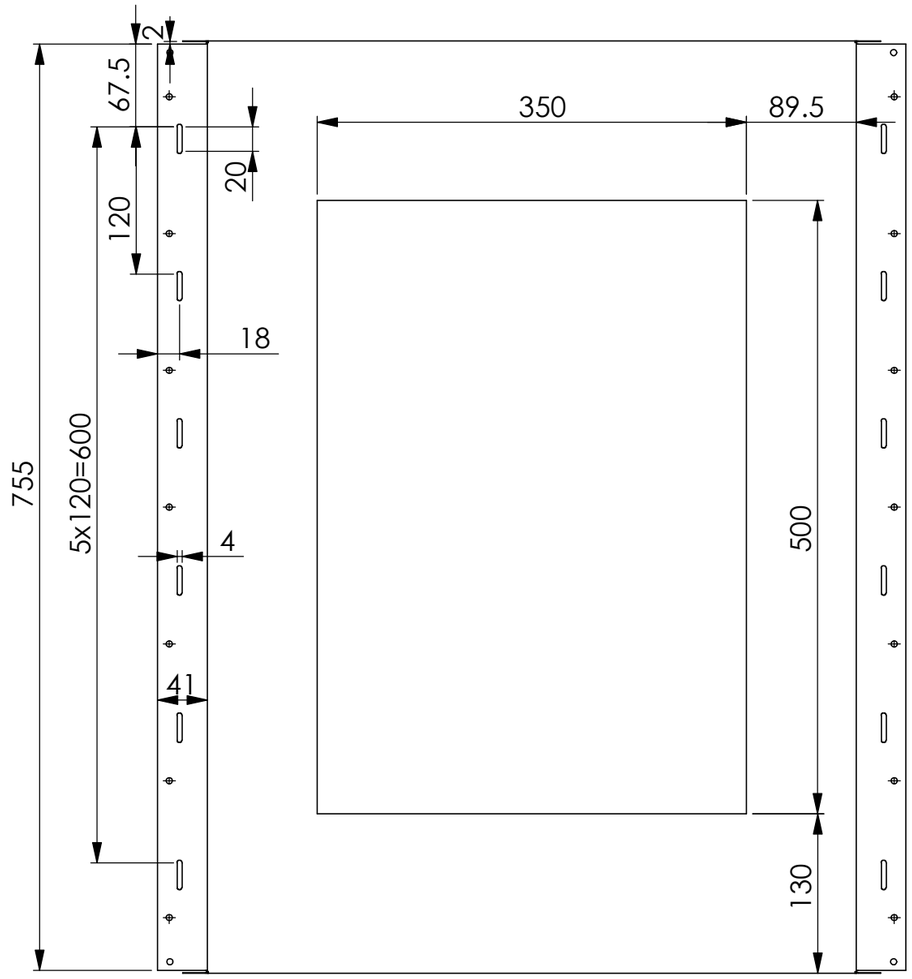

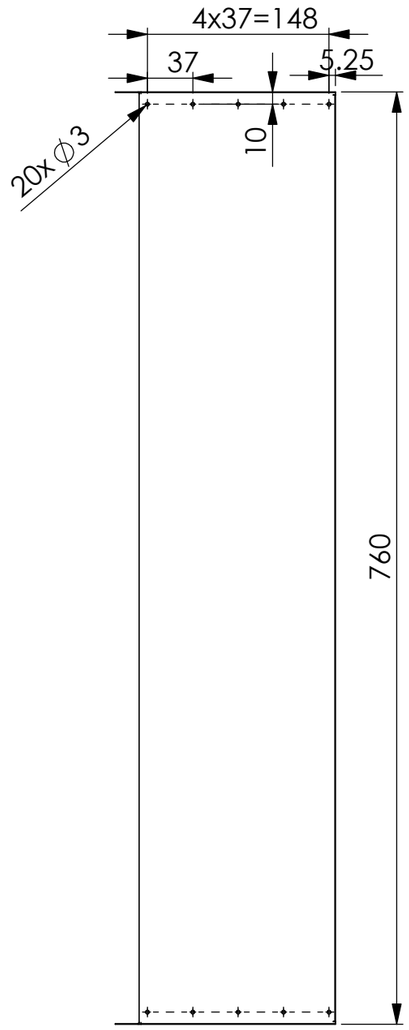

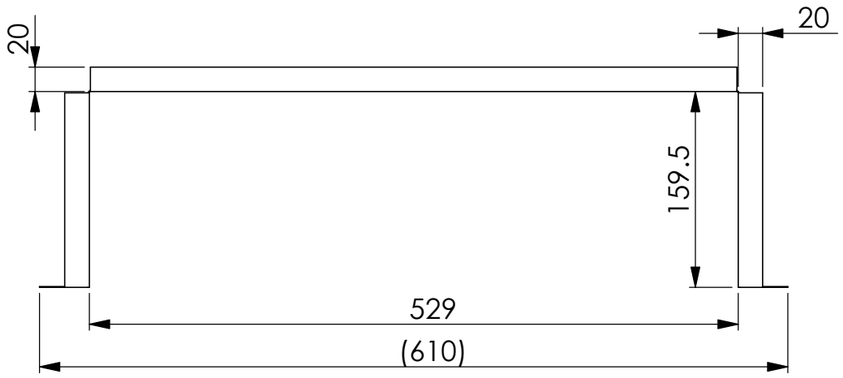

Inox AISI 304

chapa t= 0.5

Furos não cotados a fazer durante a montagem

UNLESS OTHERWISE SPECIFIED: DIMENSIONS ARE IN MILLIMETERS SURFACE FINISH: TOLERANCES: LINEAR: ANGULAR:		FINISH:		DEBURR AND BREAK SHARP EDGES		DO NOT SCALE DRAWING	REVISION
	NAME	SIGNATURE	DATE			TITLE: chapa_interior_1_fh	
DRAWN							
CHK'D							
APPV'D							
MFG							
Q.A				MATERIAL:		DWG NO. Des 2020013105	A3
				WEIGHT:		SCALE:1:10	SHEET 2 OF 2

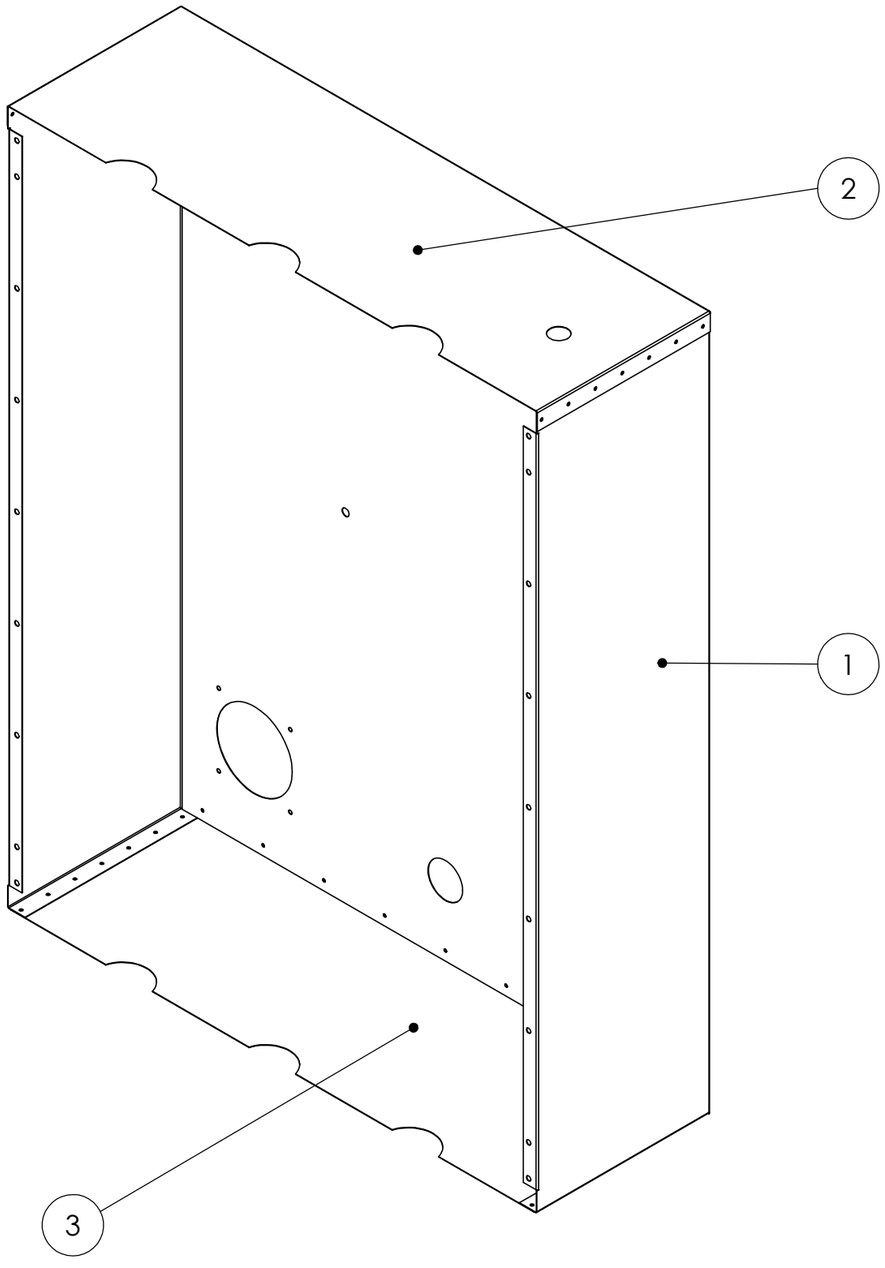

ITEM NO.	PART NUMBER	DESCRIPTION	QTY.
1	Des 2020013102	chapa_exterior_bh	1
2	Des 2020013103	chapa_top_bh	1
3	Des 2020013104	chapa_bottom_bh	1

UNLESS OTHERWISE SPECIFIED:
DIMENSIONS ARE IN MILLIMETERS
SURFACE FINISH:
TOLERANCES:
LINEAR:
ANGULAR:

FINISH:

DEBURR AND BREAK SHARP EDGES

DO NOT SCALE DRAWING

REVISION

	NAME	SIGNATURE	DATE
DRAWN			
CHK'D			
APPV'D			
MFG			
Q.A			

MATERIAL:

WEIGHT:

TITLE:
4.chamber_back_half_exterior

DWG NO. Des 2020013101

A3

SCALE:1:10

SHEET 1 OF 4

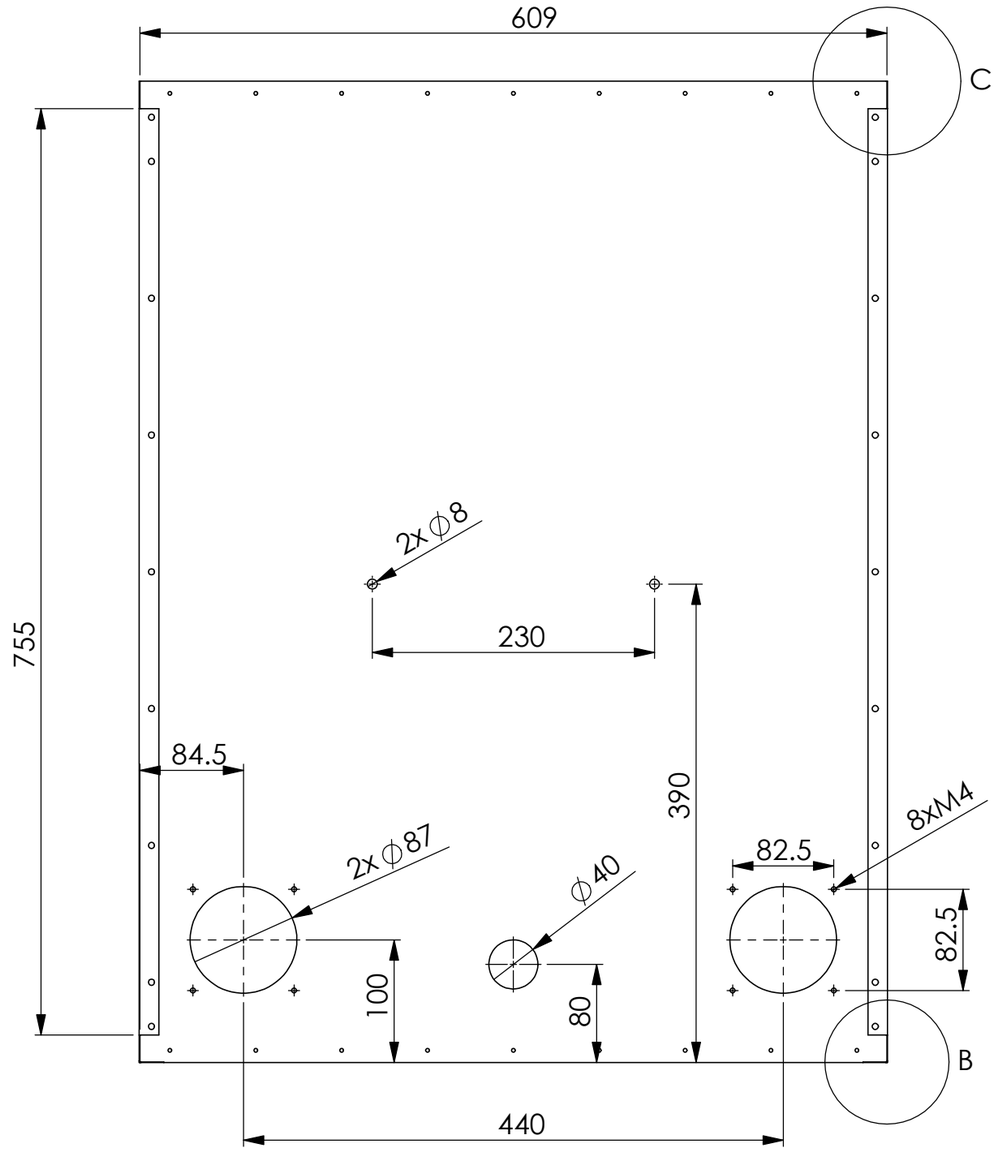

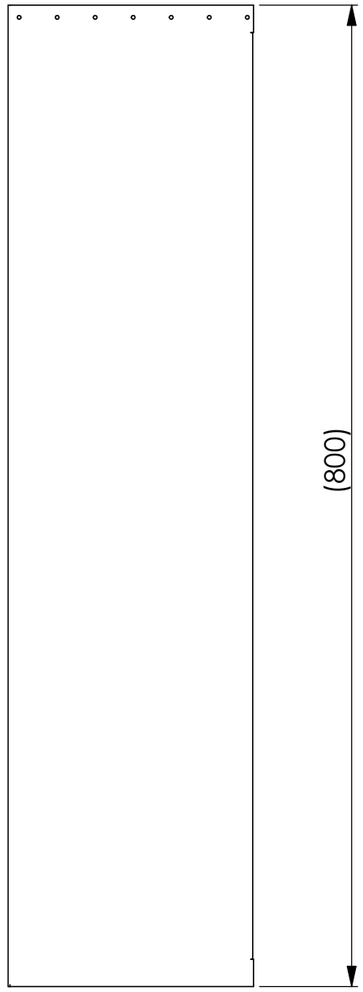

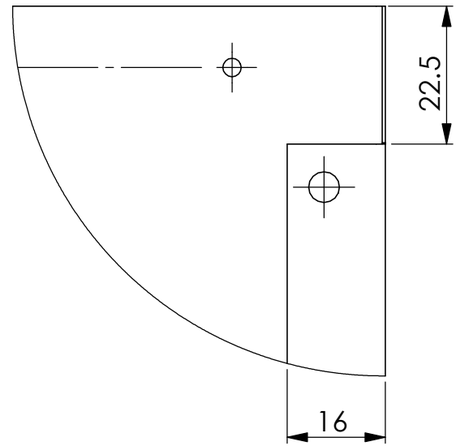

C (1 : 1)

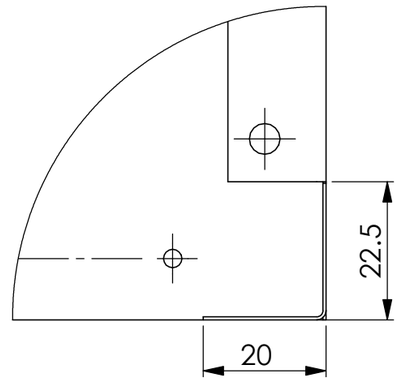

B (1 : 1)

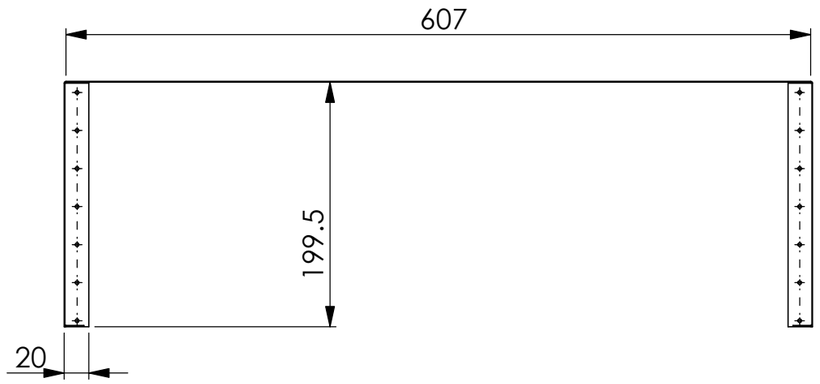

Inox AISI 304

chapa t= 0.5

Furos não cotados a fazer durante a montagem

UNLESS OTHERWISE SPECIFIED: DIMENSIONS ARE IN MILLIMETERS SURFACE FINISH: TOLERANCES: LINEAR: ANGULAR:	FINISH:		DEBURR AND BREAK SHARP EDGES	DO NOT SCALE DRAWING	REVISION	
	NAME	SIGNATURE	DATE	TITLE: chapa_exterior_bh		
DRAWN						
CHK'D						
APPV'D						
MFG						
Q.A				MATERIAL:	DWG NO. Des 2020013102	A3
				WEIGHT:	SCALE:1:10	SHEET 2 OF 4

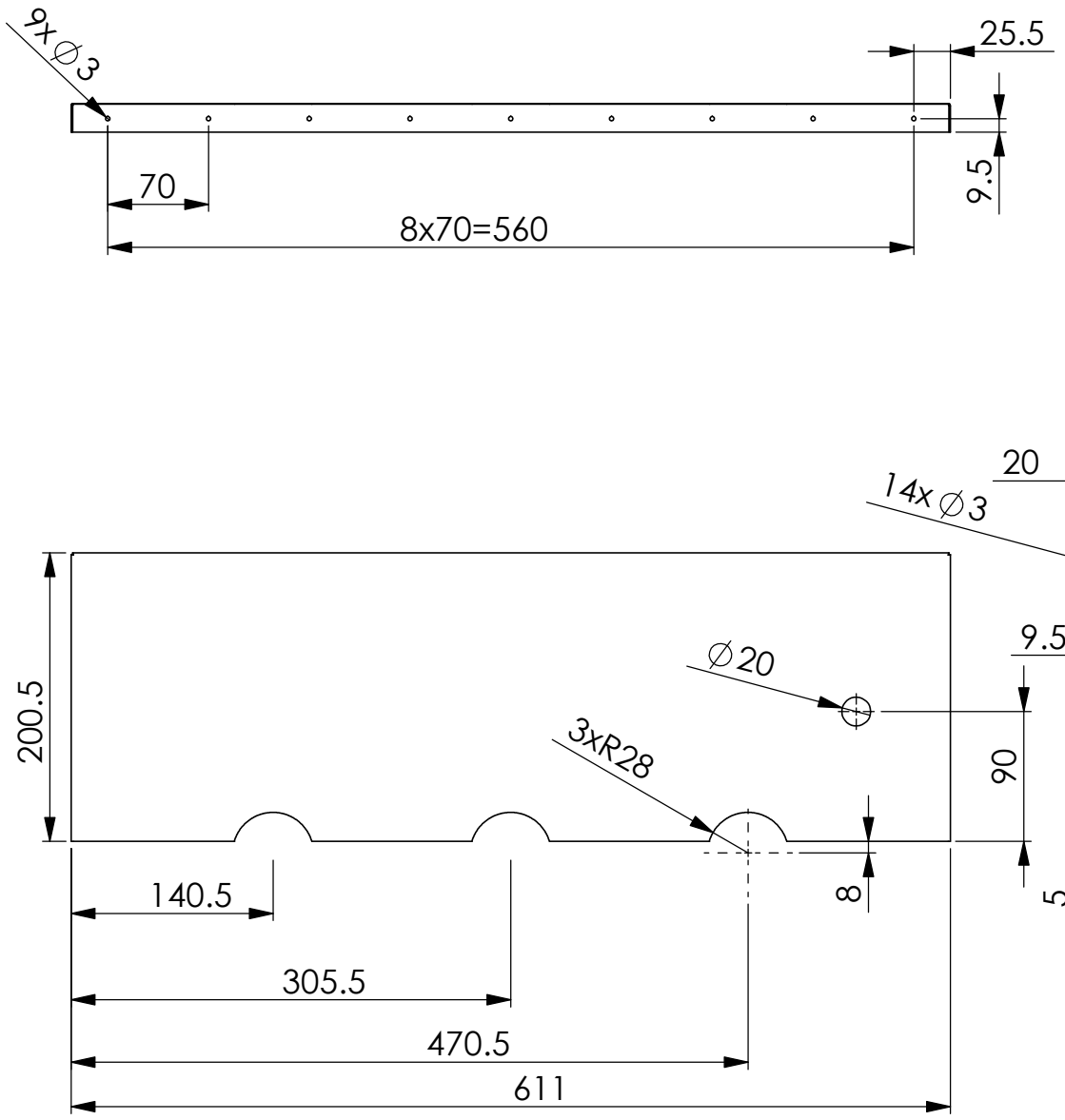

Inox AISI 304

chapa t= 0.5

UNLESS OTHERWISE SPECIFIED: DIMENSIONS ARE IN MILLIMETERS SURFACE FINISH: TOLERANCES: LINEAR: ANGULAR:	FINISH:		DEBURR AND BREAK SHARP EDGES		DO NOT SCALE DRAWING	REVISION
	NAME	SIGNATURE	DATE		TITLE: chapa_top_bh	
DRAWN						
CHK'D						
APPV'D						
MFG						
Q.A				MATERIAL:	DWG NO. Des 2020013103	A4
				WEIGHT:	SCALE:1:10	SHEET 3 OF 4

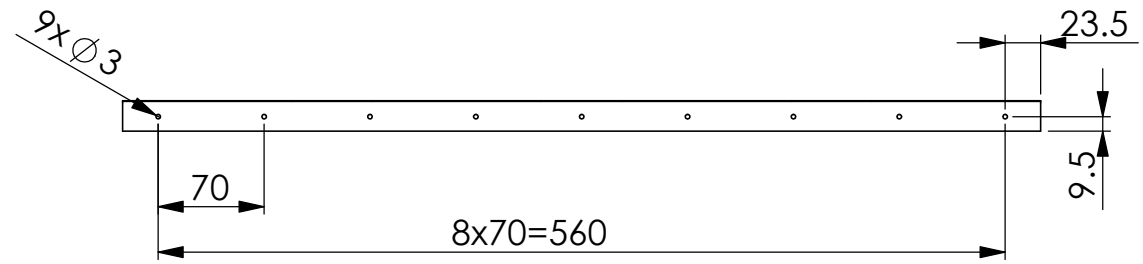

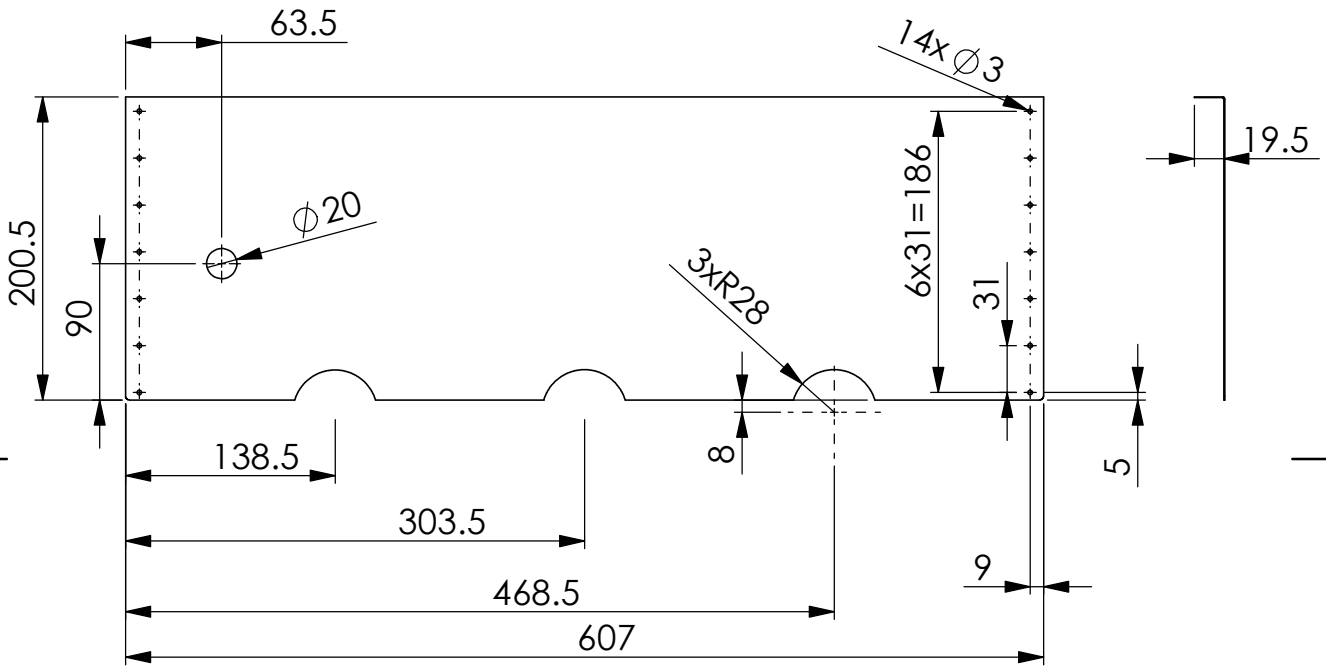

Inox AISI 304

chapa t= 0.5

UNLESS OTHERWISE SPECIFIED: DIMENSIONS ARE IN MILLIMETERS SURFACE FINISH: TOLERANCES: LINEAR: ANGULAR:	FINISH:	DEBURR AND BREAK SHARP EDGES	DO NOT SCALE DRAWING / REVISION

	NAME	SIGNATURE	DATE
DRAWN			
CHK'D			
APPV'D			
MFG			
Q.A			

TITLE: chapa_bottom_bh

MATERIAL:

DWG NO. Des 2020013104

A4

WEIGHT:

SCALE:1:10

SHEET 4 OF 4

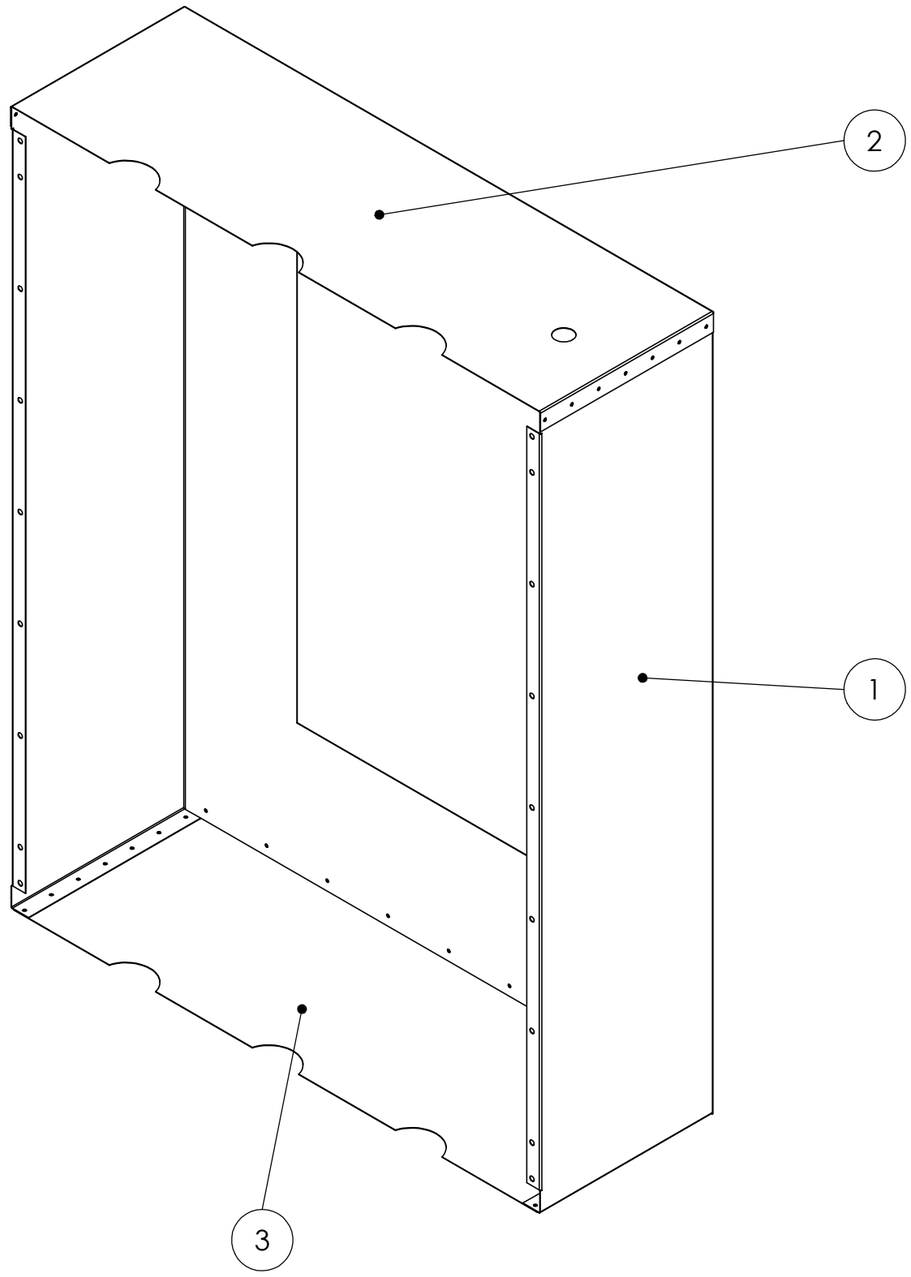

ITEM NO.	PART NUMBER	DESCRIPTION	QTY.
1	Des 2020020702	chapa_exterior_fh	1
2	Des 2020013103	chapa_top_bh	1
3	Des 2020013104	chapa_bottom_bh	1

UNLESS OTHERWISE SPECIFIED: DIMENSIONS ARE IN MILLIMETERS SURFACE FINISH: TOLERANCES: LINEAR: ANGULAR:	FINISH:		DEBURR AND BREAK SHARP EDGES		DO NOT SCALE DRAWING	REVISION
	NAME	SIGNATURE	DATE			
DRAWN						
CHK'D						
APPV'D						
MFG						
Q.A				MATERIAL:	DWG NO. Des2020020701	A3
				WEIGHT:	SCALE:1:10	SHEET 1 OF 2

TITLE: 4.chamber_front_half_exterior

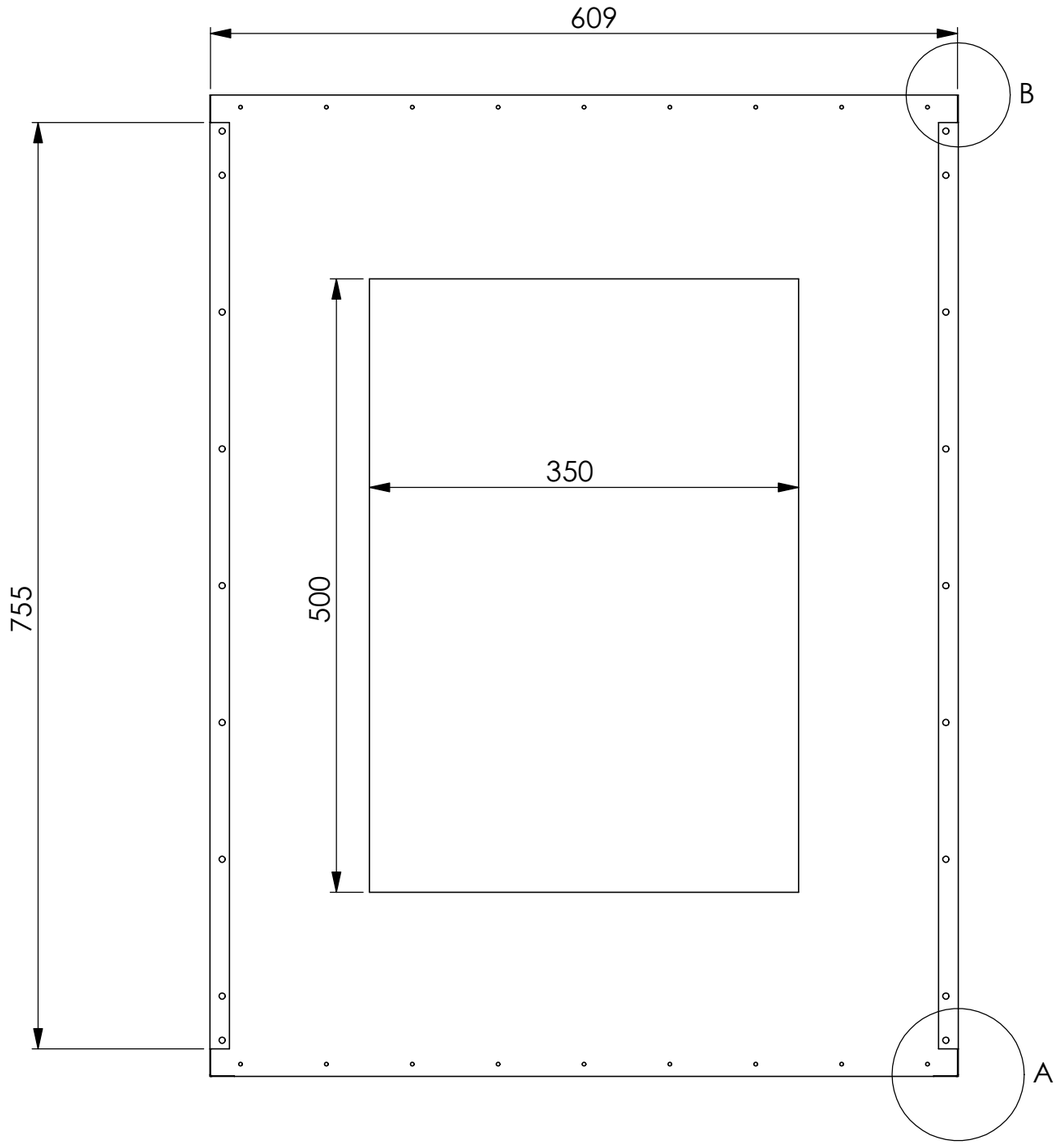

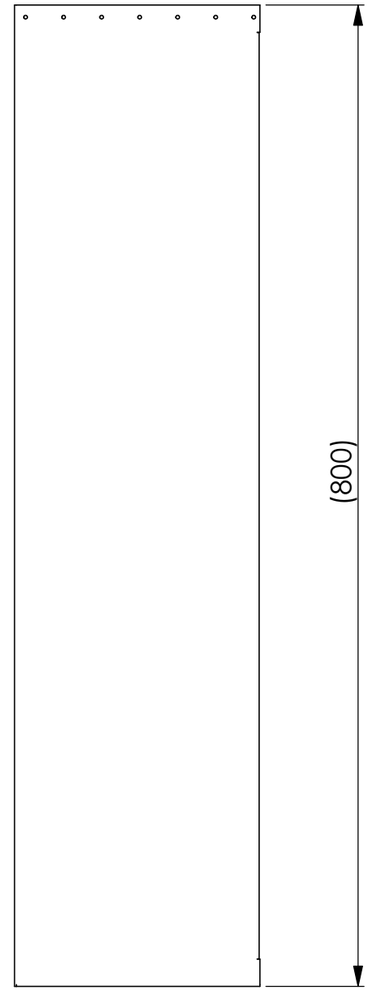

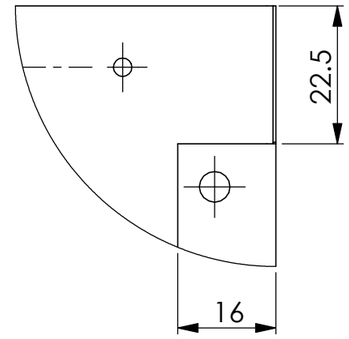

B (1 : 1)

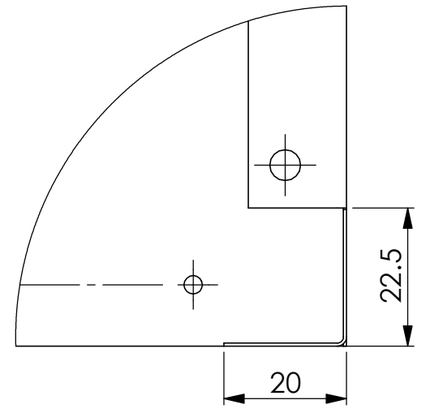

A (1 : 1)

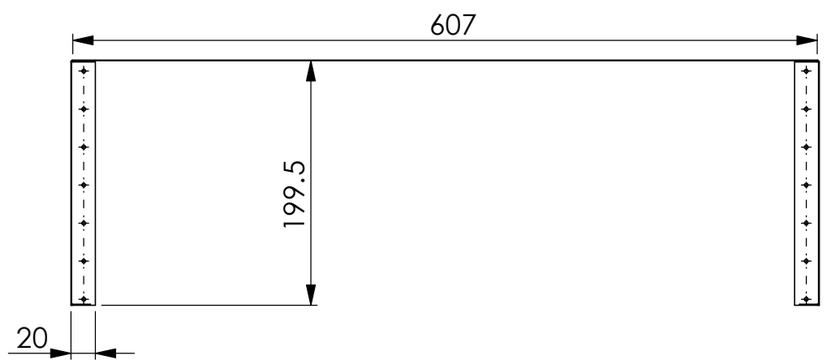

Inox AISI 304

chapa t= 0.5

Furos não cotados a fazer durante a montagem

UNLESS OTHERWISE SPECIFIED: DIMENSIONS ARE IN MILLIMETERS SURFACE FINISH: TOLERANCES: LINEAR: ANGULAR:	FINISH:		DEBURR AND BREAK SHARP EDGES	DO NOT SCALE DRAWING	REVISION	
	NAME	SIGNATURE	DATE	TITLE: chapa_exterior_fh		
DRAWN						
CHK'D						
APPV'D						
MFG						
Q.A				MATERIAL:	DWG NO. Des 2020020702	A3
				WEIGHT:	SCALE:1:10	SHEET 2 OF 2

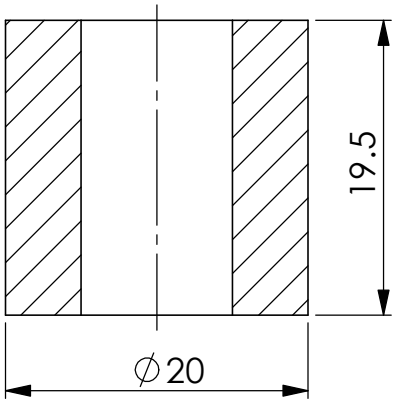

Teflon 34 peças

UNLESS OTHERWISE SPECIFIED: DIMENSIONS ARE IN MILLIMETERS SURFACE FINISH: TOLERANCES: LINEAR: ANGULAR:	FINISH:		DEBURR AND BREAK SHARP EDGES		DO NOT SCALE DRAWING	REVISION
	NAME	SIGNATURE	DATE		TITLE: batente_L19.5	
DRAWN						
CHK'D						
APPV'D						
MFG						
Q.A				MATERIAL:	DWG NO. Des 2020012903	A4
				WEIGHT:	SCALE:5:1	SHEET 1 OF 1

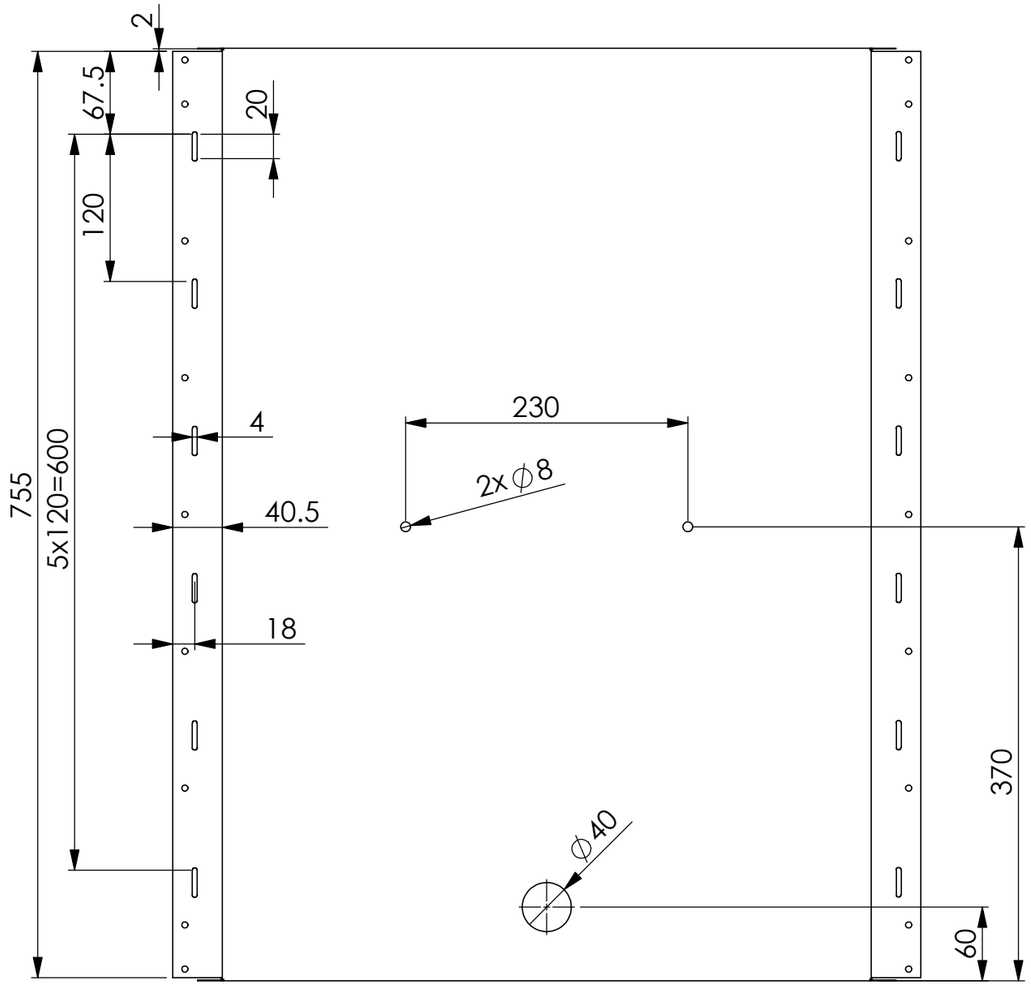

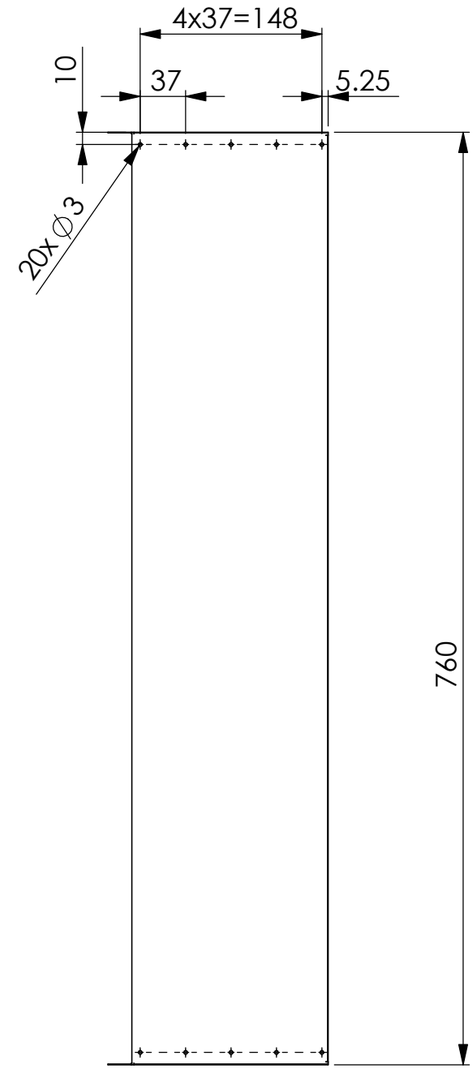

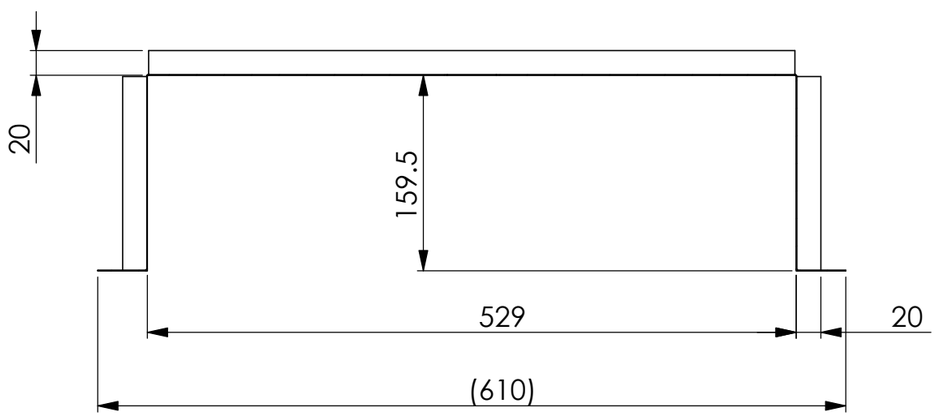

Inox AISI 304

chapa t= 0.5

Furos não cotados a fazer durante a montagem

UNLESS OTHERWISE SPECIFIED: DIMENSIONS ARE IN MILLIMETERS SURFACE FINISH: TOLERANCES: LINEAR: ANGULAR:	FINISH:		DEBURR AND BREAK SHARP EDGES	DO NOT SCALE DRAWING	REVISION	
	NAME	SIGNATURE	DATE	TITLE: chapa_interior_1_bh		
DRAWN						
CHK'D						
APPV'D						
MFG						
Q.A				MATERIAL:	DWG NO. Des 2020012901	A3
				WEIGHT:	SCALE:1:5	SHEET 1 OF 1

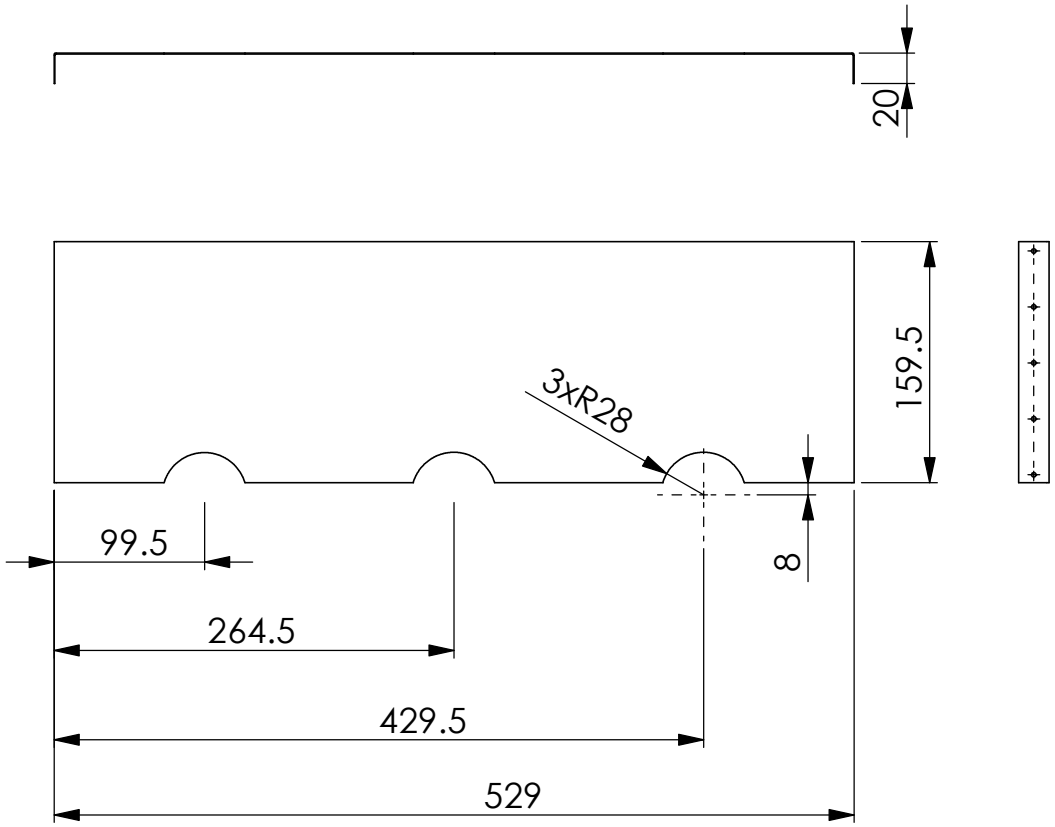

Inox AISI 304

chapa t= 0.5

Furos não cotados a fazer durante a montagem

UNLESS OTHERWISE SPECIFIED: DIMENSIONS ARE IN MILLIMETERS SURFACE FINISH: TOLERANCES: LINEAR: ANGULAR:	FINISH:		DEBURR AND BREAK SHARP EDGES	DO NOT SCALE DRAWING	REVISION	
	NAME	SIGNATURE	DATE	TITLE:		
DRAWN				chapa_interior_2_bh		
CHK'D						
APPV'D						
MFG						
Q.A				MATERIAL:	DWG NO. Des 2020012902	A4
				WEIGHT:	SCALE:1:5	SHEET 1 OF 1

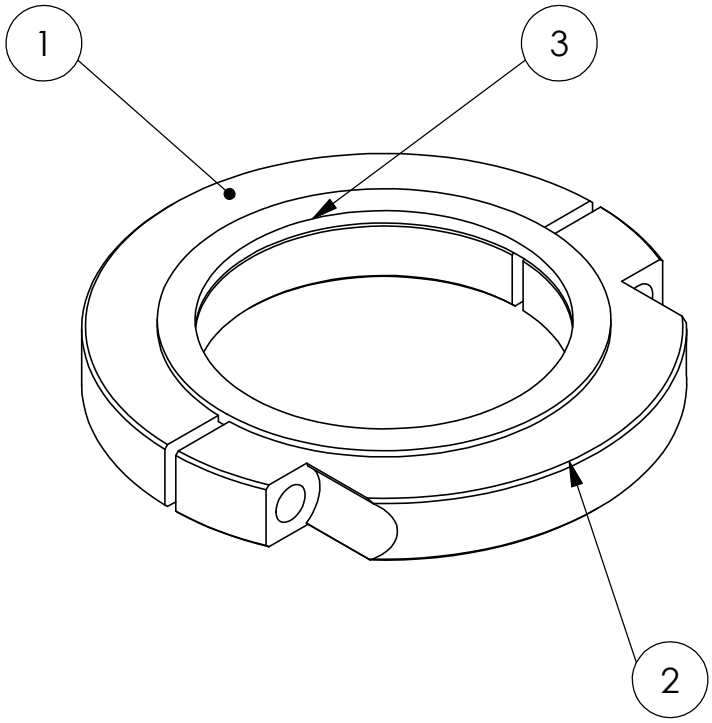

ITEM NO.	PART NUMBER	DESCRIPTION	QTY.
1	Des 2020020712	bottom_spaccer_half_one	1
2	Des 2020020713	bottom_spaccer_half_two	1
3	-	bottom_spaccer_washer	1

UNLESS OTHERWISE SPECIFIED: DIMENSIONS ARE IN MILLIMETERS SURFACE FINISH: TOLERANCES: LINEAR: ANGULAR:	FINISH:		DEBURR AND BREAK SHARP EDGES	DO NOT SCALE DRAWING	REVISION	
	NAME	SIGNATURE	DATE			
DRAWN				TITLE: bottom_spaccer		
CHK'D						
APPV'D						
MFG						
Q.A				MATERIAL:	DWG NO. Des 2020020711	A4
				WEIGHT:	SCALE:1:1	SHEET 1 OF 3

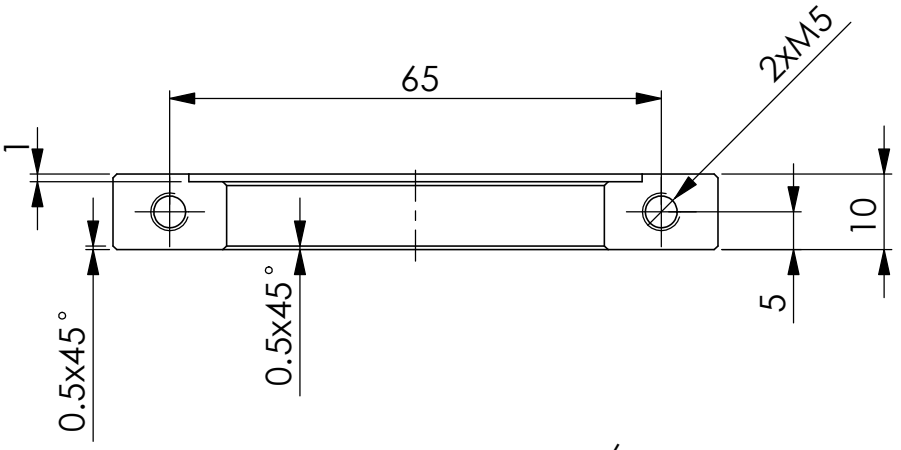

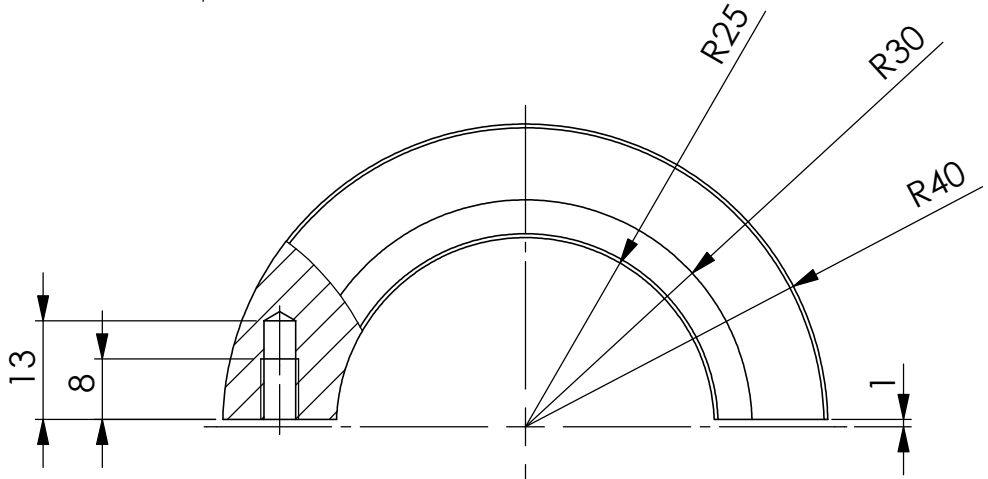

Inox AISI 304

UNLESS OTHERWISE SPECIFIED: DIMENSIONS ARE IN MILLIMETERS SURFACE FINISH: TOLERANCES: LINEAR: ANGULAR:	FINISH:		DEBURR AND BREAK SHARP EDGES	DO NOT SCALE DRAWING	REVISION	
	NAME	SIGNATURE	DATE	TITLE: bottom_spaccer_half_one		
DRAWN						
CHK'D						
APPV'D						
MFG						
Q.A				MATERIAL:	DWG NO. Des 2020020712	A4
				WEIGHT:	SCALE:1:2	SHEET 2 OF 3

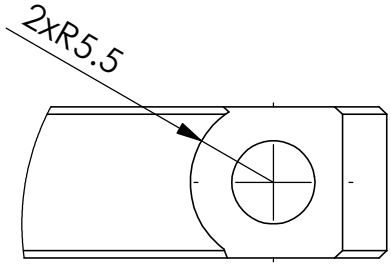

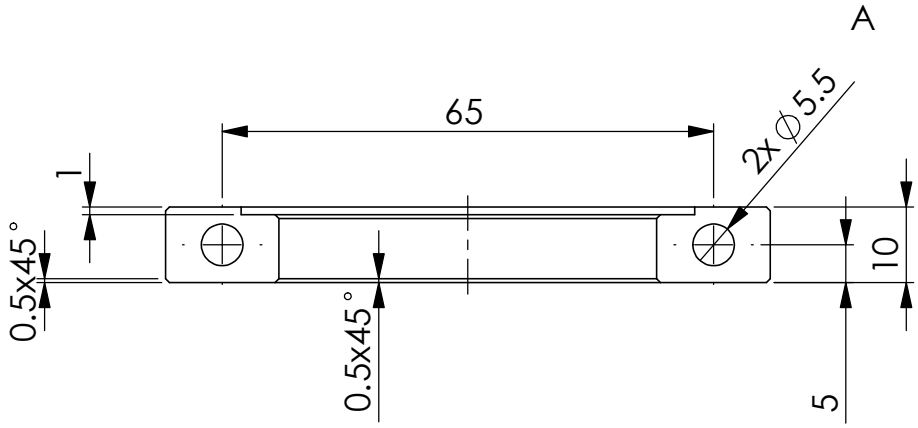

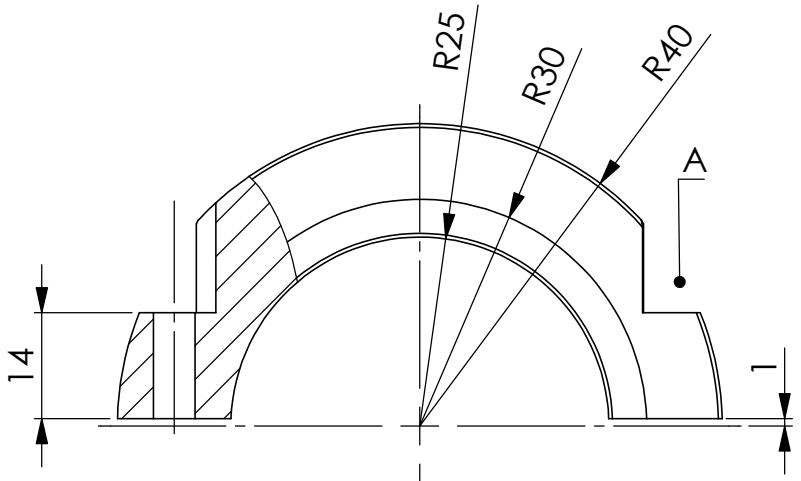

Inox AISI 304

UNLESS OTHERWISE SPECIFIED: DIMENSIONS ARE IN MILLIMETERS SURFACE FINISH: TOLERANCES: LINEAR: ANGULAR:	FINISH:		DEBURR AND BREAK SHARP EDGES	DO NOT SCALE DRAWING	REVISION	
	NAME	SIGNATURE	DATE	TITLE: bottom_spaccer_half_two		
DRAWN						
CHK'D						
APPV'D						
MFG						
Q.A				MATERIAL:	DWG NO. Des 2020020713	A4
				WEIGHT:	SCALE:1:2	SHEET 3 OF 3

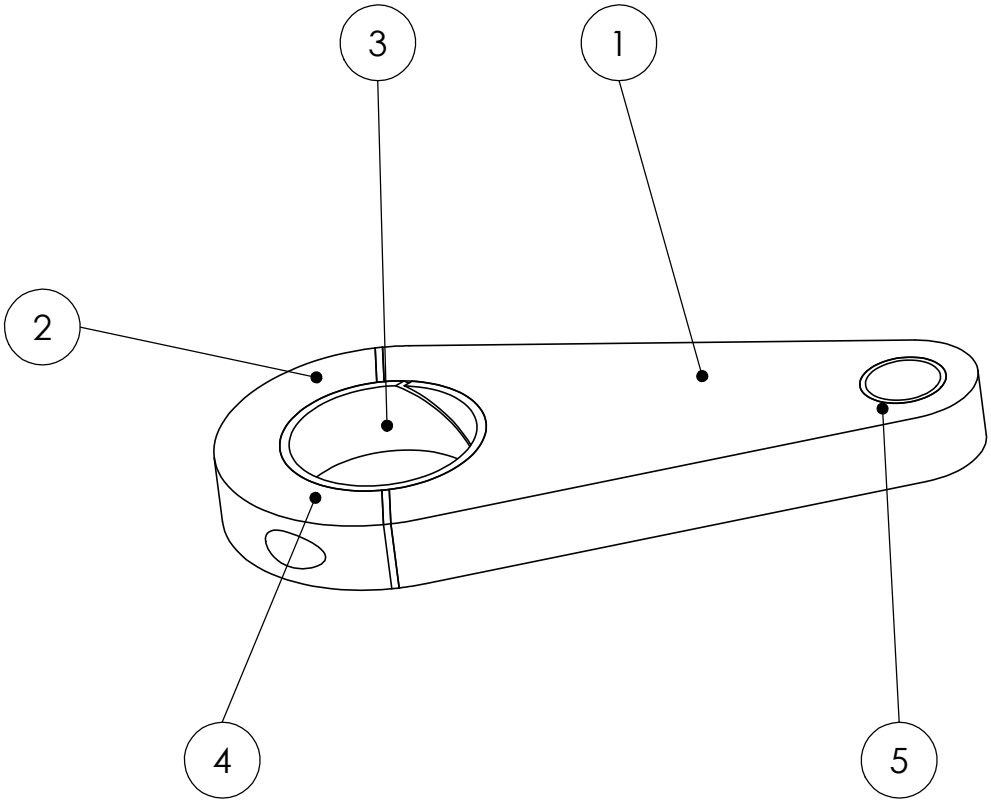

ITEM NO.	PART NUMBER	DESCRIPTION	QTY.
1	Des 2020020715	mechanical_attachment_big_half	1
2	Des 2020020716	mechanical_attachment_small_half	1
3	Des 2020020717	mechanical_attachment_spacc er	2
4	mechanical_attachment_bushing_1	∅50x∅55x20	4
5	mechanical_attachment_bushing_2	∅20x∅23x20	4

UNLESS OTHERWISE SPECIFIED: DIMENSIONS ARE IN MILLIMETERS SURFACE FINISH: TOLERANCES: LINEAR: ANGULAR:	FINISH:	DEBURR AND BREAK SHARP EDGES	DO NOT SCALE DRAWING / REVISION

	NAME	SIGNATURE	DATE
DRAWN			
CHK'D			
APPV'D			
MFG			
Q.A			

TITLE: mechanical_attachment

MATERIAL:

DWG NO. Des 20200207--

A4

WEIGHT:

SCALE:1:5

SHEET 1 OF 6

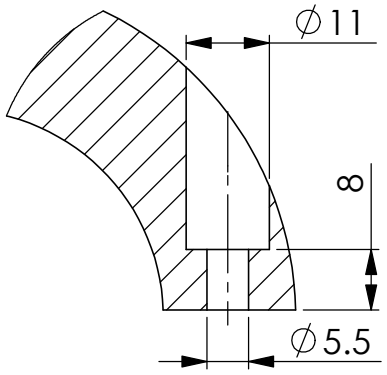

B (1 : 1)

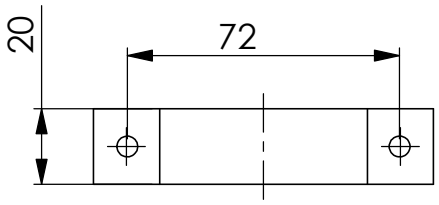

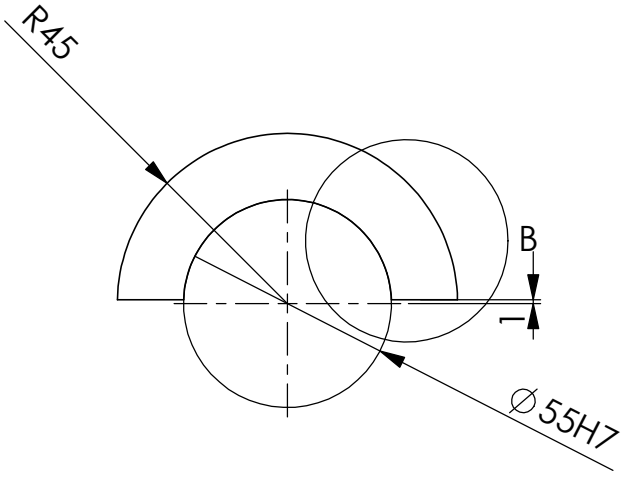

Inox AISI 304

UNLESS OTHERWISE SPECIFIED: DIMENSIONS ARE IN MILLIMETERS SURFACE FINISH: TOLERANCES: LINEAR: ANGULAR:	FINISH:		DEBURR AND BREAK SHARP EDGES	DO NOT SCALE DRAWING	REVISION	
	NAME	SIGNATURE	DATE	TITLE: mechanical_attachment_small_half		
DRAWN						
CHK'D						
APPV'D						
MFG						
Q.A				MATERIAL:	DWG NO. Des 2020020716	A4
				WEIGHT:	SCALE:1:2	SHEET 2 OF 6

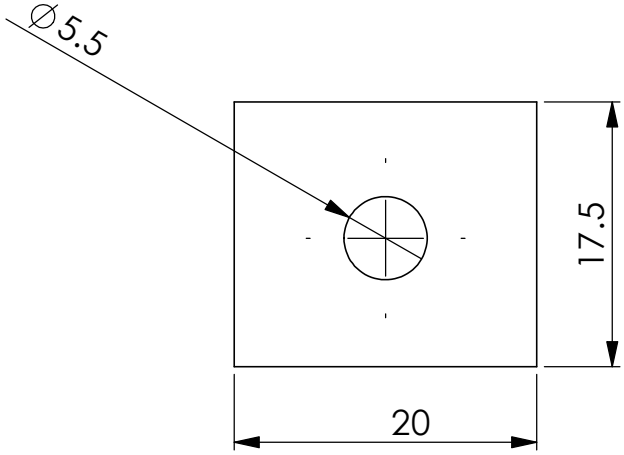

t=2mm

Inox AISI 304

UNLESS OTHERWISE SPECIFIED: DIMENSIONS ARE IN MILLIMETERS SURFACE FINISH: TOLERANCES: LINEAR: ANGULAR:	FINISH:		DEBURR AND BREAK SHARP EDGES	DO NOT SCALE DRAWING	REVISION	
	NAME	SIGNATURE	DATE	TITLE: mechanical_attachment_spacce r		
DRAWN						
CHK'D						
APPV'D						
MFG						
Q.A				MATERIAL:	DWG NO. Des 2020020717	A4
				WEIGHT:	SCALE:2:1	SHEET 3 OF 6

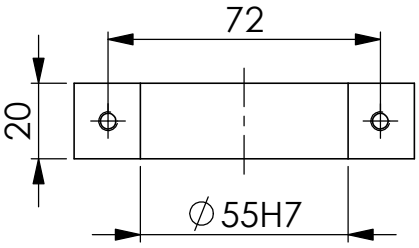

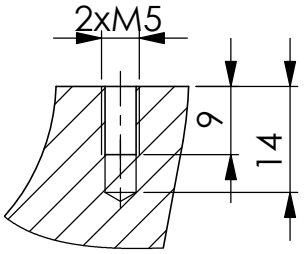

A-A (1 : 1)

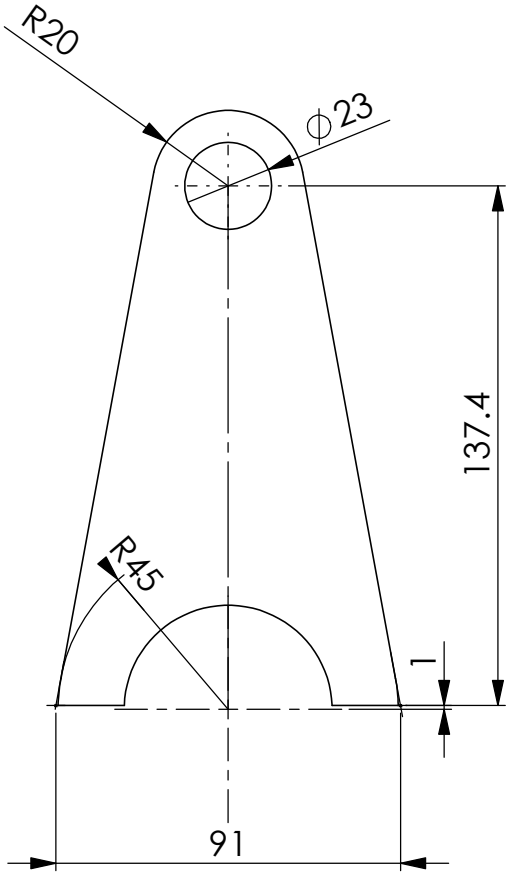

Inox AISI 304

UNLESS OTHERWISE SPECIFIED: DIMENSIONS ARE IN MILLIMETERS SURFACE FINISH: TOLERANCES: LINEAR: ANGULAR:	FINISH:		DEBURR AND BREAK SHARP EDGES	DO NOT SCALE DRAWING	REVISION	
	NAME	SIGNATURE	DATE	TITLE: mechanical_attachment_big_half		
DRAWN						
CHK'D						
APPV'D						
MFG						
Q.A				MATERIAL:	DWG NO. Des 2020020715	A4
				WEIGHT:	SCALE:1:5	SHEET 4 OF 6

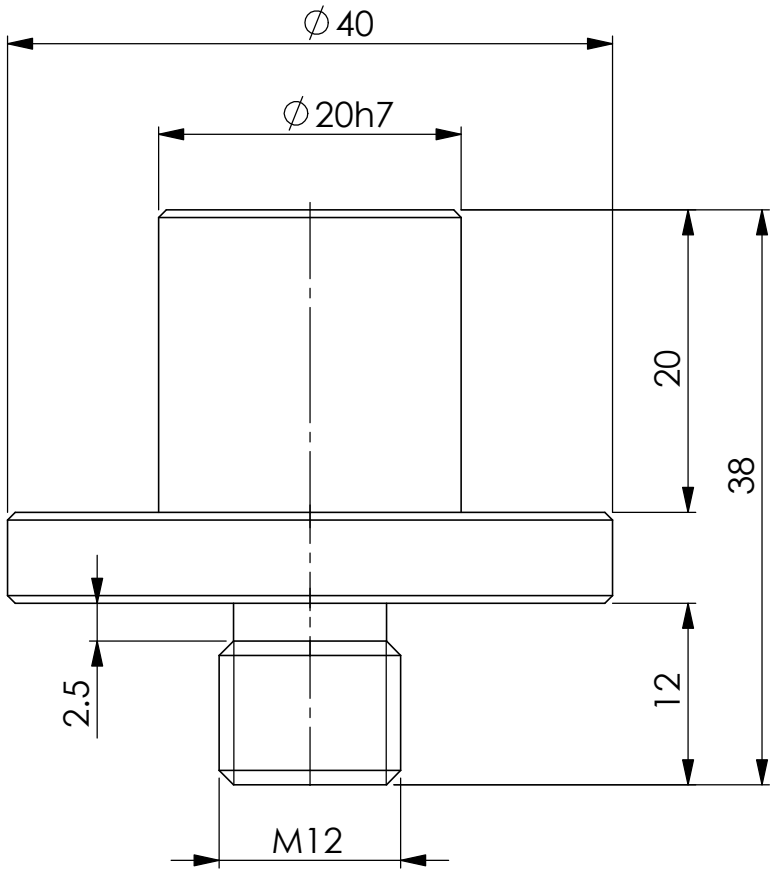

Chamfros 0.5x45

Inox AISI 304

UNLESS OTHERWISE SPECIFIED: DIMENSIONS ARE IN MILLIMETERS SURFACE FINISH: TOLERANCES: LINEAR: ANGULAR:	FINISH:		DEBURR AND BREAK SHARP EDGES	DO NOT SCALE DRAWING	REVISION	
	NAME	SIGNATURE	DATE	TITLE: Apoio_suport_1		
DRAWN						
CHK'D						
APPV'D						
MFG						
Q.A				MATERIAL:	DWG NO. Des 2020020718	A4
				WEIGHT:	SCALE:1:1	SHEET 5 OF 6

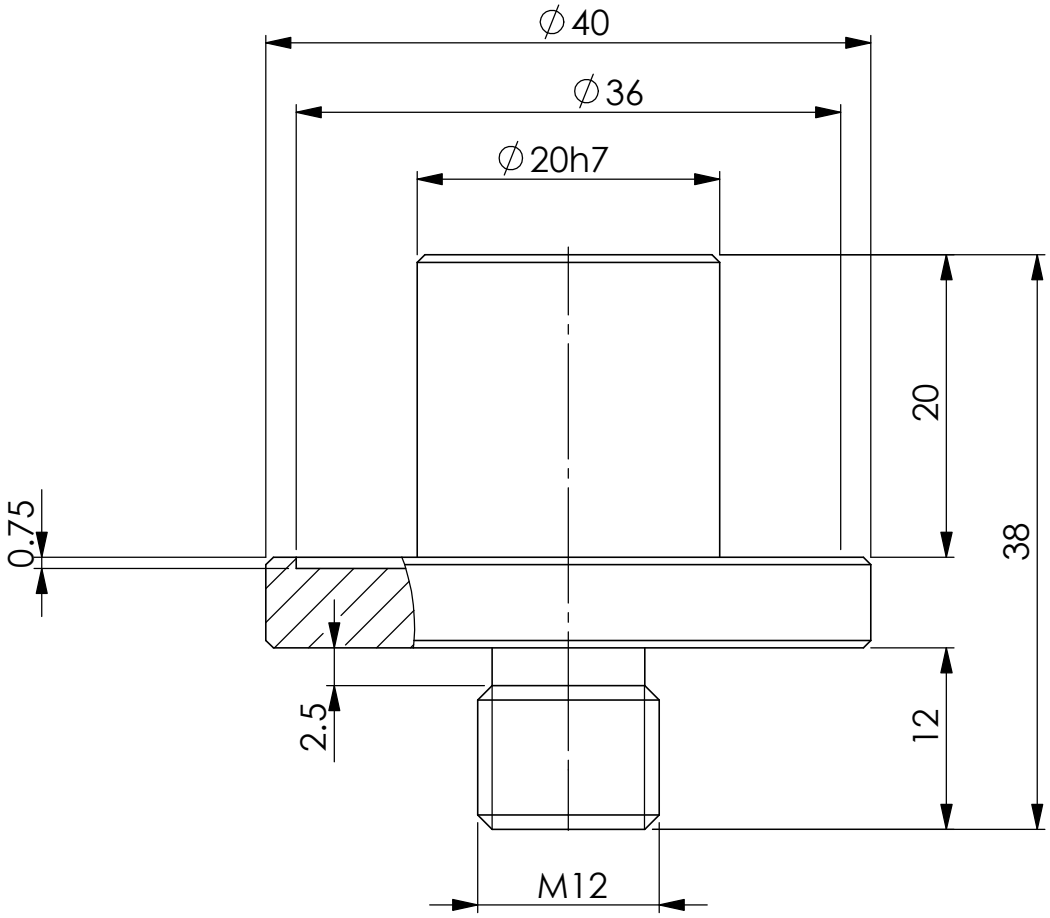

Chamfros 0.5x45

Inox AISI 304

UNLESS OTHERWISE SPECIFIED: DIMENSIONS ARE IN MILLIMETERS SURFACE FINISH: TOLERANCES: LINEAR: ANGULAR:	FINISH:		DEBURR AND BREAK SHARP EDGES	DO NOT SCALE DRAWING	REVISION	
	NAME	SIGNATURE	DATE	TITLE: Apoio_suport_2		
DRAWN						
CHK'D						
APPV'D						
MFG						
Q.A				MATERIAL:	DWG NO. Des 2020020719	A4
				WEIGHT:	SCALE:1:1	SHEET 6 OF 6

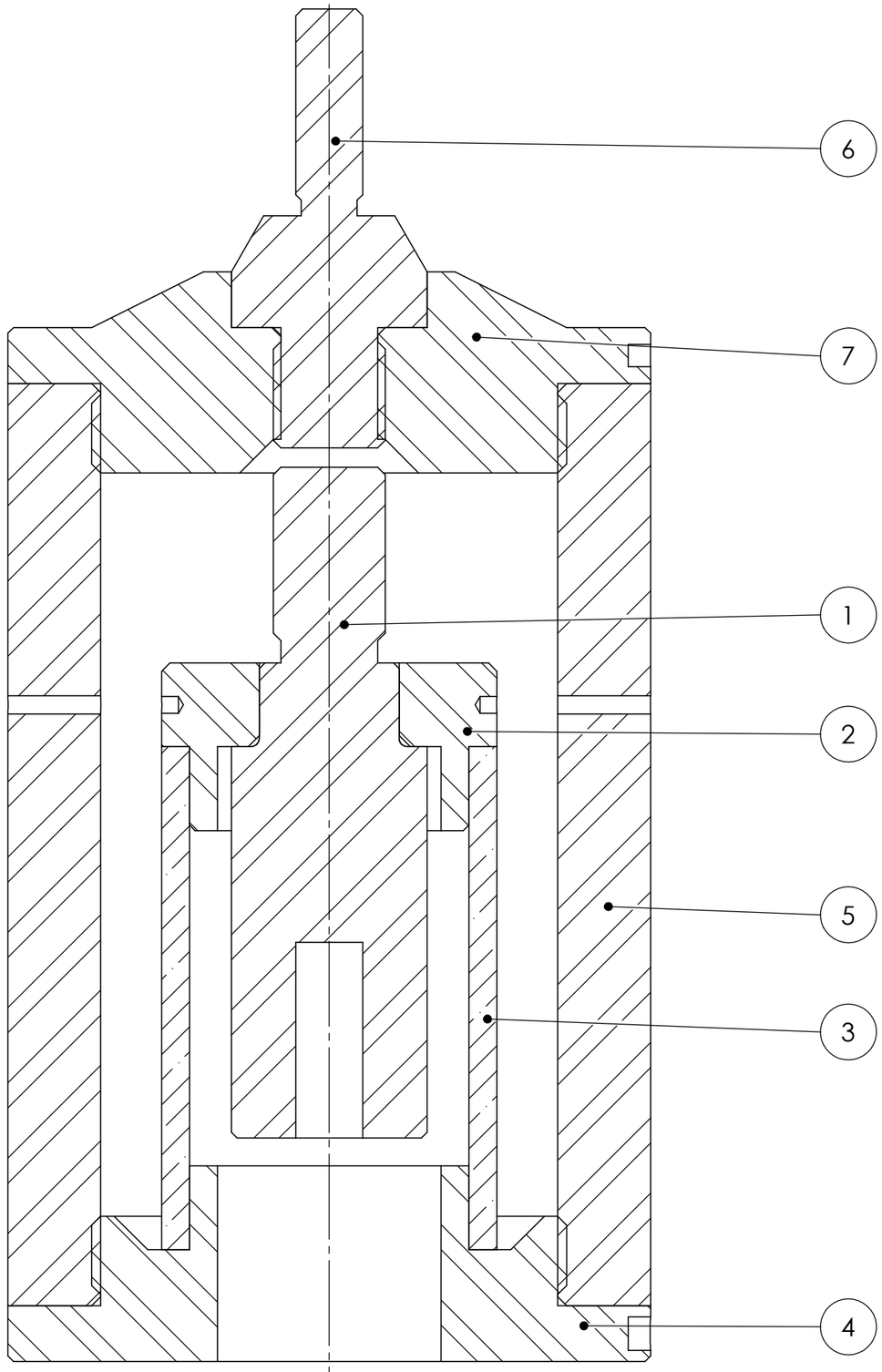

ITEM NO.	PART NUMBER	DESCRIPTION	QTY.
1	Des 2020020704	upper_coupling_modified_1.4	1
2	Des 2020020705	disc.4	1
3	Des 2020020706	insulator.4	1
4	Des 2020020710	lower_cover.4	1
5	Des 2020020707	side_cover_modified.4	1
6	Des 2020020708	upper_coupling_modified_2.4	1
7	Des 2020020709	upper_cover_modified.4	1

UNLESS OTHERWISE SPECIFIED:
DIMENSIONS ARE IN MILLIMETERS
SURFACE FINISH:
TOLERANCES:
LINEAR:
ANGULAR:

FINISH:

DEBURR AND BREAK SHARP EDGES

DO NOT SCALE DRAWING | REVISION

	NAME	SIGNATURE	DATE
DRAWN			
CHK'D			
APPV'D			
MFG			
Q.A			

TITLE:

Assem4

MATERIAL:

DWG NO. Des 2020020703

A3

WEIGHT:

SCALE:1:5

SHEET 1 OF 8

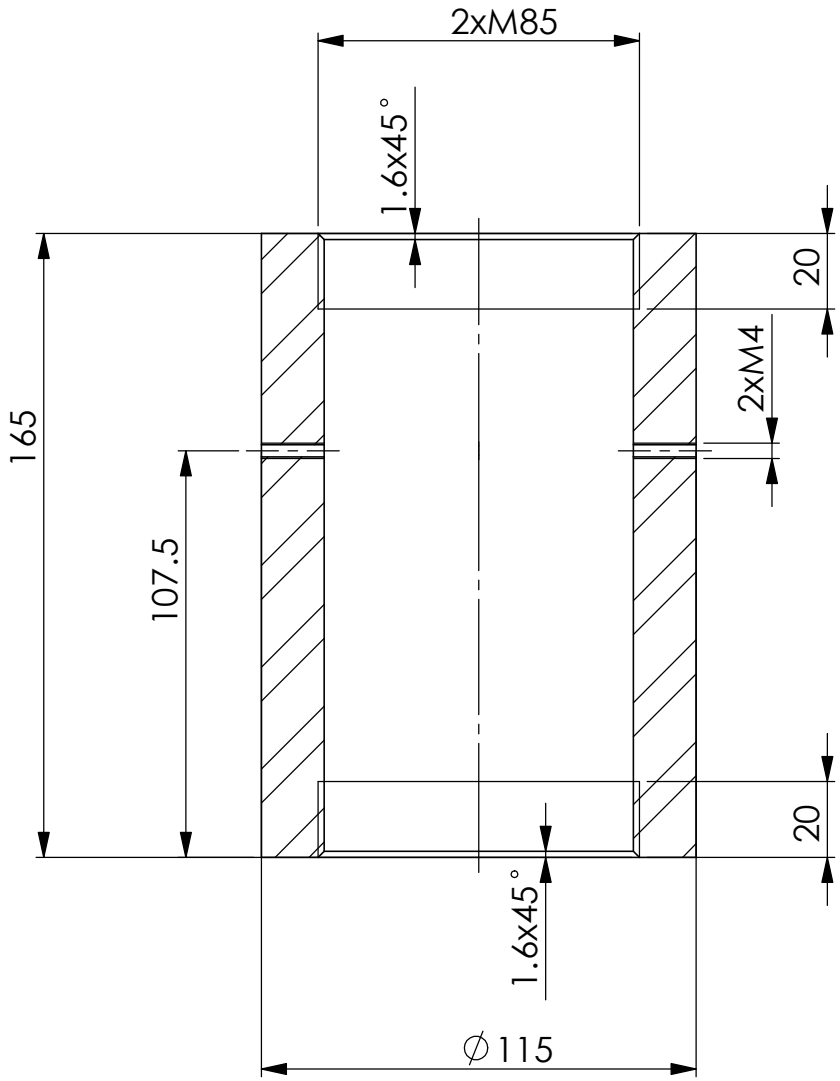

Inox AISI 304

UNLESS OTHERWISE SPECIFIED: DIMENSIONS ARE IN MILLIMETERS SURFACE FINISH: TOLERANCES: LINEAR: ANGULAR:	FINISH:		DEBURR AND BREAK SHARP EDGES	DO NOT SCALE DRAWING	REVISION	
	NAME	SIGNATURE	DATE	TITLE: side_cover_modified.4		
DRAWN						
CHK'D						
APPV'D						
MFG						
Q.A				MATERIAL:	DWG NO. Des 2020020707	A4
				WEIGHT:	SCALE:1:2	SHEET 2 OF 8

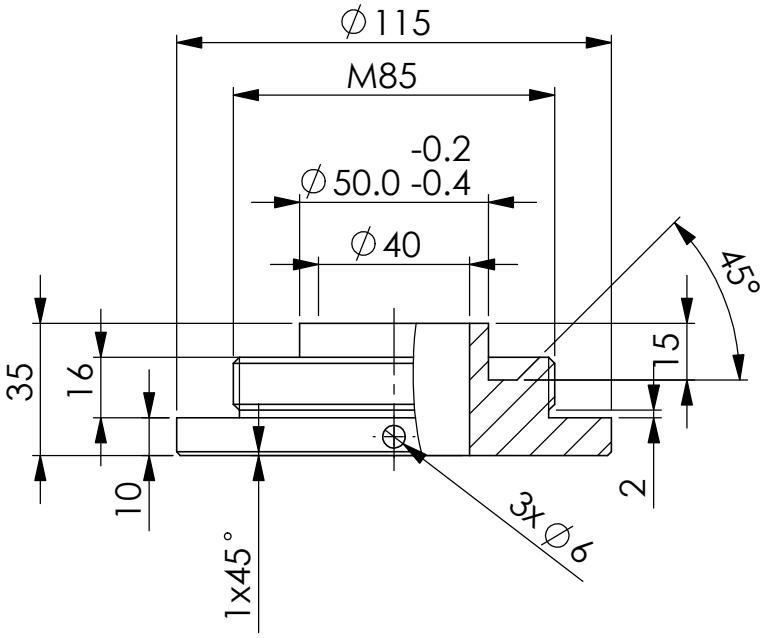

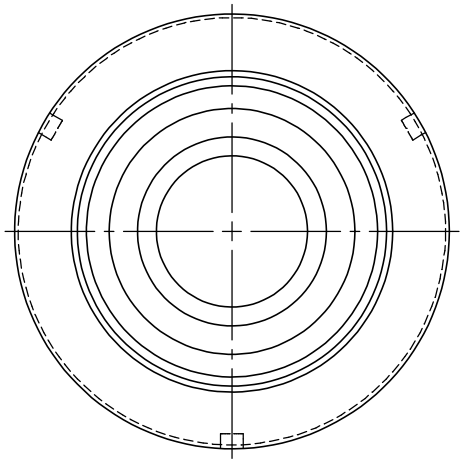

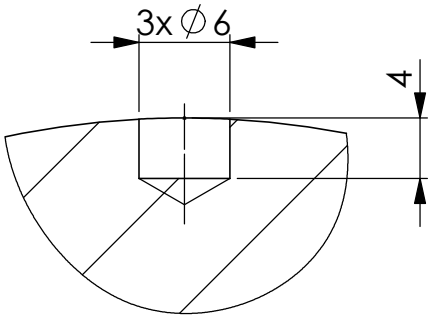

Inox AISI 304

A-A (2 : 1)

UNLESS OTHERWISE SPECIFIED: DIMENSIONS ARE IN MILLIMETERS SURFACE FINISH: TOLERANCES: LINEAR: ANGULAR:	FINISH:		DEBURR AND BREAK SHARP EDGES	DO NOT SCALE DRAWING	REVISION	
	NAME	SIGNATURE	DATE	TITLE: lower_cover.4		
DRAWN						
CHK'D						
APPV'D						
MFG						
Q.A				MATERIAL:	DWG NO. Des 2020020710	A4
				WEIGHT:	SCALE:1:2	SHEET 3 OF 8

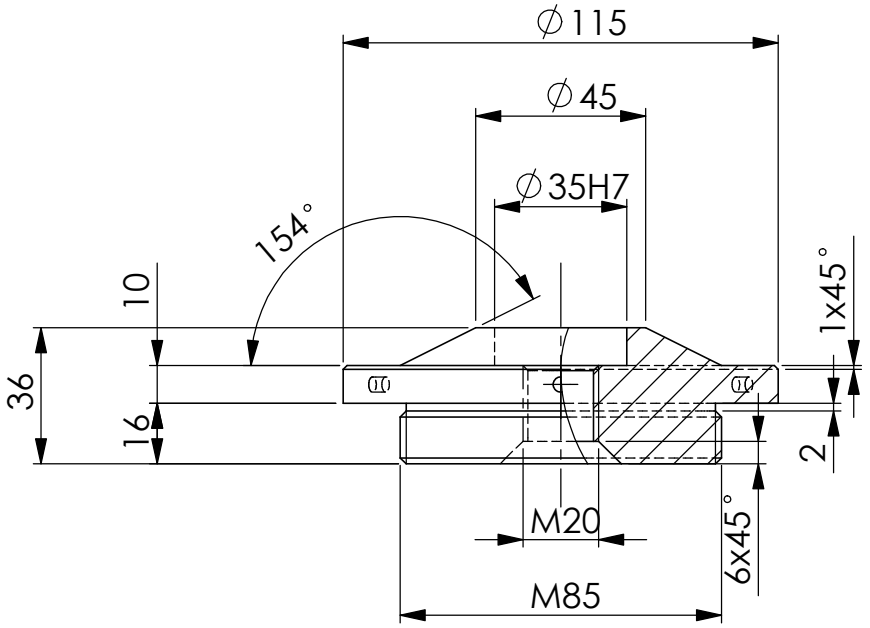

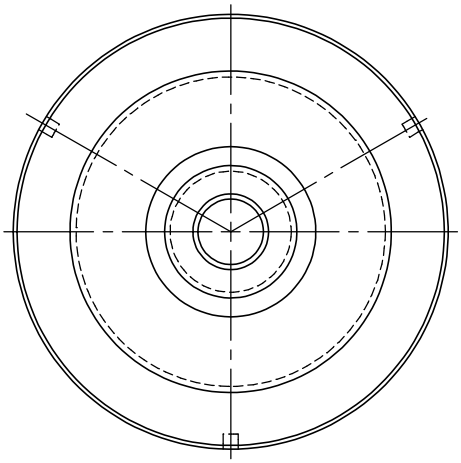

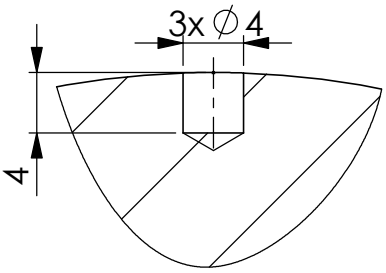

B-B (2 : 1)

Inox AISI 304

UNLESS OTHERWISE SPECIFIED: DIMENSIONS ARE IN MILLIMETERS SURFACE FINISH: TOLERANCES: LINEAR: ANGULAR:	FINISH:		DEBURR AND BREAK SHARP EDGES		DO NOT SCALE DRAWING	REVISION
	NAME	SIGNATURE	DATE		TITLE: upper_cover_modified.4	
DRAWN						
CHK'D						
APPV'D						
MFG						
Q.A				MATERIAL:	DWG NO. Des 2020020709	A4
				WEIGHT:	SCALE:1:2	SHEET 4 OF 8

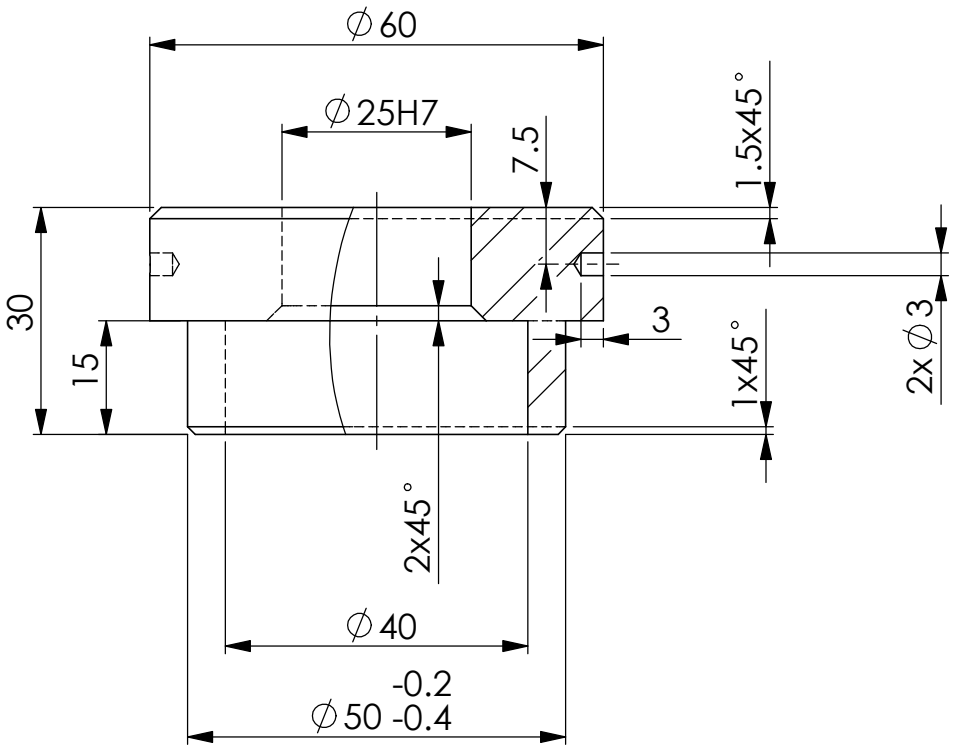

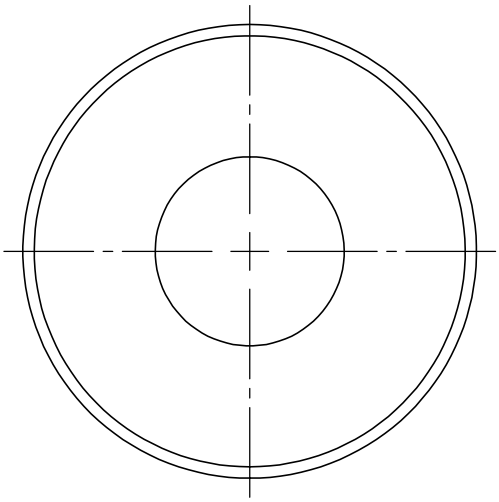

Inox AISI 304

UNLESS OTHERWISE SPECIFIED: DIMENSIONS ARE IN MILLIMETERS SURFACE FINISH: TOLERANCES: LINEAR: ANGULAR:		FINISH:		DEBURR AND BREAK SHARP EDGES	DO NOT SCALE DRAWING	REVISION
	NAME	SIGNATURE	DATE		TITLE: disc.4	
DRAWN						
CHK'D						
APPV'D						
MFG						
Q.A				MATERIAL:	DWG NO. Des 2020020705	A4
				WEIGHT:	SCALE:1:2	SHEET 5 OF 8

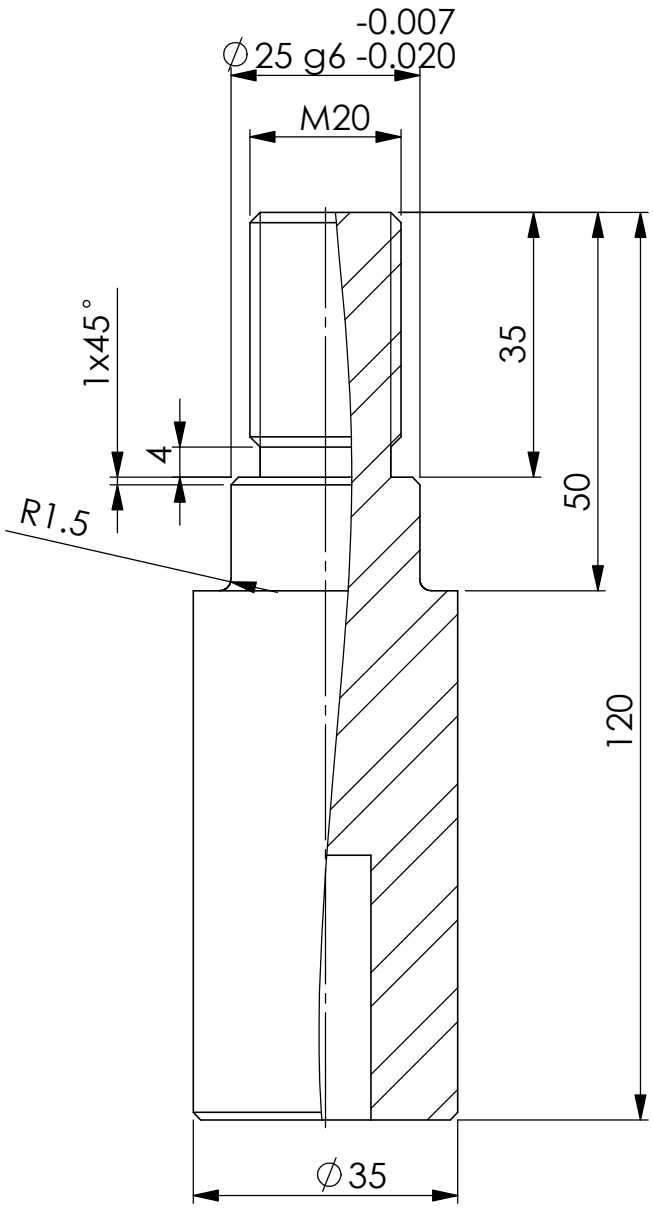

Inox AISI 304

UNLESS OTHERWISE SPECIFIED: DIMENSIONS ARE IN MILLIMETERS SURFACE FINISH: TOLERANCES: LINEAR: ANGULAR:		FINISH:		DEBURR AND BREAK SHARP EDGES	DO NOT SCALE DRAWING	REVISION
	NAME	SIGNATURE	DATE		TITLE: upper_coupling_modified_1.4	
DRAWN						
CHK'D						
APPV'D						
MFG						
Q.A				MATERIAL:	DWG NO. Des 2020020704	A4
				WEIGHT:	SCALE:1:1	SHEET 6 OF 8

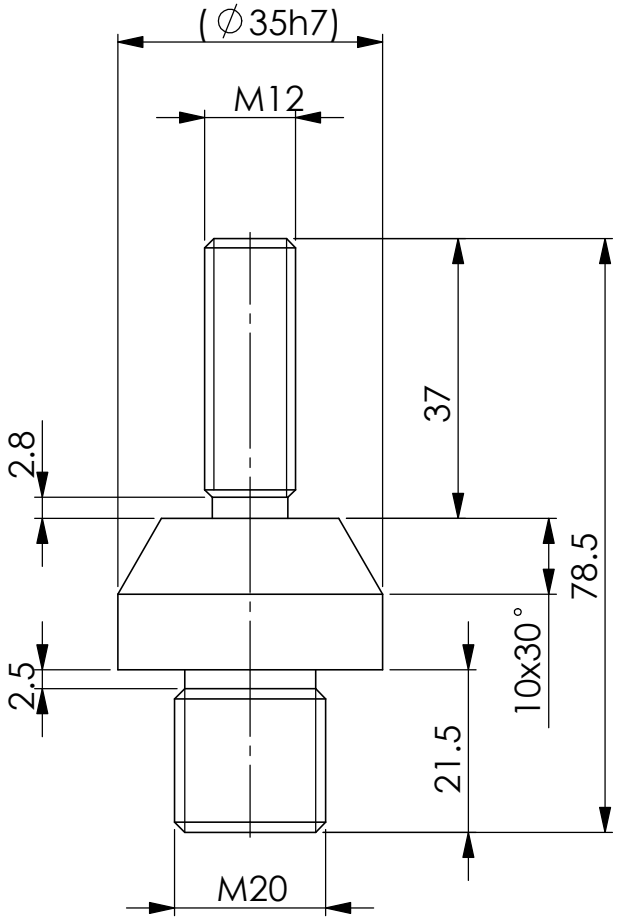

Inox AISI 304

UNLESS OTHERWISE SPECIFIED: DIMENSIONS ARE IN MILLIMETERS SURFACE FINISH: TOLERANCES: LINEAR: ANGULAR:	FINISH:		DEBURR AND BREAK SHARP EDGES	DO NOT SCALE DRAWING	REVISION	
	NAME	SIGNATURE	DATE	TITLE: upper_coupling_modified_2.4		
DRAWN						
CHK'D						
APPV'D						
MFG						
Q.A				MATERIAL:	DWG NO. Des 2020020708	A4
				WEIGHT:	SCALE:1:1	SHEET 7 OF 8

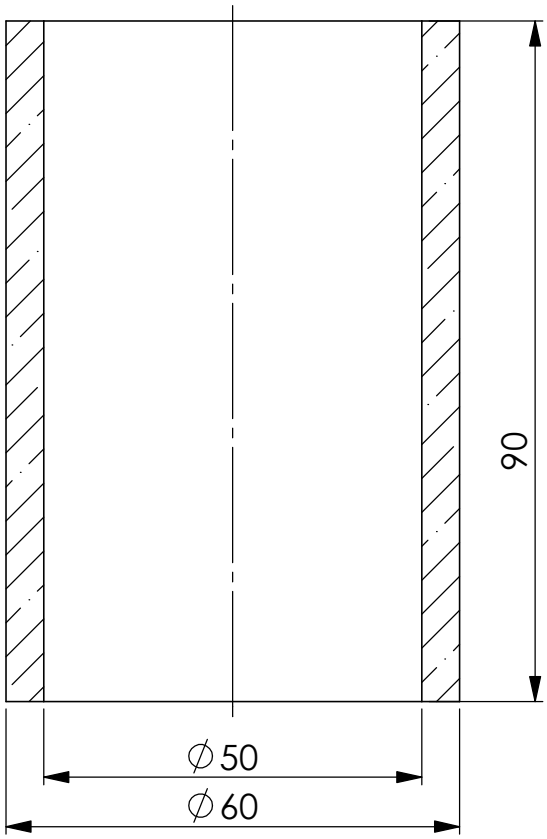

cordierite

UNLESS OTHERWISE SPECIFIED: DIMENSIONS ARE IN MILLIMETERS SURFACE FINISH: TOLERANCES: LINEAR: ANGULAR:	FINISH:	DEBURR AND BREAK SHARP EDGES	DO NOT SCALE DRAWING / REVISION

	NAME	SIGNATURE	DATE
DRAWN			
CHK'D			
APPV'D			
MFG			
Q.A			

TITLE: insulator.4

MATERIAL:

DWG NO. Des 2020020706

A4

WEIGHT:

SCALE:1:2

SHEET 8 OF 8